# POLITECNICO DI TORINO

Master's degree in Environmental and Land Engineering


Master's degree Thesis

# Transport of nanoplastics in water treatment systems

**Supervisor**:
Prof. Rajandrea Sethi

**Candidate**:
Leonardo Magherini

**Co-supervisors**:
Carlo Bianco
Amelia Piscitello

**External supervisor**:
Gerardo Pulido Reyes

Academic Year 2019/2020

# ABSTRACT

Microplastics (MPs) and nanoplastics (NPs) are contaminants of emerging concern due to their pervasive presence in environmental compartments, and in particular in water bodies. The increasing interest of the scientific and public authorities on the matter has caused in the last decade an exponential growth of scientific research on this topic. Wastewater treatment plants (WWTPs) are currently considered one of the main sources of micro- and nanoplastics due to the fact that they treat sewages, which usually transport high loads of primary plastic particles. On the other hand, water treatment plants (WTPs) are required to guarantee sufficient standards of quality, which can be reduced by the presence of micro- or nanoplastics in the water supply source.

The aim of this thesis is to assess the capability of conventional WTPs, and in particular of the filtration stage, to remove plastic particles from the Lake Zürich water. To this purpose, the lake water was spiked with palladium doped NP (190 nm) before being introduced in a pilot scale WTP (1.85 m). The rare metal, which is not naturally present in the lake water, was used as a marker to track the particle mobility and quantify their concentration in water. The NP removal efficiency was tested in two granular filtering media frequently present in the treatment chain of WWTPs and WTPs, i.e. a sand ($d_{50}$ = 450 μm) and an activated carbon ($d_{50}$ = 1050 μm) bed filter.

This study originated from the collaboration of Eawag - Swiss Federal Institute of Aquatic Science and Technology, which conducted the experimental part of the study, and the Groundwater Engineering Research Group – GW of Politecnico di Torino, which was responsible for the data interpretation and modelling.

At first, the particle behaviour within the filtering media was characterized at laboratory scale. Eawag conducted several column filtration tests exploring different operating conditions. The experimental data were elaborated and analysed to understand the interaction mechanism between nanoplastics and the filter material. The filtration mechanism and the related kinetic parameters were estimated using the numerical model MNMs, developed at Politecnico di Torino, to fit the column experimental breakthrough curves. These parameters were then applied to predict the particle behaviour within the pilot plant and to support the design of the larger scale experiments. Finally, the modelled and experimental data were compared to refine the pilot model and enhance its reliability and prediction capability.

From this study emerged that the filtration mechanism that better describes the particle behaviour in a sand or in an activated carbon filter is “blocking”. Blocking is a saturative single-layer deposition mechanism, typical of systems where physico-chemical surface interactions are predominant. This is the case of NPs, which are characterized by a high negative surface charge. As a consequence, the filtration efficiency is expected to approach zero for both filtering materials once all the active sites available for deposition are occupied by particles and the porous medium saturation is achieved. According to the model, given the same filtration time and filter length, a higher retention capacity was

predicted for the sand bed, thanks to the lower filtration rate and smaller grains size compared to activated carbon. From an operational point of view, this means that a periodic backwashing of the filters is necessary to achieve and keep acceptable NP retention capacities in WTPs. In conclusion, knowing the behaviour of nanoplastics in granular media filters used in WTPs and WWTPs is a potential asset to firstly count, and eventually reduce, the amount of plastic particles released in water bodies and secondly to increase the drinking water quality.

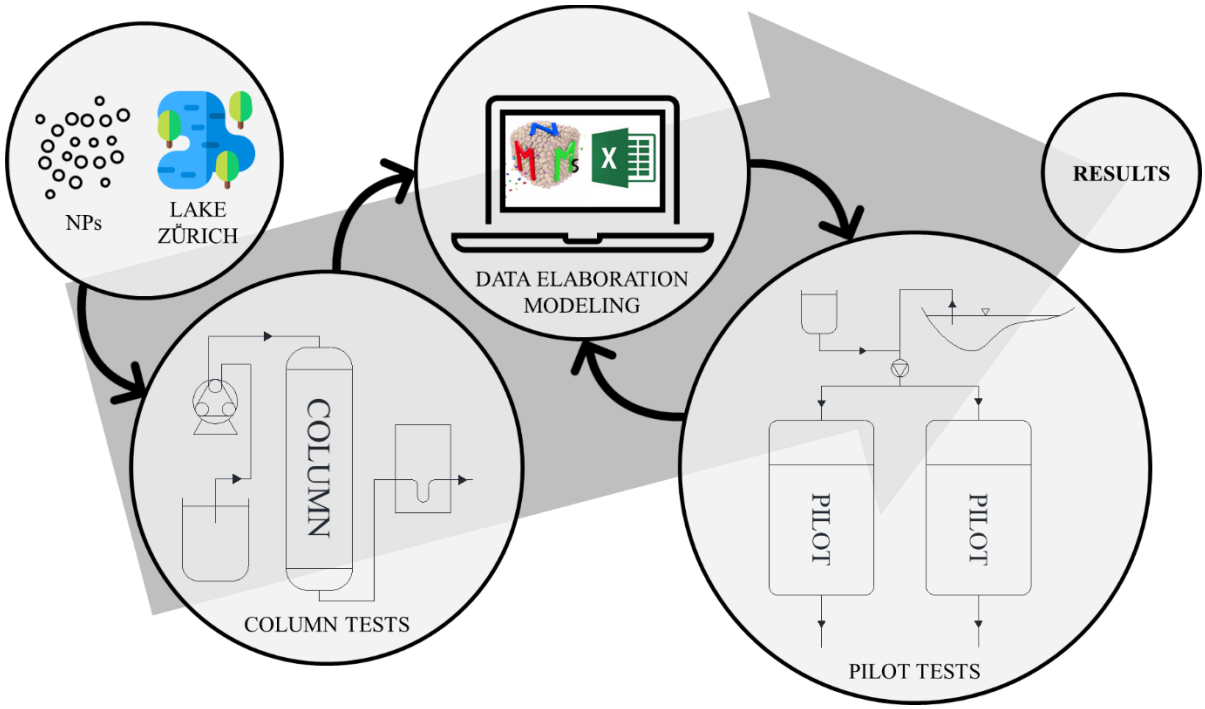


*Graphical abstract*

# Contents

# INTRODUCTION

The pervasive presence of microplastics (MPs) and nanoplastics (NPs) in various environmental compartments fostered an increasing research on their possible implications on human health and environment protection. A scientific development regarding microplastics is therefore necessary, starting from collecting methods, identification methods, sources identification, to toxicity studies. A general presentation of micro- and nanoplastics is here provided with the aim of showing the key aspects necessary to better understand the goal of this research. The knowledge on plastic debris is increasing rapidly, in the following paragraphs only few key aspects are reported.

A crucial and preliminary aspect of the research is the definition of plastic. The International Organization for Standardization defines plastic as a "material which contains as an essential ingredient a high polymer and which, at some stage in its processing into finished products, can be shaped by flow" in ISO 472:2013. The same institution excludes from the definition the elastomeric materials, which "are also shaped by flow" but "are not considered to be plastics" (ISO 472:2013). However, from an environmental point of view, plastic and rubber can be both considered potential sources of MPs independently from their definitions [1]. A consensus on which material to include in the MP definition is therefore necessary to support the drafting of regulations [2]. However, a unification of the terminology potentially restricts the scientific freedom, and should therefore be avoided [2].

Secondly, it is essential to differentiate plastic particles according to their sizes. The modern term to define plastic particles, "*microplastics*", was used for the first time in 2004 [3]. However, the first small plastic debris was found in 1972 floating on the Sargasso Sea [4]. This new term is now used by the scientific community, but up until now a standard size classification has not been defined yet. The first upper size limit was proposed by NOAA in 2009 during an International Research Workshop at the University of Washington Tacoma [5]. The limit of 5 mm was established to encourage the discussion on possible ecological effects and not the physical blockage of gastrointestinal tracts. Since then, the upper limit of 5 mm has become the most used. Therefore, it is now used by some international expert groups like GESAMP in 2015 [6], and 2020 [7], or like the JRC of the European Commission [8]. In addition to the upper limit, it is crucial to define the lower limit, which is nowadays defined by the class of "*nanoplastics*". The definition of nanomaterial, adopted by the EU in 2011 (2011/696/EU), is "*A natural, incidental or manufactured material containing particles, in an unbound state or as an aggregate or as an agglomerate and where, for 50 % or more of the particles in the number size distribution, one or more external dimensions is in the size range 1 nm - 100 nm.*" [9]. In conclusion, an international size definition has not been defined yet, hence, there are several size classifications of plastic particles available, each of which considers different parameters. Figure 0.1 provides a summary of particle size classifications from literature articles and from institutional reports [2]. The four classes considered are: *macroplastics*, *mesoplastics*, *microplastics*, and *nanoplastics*. The class definition varies according to different reasons, such as: identification limits, sampling net mesh, particle definitions, or general agreement.

Micro- and nanoplastics can be also classified in two groups in relation to their source: *primary microplastics* and *secondary microplastics*. Primary micro- and nanoplastics are plastic particles that are manufactured as such. Instead, the secondary ones are generated by the fragmentation of bigger plastic debris. Primary plastic particles include mainly plastic pellets used in the plastic industry and microbeads, which are spheres or granules used in toothpastes or scrubs to increase the exfoliating properties or in cosmetics to increase their light-reflection [10]. Secondary micro- and nanoplastics, which are generated by grater plastic debris, are produced when them are exposed to physical, biological and chemical processes [11]. It is estimated that between about 80 000 and 220 000 of primary MPs, of which between 3.2% and 4.1% are microbeads, are emitted into the seas from Europe. Annually Europe releases from 68 500 to 275 000 tonnes of secondary MPs in seas [12].

Because a unique definition of micro- and nanoplastics does not exist yet, for the definition and categorization of plastic particles three main characteristics are often used: shape, colour, and density. The first one, shape, is function of the source of the MPs. Primary MPs tend to have a manufactured shape while secondary MPs have a inhomogeneous appearance [13]. The shape is also affected by the weathering, that can change the aspect of the plastic debris. Crawford et al. [12] defined six different shapes: pellet, microbead, fragment, fibre, film, and foam. Instead, Hartmann et al. [2] selected only four shapes: spheres, fibres, films, and irregular particles. One other important characteristic of plastic debris is colour. MPs can assume a vast variety of colours, which affect the identification and the interaction with the biota [12]. The last one is density, which influences the fate of micro- and nanoplastics in the environment. Density is affected by the plastic type, structure (e.g. the presence of air bubbles), and presence of external material (e.g. fouling). The main aspect that characterises density is the plastic typology. The most common types of MPs are polyethylene, polypropylene, and polystyrene. Since MPs are mainly present in environmental compartments – which are not stable but characterized by currents, forces and environmental factors that affect the buoyancy of the particles – microplastics with a density higher than water can be found on the surface, while debris with a density lower than water can sink due to fouling or interaction with marine aggregates [12].

After having classified the MPs and NPs, it is important to identify their fate and the possible sources. The most studied environmental compartment is water because it is where MPs and NPs mainly merge.

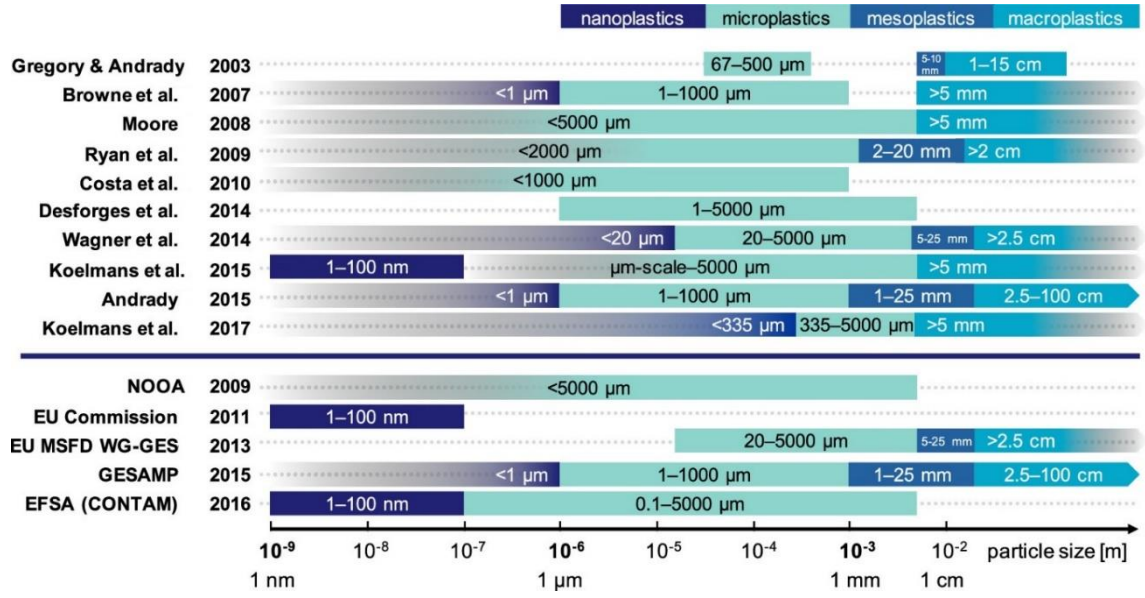


*Figure 0.1 - Different plastic debris categorizations according to size. Them are classified in scientific literature, over the line, and in institutional reports, under the line. Modified from Hartmann [2]*

In particular, the marine environment is the most studied. MPs are detected in many different domains of the marine system, including the garbage patches in the subtropical gyres [14], sandy beaches and sea bottoms. An estimation of the plastic debris mass present on the surface of the world's ocean was performed by Eriksen et al. in 2014. A mass of about 35 450 tonnes of MPs was estimated analysing data collected from 2007 to 2013 [15]. The plastic particles present in saltwater also derive from the confluence of freshwater bodies. Indeed, the concentration of MPs in freshwater is similar to the marine one. MPs are found in lakes, rivers, and estuaries in all the sections: surface, column and sediments [16]. The distribution in freshwater bodies is affected by the characteristics of the MPs. It is also reasonable to assume that MP concentration is directly related to the presence of human activities [16]. As a consequence, the concentration values vary in a wide range, from few particles to thousands of particles for cubic meter [14]. For instance, all the samples collected in the top six larger lakes of Switzerland, contain MPs with an average concentration from 11 000 to 220 000 particles/$km^2$ [17].

The mainly possible sources of MPs and NPs in water bodies can be found in the 2019 report of SAPEA [14]. The sources identified in the report are: city dust, which is generated by the abrasion of tyres; the degradation products of the protective layers of fishing and marine vessels; and the deterioration of lost or discharged fishing gear. Synthetic clothes are another source of plastic debris because they release synthetic fibres due to abrasion during laundry [18]. WWTPs and WTPs are also considered an important source of microplastics, even though they are not a direct cause of MPs and NPs production. The reason lies in the fact that they transport MPs and NPs from their sewers. Their effluent is function of the input concentration and the kind of technologies present into the plants.

The domestic water treated by a WWTP or WTP contains mainly synthetic textile fibres from washing machines, microbeads and secondary plastic particles [19, 20]. Plastic debris are removed efficiently by filtration treatments but in any case a portion is released [21, 22]. It is demonstrated that WWTPs retain 87-99% of the MPs. Even if most of them are found in the sludge that can be used as fertilizer and consequently, MPs potentially achieve the soil [14]. The effluent concentration instead ranges from 10 to $10^7$ particles/$m^3$ [14]. Focusing on the filters, which are present in the WWTPs and in the WTPs and are the subject of this study, the suspicion that filters retain the MPs is not supported by the measure of MPs in the backwash solution [10, 23].

This study is divided into two parts, the first one is a literature analysis of publications regarding microplastics (MPs) and nanoplastics (NPs), while the second one is the study of the NP filtration by water treatment systems.

In PART I Scopus was employed to create a dataset of documents (whose topic is MPs and NPs), which was also used to perform a statistical analysis creating graphs, ranks and categorizations. *SciVal* was used to support the work and to obtain more complex representation of the dataset. The main goal of the first part was to realise the significance of the research on micro- and nanoplastics and consequently of the most studied environmental compartments, subjects and topics that need further investigations. In order to understand which environmental compartments was more investigated, a classification was done focusing the attention on wastewater treatment plants (WWTPs) and water treatment plants (WTPs), which are the topic of the second part of the thesis.

As previously mentioned, in PART II, the study of NP transport in water treatment filters is described. The main goal was to identify the behaviour of NPs in two common filters of water treatment systems: sand filters and activated carbon filters. Once the dynamic was known, it was possible to estimate the filtration efficiencies and consequently evaluate the number of particles that potentially reach the

environment and humans. The study originated from the collaboration of *Eawag* - *Swiss Federal Institute of Aquatic Science and Technology*, which conducted the experimental part of the study, and the *GW* - *Groundwater Engineering Group* of Politecnico di Torino, which was responsible for the data interpretation and modelling.

# PART I

## Literature analysis

A dataset of articles from *Scopus* was created to study the trend of *microplastics* and *nanoplastics* publications and to perform a statistical analysis on them. All the results are referred to 07 July 2020, when the dataset used for the analysis was created. The dataset was defined searching some *keywords* in *Scopus* and applying a filtration and extending procedure to collect the greater number of documents inherent to the topic. Graphs, tables and ranks were created using the information related to the documents, thanks also to the *Analyse search results* tool. Moreover, the dataset was imported in *SciVal,* where a more accurate analysis was performed, and more complex graphs were produced. Since an environmental compartment classification does not exist in *Scopus* or *SciVal* yet, a classification method was developed during the statistical analysis. Similar studies on the matter already exists [24].

Currently, research on MPs and NPs is achieving resounding success, the topic parallels with the global problem of the marine litter. Literature on the matter principally focus on: micro- and nanoplastic composition, sources, fate and measuring methods. The research on the effects of plastic particles on human and animal health is also an important issue studied. It is crucial to understand if MPs and NPs are a threat to the environment and human health.

## 1.1 Dataset definition

The goal was to create a dataset trying to include the highest number of articles regarding the topic, paying attention not to add documents far from the subject. The first step was to research on *Scopus* some keywords to get the set of documents. *Scopus* allows to define the fields of research and keywords were looked for in the *title*, *abstract* and *keywords* of the articles. The keywords were selected to find the highest number of documents and to reduce the probability of losing some of them. The list of words was: *microplastic*, *microplastics*, *nanoplastic*, *nanoplastics*, *micro-plastic*, *micro-plastics*, *nano-plastic*, *nano-plastics*.

Articles, which were not inherent to the topic, were included in the set of documents, regarding stress and deformation of metals for example. The second step of the procedure, to define the MP and NP database, was a filtering process. It was made by three steps: select a fair number of the most cited articles and save their title and source title, define a selection rule, and apply the filtering method to create a subset. In this case of study, the selection rule was that an article is chosen only if it had at least a most cited article into its bibliography, or it was published at least in one of the sources.

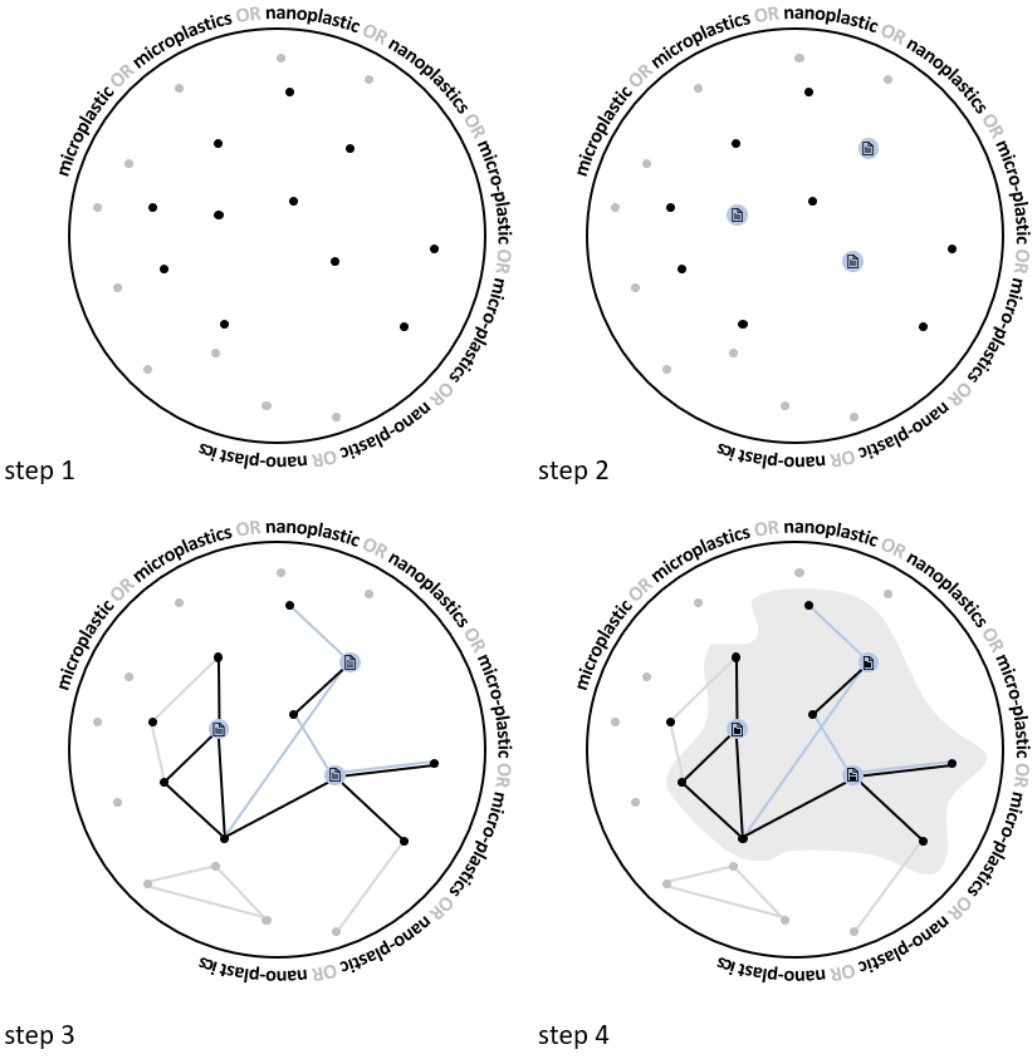


*Figure 1.1 - Visual representation of dataset definition and filtration method: step-1) Research of documents by using keywords; step-2) Select the most cited articles and their source title; step-3) Define a rule of filtering; step-4) Define the sub set of documents.*

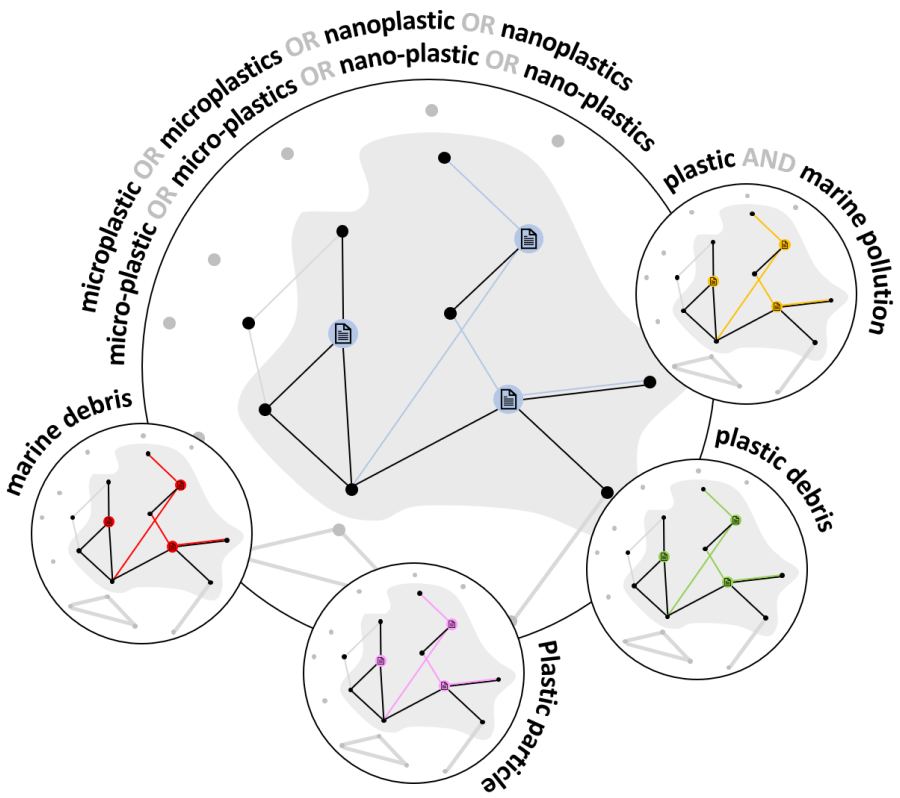


*Figure 1.2 - Dataset extension by adding four groups of articles created from key reference publications.*

A visual representation of the *Scopus* search and filtration are visible in Figure 1.1. In *step-1* the circle represents the set of articles found in which the black or grey dots are the single article. The colour is linked to the inherence, the black ones regard the topic while the grey ones do not. In *step-2* the icons of a document represent the most cited articles and the light blue dot the source where they were published. The graphic representation of the selection rule is in *step-3* where the black line is the link with a most cited document and the light blue one the connection with the source. The grey area in *step-4* is the subset.

Reading articles that regard MPs or NPs, some documents were cited a lot of times but some of them were not included into the dataset. They had not one of the keywords used before to create the set of articles. Mainly these documents were written before the common use of the words *microplastics* and *nanoplastics,* but they are founders of the research argument. Therefore, a methodology to include them was done. Firstly, four articles were selected [3, 4, 25, 26], which were reputed key reference and were not included in the previous dataset. Then a set of keywords, respectively "*plastic particle*", "*marine debris*", "*plastic AND marine pollution*", and "*plastic debris*", were chosen for each article. As in the dataset definition, each group of keywords was researched in the *title*, *abstract* and *keywords*. The articles found were filtered with the same procedure explained before. At the end, the newest datasets were added up to the main one. A schematic representation of the procedure is visible in Figure 1.2.

### 1.1.1 Graphs and results of the dataset

The set of articles obtained after having used the list of keywords, includes 4876 documents. Applying the filtration procedure explained in chapter 1.1 and visible in Figure 1.2, the total decreases to 3501.

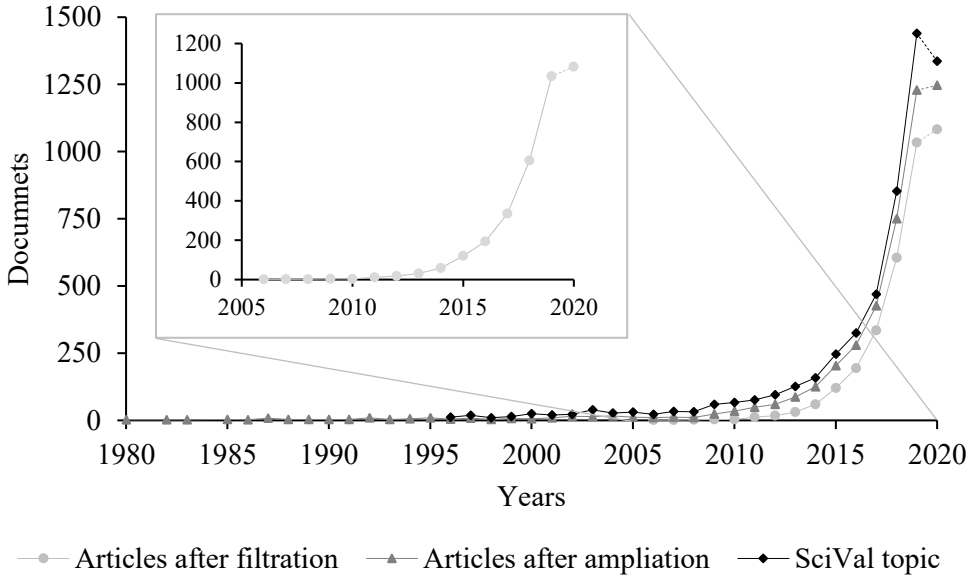


*Figure 1.3 - Comparison of documents publication increasing in time.*

Scrolling the list of articles, any publication is present that is not inherent to the main topic. The older document present in the set was published in 2006, which is around the period of the creation of the term microplastics. A total of 1033 articles were published in 2019. The trend in time of the filtered documents is visible in the zoom of Figure 1.3.

The process of extending whose method is explained in chapter 1.1 allowed simultaneously to increase the number of documents regarding MPs or NPs for each year and to expand the timeline to the period before the creation of the term *microplastics*. As it is possible to see in Figure 1.3 the line of the set of documents after extension is greater than the first explained and it begins in the eighties. The extension generated an increase of 164 publications in 2019.

A good time graph for a comparison is the timeline of the SciVal topic “Microplastic; Marine Debris;

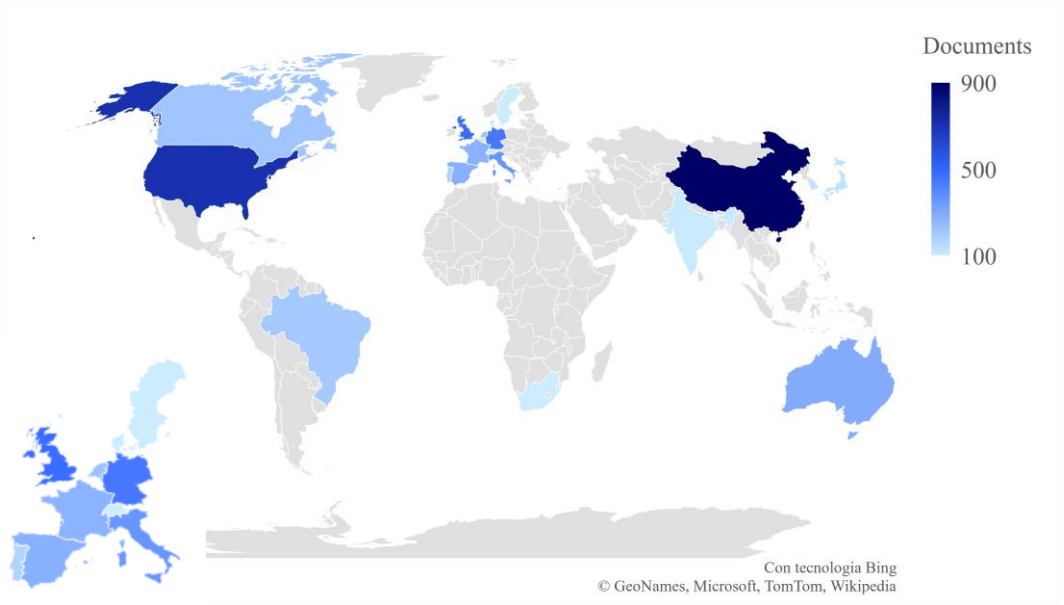


*Figure 1.4 – Distribution of documents by country*

*Table 1.1 - Top twenty World countries and Top twelve European countries*

**WORLD**

| Ranking | Country | n° | Ranking | Country | n° |
|---|---|---|---|---|---|
| 1 | China | 907 | 11 | Brazil | 202 |
| 2 | United States | 709 | 12 | Portugal | 177 |
| 3 | United Kingdom | 483 | 13 | Japan | 131 |
| 4 | Germany | 449 | 14 | South Korea | 130 |
| 5 | Italy | 361 | 15 | Norway | 115 |
| 6 | Australia | 291 | 16 | India | 104 |
| 7 | Spain | 280 | 17 | Denmark | 94 |
| 8 | France | 271 | 18 | South Africa | 91 |
| 9 | Netherlands | 229 | 19 | Sweden | 88 |
| 10 | Canada | 213 | 20 | Switzerland | 80 |

**EUROPE**

| Ranking | Country | n° | Ranking | Country | n° |
|---|---|---|---|---|---|
| 1 | United Kingdom | 483 | 7 | Netherlands | 229 |
| 2 | Germany | 449 | 8 | Portugal | 177 |
| 3 | Italy | 361 | 9 | Norway | 115 |
| 4 | Australia | 291 | 10 | Denmark | 94 |
| 5 | Spain | 280 | 11 | Sweden | 88 |
| 6 | France | 271 | 12 | Switzerland | 80 |

Litter". It starts in 1996 but includes more documents than the ampliated set. The documents counted in 2019 are 1439, 403 more than the filtered set and 242 more than the ampliated one. It is possible to see in Figure 1.3 that the trend is the same for all three, an exponential increase.

From the *analyse search results* tool of *Scopus* it is possible to visualize, elaborate and download some graphs. The data used come from the filtered and extended set of articles. The most interesting classifications that were selected are showed in this study. The top twenty countries, which are producing articles about MP and NP are highlighted in blue in Figure 1.4. The podium is composed in order of China, United States and United Kingdom. Italy is fifth with 361 documents produced. In the corner of Figure 1.4, a zoom on Europe was done to better read the chart. To support the world map chart, the number of documents published from the top twenty countries is visible in Table 1.1. In the same table is also present the Europe rank. Twelve of the top twenty countries are European.

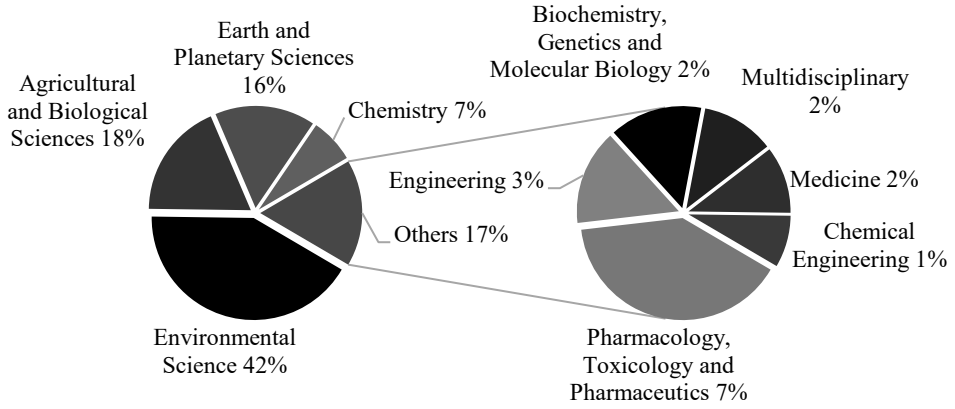


*Figure 1.5 - Distribution of documents by subject area*

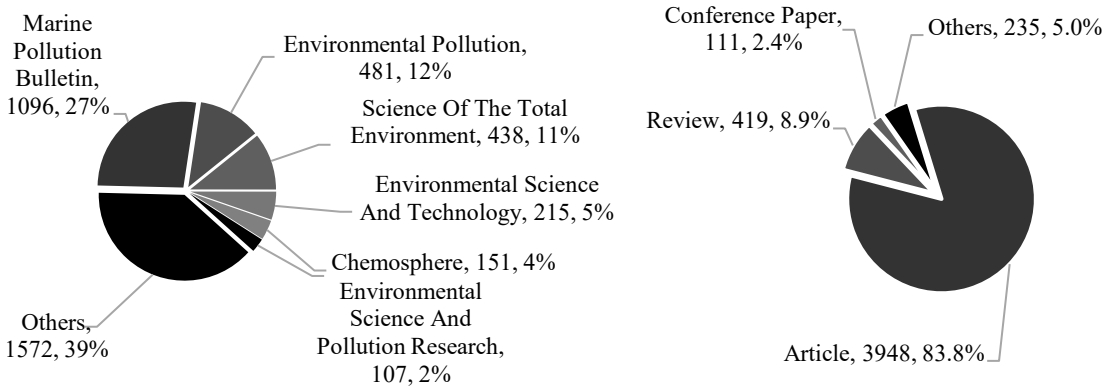


*Figure 1.6 - Top sources and documents' type*

Another graph obtained from *Scopus* is the distribution of documents by subject area. The top ten subject areas were selected to generate the pie chart of Figure 1.5. As can be seen from the graph, the most developed sector regarding the studied topic is *Environmental Science,* followed by *Agricultural and Biological Sciences,* and *Earth and Planetary Sciences*, respectively. A substantial cut of the pie chart is also referred to *Chemistry* and *Pharmacology, Toxicology and Pharmaceutics*.

Therefore, an import aspect is the type of publication that is published regarding MPs and NPs. Related to the kind of documents, the top source can be showed. In the two pie charts of Figure 1.6 the percentages and the number of documents published are readable for the most specialized sources and the usual type of articles. *Marine Pollution Bulletin* with 1096 documents is the source with the highest number of publications. Three of the most cited publications, visible in Table 1.2, are published in the mentioned source. The greater pie's cut of documents are articles with a percentage of 83.8%.

At the end, the analysis of the most cited articles and the top authors classified regards to the number of publications was done. As can be seen in Figure 1.7 the podium is made by *Thompson*, *Koelmans* and *Shi* with respectively 65, 53 and 52 documents published. The country of the affiliation can be read over the bar. In Table 1.2 the list of the top ten articles for citations is visible with the main details: *First Authors*, *Title*, *Year, Source Title* and *Type*. As it was possible to imagine, most of the characteristics of Figure 1.7 and Table 1.2 reflect the behaviour of the previous graphs and tables.

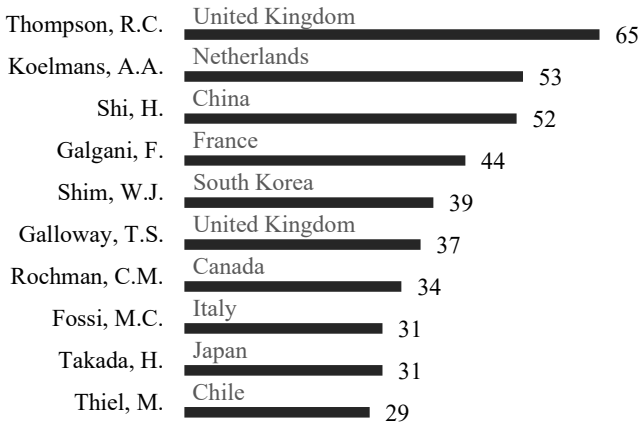


*Figure 1.7 - Top ten authors for number of publications regarding* microplastics *and* nanoplastics

*Table 1.2 - Top ten documents for number of citations regarding* microplastics *and* nanoplastics

| | First Author | Title | Source title | Year | Citations | Type |
|---|---|---|---|---|---|---|
| [27] | Jambeck | Plastic waste inputs from land into the ocean | Science | 2015 | 2072 | Article |
| [28] | Andrady | Microplastics in the marine environment | Marine Pollution Bulletin | 2011 | 1642 | Review |
| [29] | Barnes | Accumulation and fragmentation of plastic debris in global environments | Philosophical Transactions of the Royal Society B: Biological Sciences | 2009 | 1622 | Article |
| [25] | Derraik | The pollution of the marine environment by plastic debris: A review | Marine Pollution Bulletin | 2002 | 1518 | Review |
| [3] | Thompson | Lost at Sea: Where Is All the Plastic? | Science | 2004 | 1406 | Article |
| [13] | Cole | Microplastics as contaminants in the marine environment: A review | Marine Pollution Bulletin | 2011 | 1319 | Review |
| [18] | Browne | Accumulation of microplastic on shorelines worldwide: Sources and sinks | Environmental Science and Technology | 2011 | 1160 | Article |
| [15] | Eriksen | Plastic Pollution in the World's Oceans: More than 5 Trillion Plastic Pieces Weighing over 250,000 Tons Afloat at Sea | PLoS ONE | 2014 | 1141 | Article |
| [30] | Wright | The physical impacts of microplastics on marine organisms: a review. | Environmental pollution (Barking, Essex: 1987) | 2013 | 1098 | Review |
| [31] | Hidalgo-Ruz | Microplastics in the marine environment: A review of the methods used for identification and quantification | Environmental Science and Technology | 2012 | 1086 | Article |

### 1.1.2 *SciVal* graphs

A representative graph that can be taken from SciVal is visible in Figure 1.8. The documents of the dataset are classified with SciVal topics. Each topic is represented by a bubble. Those are into a wheel of subject areas. The bubble diameter is related to the number of articles inherent to the topic while the distance from the middle of the graph represent the relation with ASJC. ASJC, *All Science Journal Classification*, is a method used in *Scopus* and *SciVal* to classify the documents based on their sources. The more influence an ASJC has over a topic, the closer it will bring the topic to its side of the wheel of science. As a result, the topics closer to the centre of the wheel are more likely to be multidisciplinary, compared to the topics towards the edge of the wheel.

As can be seen the biggest bubble is the green one in the bottom right corner, which topic is "*Microplastic; Marine Debris; Litter*". This graph demonstrates that the dataset created is made by documents, which are for the most part regard to the topic of MPs and NPs. Most of the bubbles are near the wheel where the more influence ASJC are *Engineering*, *Energy*, *Environmental Science*, *Earth* and *Planetary Sciences*, *Agricultural* and *Biological Sciences*, *Biochemistry Genetics,* and *Molecular Biology*.

## 1.2 Environmental compartments classification

*Scopus* or *SciVal* do not have the possibility to classify the articles basing on the environmental matrix where MPs or NPs potentially are present. To obtain a classification based on the pollutant fate, a simple method was developed.

At the beginning was necessary to design the classification choosing the environmental compartments that are inherent to the study. As can be seen in Figure 1.9 the chosen sectors for this analysis are: *air,*

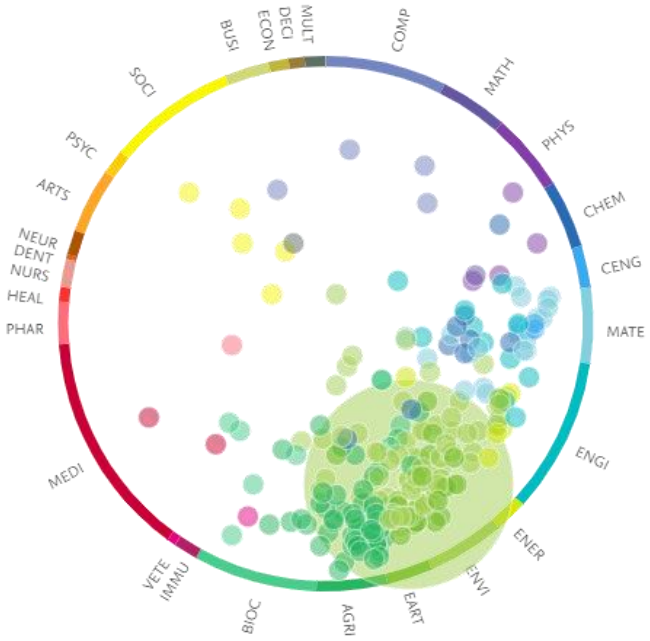


*Figure 1.8 - Bubble graph of documents classified with SciVal topics*

*COMP - Computer Science, MATH – Mathematics, PHYS - Physics and Astronomy, CHEM – Chemistry, CENG - Chemical Engineering, MATE - Materials Science, ENGI – Engineering, ENER – Energy, ENVI - Environmental Science, EART - Earth and Planetary Sciences, AGRI - Agricultural and Biological Sciences, BIOC - Biochemistry, Genetics and Molecular Biology, IMMU - Immunology and Microbiology, VETE – Veterinary, MEDI – Medicine, PHAR - Pharmacology, Toxicology and Pharmaceutics, HEAL - Health Professions, NURS – Nursing, DENT – Dentistry, NEUR – Neuroscience, ARTS - Arts and Humanities, PSYC – Psychology, SOCI - Social Sciences, BUSI - Business, Management and Accounting, ECON - Economics, Econometrics and Finance, DECI - Decision Sciences, MULT - Multidisciplinary*

*wastewater, saltwater, fresh water, groundwater, soil, biota*. For each environmental sector, a list of keywords was established with the goal to find them in the title of the articles. They were selected after an attention reading of the list of documents present in the dataset generated. They must be selected carefully because they must be representative of the main sector. They must not be repeated in different environmental compartments not to generate ambiguity. In Figure 1.9 it is possible to see the lists for every sector. When the keywords were defined, it was necessary to verify in which article title was present one or more keywords. So, it is possible to know how many articles have in the title one of the keywords and consequently a possible relation with the environmental compartment. In one title more keywords can be found and therefore, a document can be classified in more environmental sector. Only documents in which at most two keywords are present in the title were chosen to simplify the statistical analysis. The results of the previous point can be elaborated to obtain some statistical relation.

The number of articles that have these characteristics are: 3014. The result obtained follows the procedure explained before and it is visible in Figure 1.9. In the table it is readable the number of documents in which the keywords, assembled in the environmental compartment, are present in the title. Some of them have only keyword regarding one theme and the values are in the diagonal of the table. As can be seen from the table the most studied environmental compartment is salt water with 1207 documents. It has also a lot of intersection with other environmental compartments as: *soil*, *animal,* and *human*. The lowest sectors are *air* and *ground water*. The total number of articles regarding one environmental compartment is obtained by summing the values present in its column and row. In Figure 1.9 the totals are represented by a pie chart that confirms that salt water is the most studied field regarding micro- and nanoplastics.

## 1.3 Conclusions

In the last decade, the increasing interest of the scientific and public authorities on MPs and NPs has caused an exponential growth of scientific research. Considering the *SciVal* curve, (Figure 1.3), 1439 documents were published in 2019 with an increase of the 69% compared to 2018 and of the 207% compared to 2017. The study of MPs and NPs is continued by the most developed countries, but also by countries inspecting the seas and oceans. The podium, for number of documents, is occupied by China, USA and UK with respectively 907, 709 and 483 publications. Europe plays an important role in the research on MPs and NPs so much that twelve of the top twenty countries are Europeans. The European podium is occupied by UK, Germany and Italy with a total of 483, 449 and 361 documents respectively. MPs and NPs are studied mainly to define sources, fates and concentrations. Indeed, the percentage of documents regarding *Environmental Science* is 42%, *Agricultural and Biological Sciences* 18% and *Earth and Planetary Sciences* 16%. A substantial cut of the pie chart is also referred

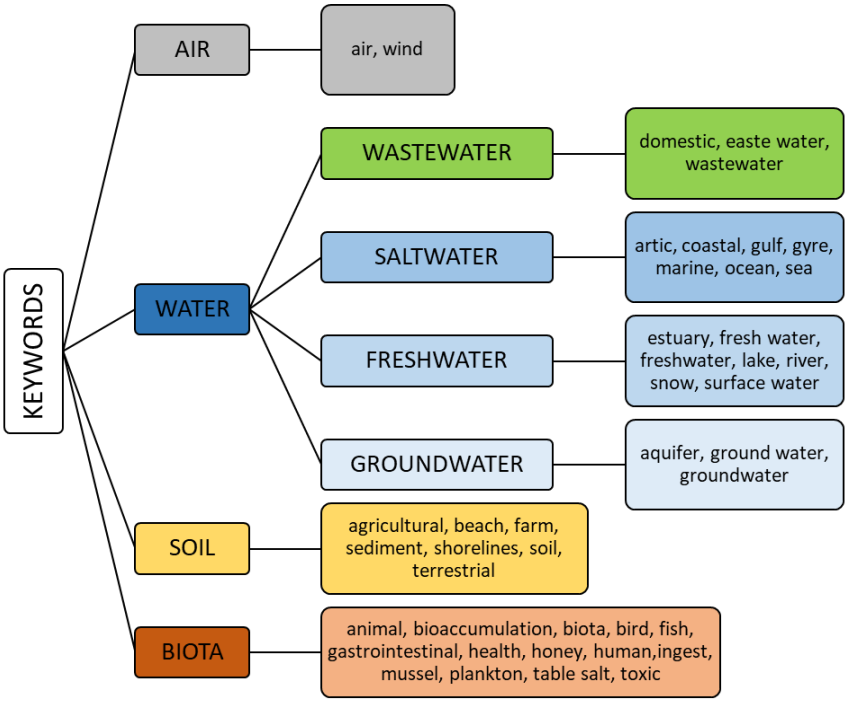


| | AIR | WASTEWATER | SALT WATER | FRESH WATER | GROUND WATER | SOIL | BIOTA |
|---|---|---|---|---|---|---|---|
| AIR | 23 | | | | | | |
| WASTEWATER | 0 | 83 | | | | | |
| SALT WATER | 12 | 14 | 1207 | | | | |
| FRESH WATER | 3 | 8 | 63 | 203 | | | |
| GROUND WATER | 0 | 0 | 1 | 0 | 3 | | |
| SOIL | 1 | 1 | 188 | 43 | 0 | 337 | |
| BIOTA | 7 | 3 | 257 | 26 | 0 | 28 | 503 |

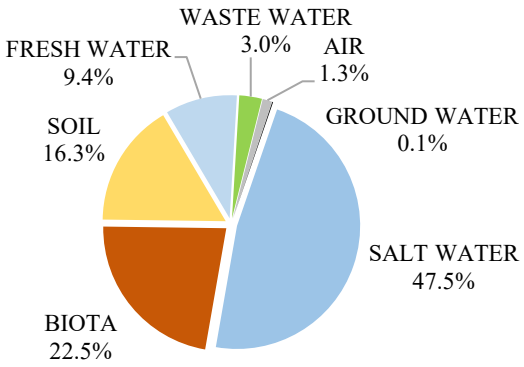


*Figure 1.9 - Documents distribution and intersections by environmental compartments*

to *Chemistry* and *Pharmacology, Toxicology and Pharmaceutics,* both of which have the 7%. The last two field of research study the composition of MPs and NPs and the possible impacts on human health and environment. From the environmental compartment classification is possible to confirm that saltwater is the most studied environmental compartment with 1742 documents that correspond to the 47.5%. the second compartment is, Biota with the 22.5% and the third is Soil with the 16.3%.

Wastewater, which is of interest for the topic of the thesis, is cited in about 109 documents. As explained in the introduction, WWTPs and WTPs are considered one of the main sources of MPs and NPs in the environment because they have to treat sewages in which the concentration of primary plastic particles can be relevant. However, WWTPs and WTPs are not well studied yet, even if they are crucial for the safeguard of humanity and environment. The lack of documents inherent to the water treatment was discovered thanks to the literature analysis, in particular the environmental compartment classification, which was developed in this thesis. A specific classification is crucial to identify the highest or lowest studied compartments and to establish the direction of the further scientific research.

# PART II

# Nanoplastic filtration in water treatment systems

The study of the transport of NPs in filter media originated from the collaboration between *Eawag* and the *Groundwater Engineering Group*. Synthetic nanoplastics were designed to study their transport through two filters, a sand one and an activated carbon one, of a WTP, which treats the water of the Zürich Lake. At the beginning, the physical and chemical characteristics of the materials (NP particles, lake water, sand and activated carbon) were measured. The results were used to support the next experiments and their interpretation. The second step was to perform the column tests to simulate the NP flow through the filters at different conditions. The column tests included two passages: the tracer test to identify the hydraulic characteristics, and the particle test to identify the interaction mechanism and the attachment/detachment parameters. The experimental curves were elaborated and analysed with the help of MNMs, which estimated the necessary parameters. To better understand the program outputs, a brief theoretical base is added to this chapter to describe the equations that are present in the software. The results of the column tests were exploited to create a model to simulate the transport in pilot-scale filters. The simulation was necessary to design the pilot-scale experiment. Once the pilot experiments were designed and completed, the experimental data were compared with the simulation in order to refine and recalibrate the model. At the end, the main properties of the transport of NPs in granular media filter were defined, and an estimation of the efficiencies was carried out. In conclusion, to better describe the fate of the plastic particles in the water treatment plant, the graphs of efficiency in function of time were created.

## 2.1 Materials

In this chapter all the main material is presented, the plastic nanoparticles and two different filter media. A general description is present with their main chemical and physical characteristics. They were used for the experiments in the laboratory of *Eawag* and the results were elaborated to understand the interaction mechanism between particles and filters.

### 2.1.1 Particles

NPs are suspected to be present in the environment, but analytical measuring methods are complicated. Laboratory experiments can help to identify the behaviour of them in the environment. In the *Eawag* laboratory synthetic nanoplastics were designed and made [32].

Nanoplastics are made by a core of polyacrylonitrile (PAN) containing the metal tracer Figure 2.1(b), palladium, and covered by the addition of a crosslinked polystyrene shell Figure 2.1(c). The acrylonitrile is capable to complex the *Pd* in the water phase while the core-shell structure reduces the metal leaching to a minimum [32]. The most used particles during the experiments inherent to this study has a raspberry shell Figure 2.1(a).

The palladium doped core allows to measure the particle concentration using an ICP-MS thanks to the linear correlation between *Pd* concentration and number of particle concentration, Figure 2.2. The detection limit in terms of *Pd* is of 0.005 µg/L, which is about $9.8 \cdot 10^8$ particles per litre [32]. From the Figure 2.2 a relation coefficient between palladium and particle concentration was extrapolated. It was assumed equal to the slope of straight line passing through the experimental points. The conversion factor obtained is approximately $2.0 \cdot 10^{11}$ particles/µg. Instead, from experimental data obtained during the test in the laboratory, a conversion factor of $4.0 \cdot 10^{11}$ particles/µg was found. The last one value was used for all the study as conversion factor between palladium concentration to particle one.

Synthetic NPs with a raspberry shell have an average diameter of 190 nm. The diameter was measured by DLS and the values can find in the supplementary material of Mitrano article [32]. The density of 1140 kg/m$^3$ was estimated by *Eawag.* knowing the particle structure.

A conversion factor to convert particle concentration in mass concentration is necessary for a correct use of the software MNMs. It is possible to estimate the conversion factor knowing the particle average density and assuming that the nanoparticles are homogeneous spheres. The mass of a particle proves to be $4.1 \cdot 10^{-18}$ kg and consequently the conversion factor. From experimental data the conversion factor is slightly different. It is equal to $1.0 \cdot 10^{-18}$ kg/particle. The last one value was used for all the study as conversion factor between particle concentration to mass one.

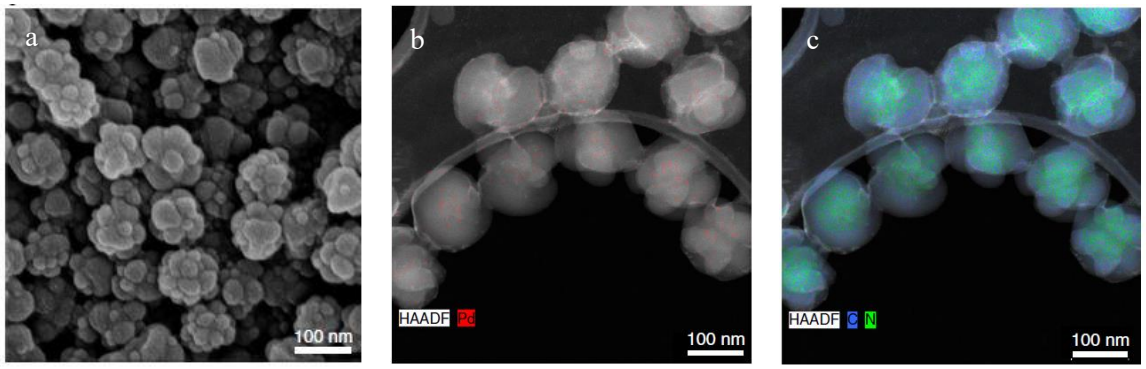


*Figure 2.1 – Synthetic nanoplastics details: a) final core-shell particles with a raspberry shell, b)* Pd *distribution in the particle core, c) core-shell structure with more PAN nitrogen in the core and PS carbon in the shell. Modified from Mitrano [32]*

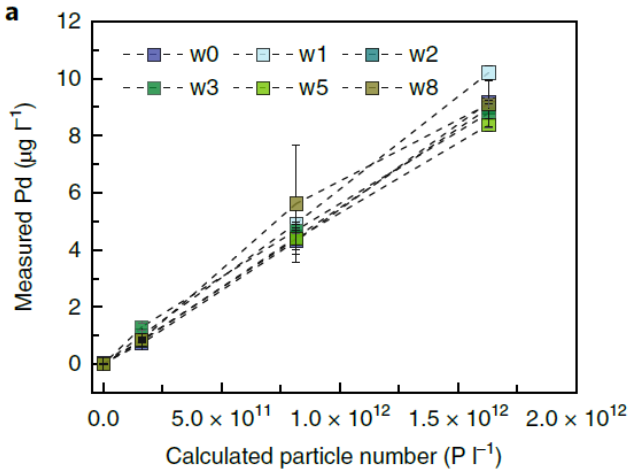


*Figure 2.2 – Linear relation of* Pd *concentration and particle concentration. Modified from Mitrano [32].*

### 2.1.2 Filters' media

Two different filter media were used: sand and activated carbon. The filters' media were chosen to reflect the most used filtering material in a water treatment plant. Grain diameter and density were not measured experimentally but found in literature. In Table 2.1 it is possible to see their values.

*Table 2.1 - Filters' media main literature parameters*

| Filters' media | Density (kg/m$^3$) | Grain diameter (µm) |
|---|---|---|
| Sand | 2650 | 450 |
| Activated carbon | 448.5 | 1050 |

Granular media filtration is used in water and wastewater treatment plant. In the first case filtration is necessary for aesthetic and public health reasons while, in the second case, it reduces particles and biochemical oxygen demand [33].

The historic filtration method is called "slow" filtration and it is still used thank to its simplicity of

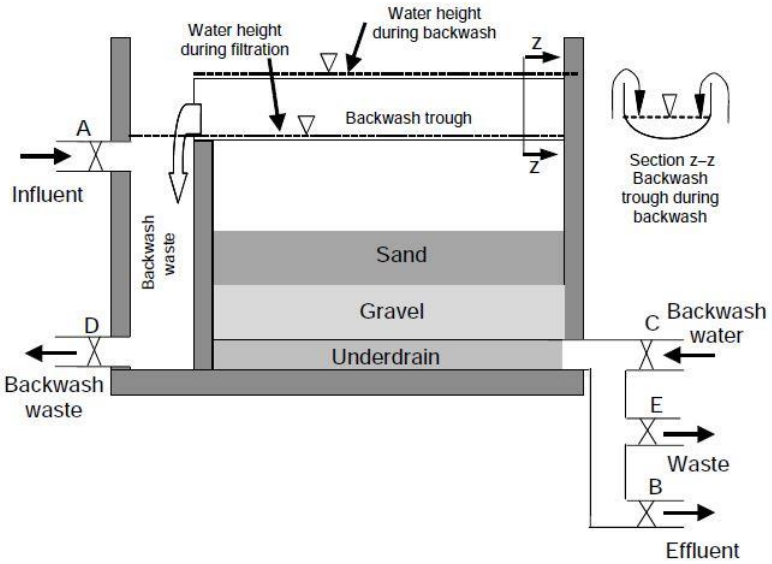


*Figure 2.3 - Schematic diagram of a gravity-driven granular media filter. Modified from Benjamin [33].*

maintenance and use. A biologically active layer grows up above the media and reduces the organic load. Furthermore, the granular media captures particles thanks to their deposition on the filter media. The difference between slow and rapid filtration is the biological active layer, which is less important. Granular activated carbon is now frequently used as a filter media because it allows adsorption of various soluble contaminants to occur in the same treatment unit as particle removal [33].

A granular media filter has two modes of operation: filtration and backwashing. Sand, activated carbon, or other media are supported usually by a gravel layer in a gravity filter. Water flows through the filter until a maximum head loss or a maximum allowable concentration are reached. When one of the maximum allowable conditions is exceeded a backwashing of the filter is necessary. The backwash water flows upstream, it has a flow higher than the filtered one to fluidize the granular media to get a better wash of grains [33]. The removal mechanism of particles in a granular media filter is described in the chapter 2.1.4.1.

### 2.1.3 Carrier fluid

The goal of the study is to describe the transport of NPs in different filter, which are usually present in a WTP or in a WWTP. The experiments, which were done by *Eawag*, were executed with water coming from the Lake Zürich because usually treated by the federal institute in a WTP. The particles behaviour is also affected by the kind of water and so is useful to illustrate some water characteristics. One of the main parameters is the water salinity. In Table 2.2 is possible to see the main ions, which are present in Lake Zürich water.

*Table 2.2 – Lake Zürich water ions analysis from Eawag*

| DOC | $N\text{-}NH_4^+$ | $CL^-$ | $N\text{-}NO_2^-$ | $N\text{-}NO_3^-$ | $P\text{-}PO_4^-$ | $SO_4^{2-}$ | $Na^+$ | $K^+$ | $Ca^{2+}$ | $Mg^{2+}$ | Alkalinity |
|---|---|---|---|---|---|---|---|---|---|---|---|
| mg/L | mg/L | mg/L | mg/L | mg/L | mg/L | mg/L | mg/L | mg/L | mg/L | mg/L | Mmol $HCO_3$/L |
| 1.67 | 0.03 | 4.90 | <0.20 | 0.54 | <0.20 | 12.55 | 4.45 | 1.13 | 48.75 | 6.18 | 3.48 |

Some experiments were done also with deionized water because it was deemed necessary during the experimental phase to compare two different waters.

### 2.1.4 Software

The design of a pilot-scale experiment or the study of NPs behaviour in a filter media require both the support of mathematical tools. They are necessary to analyse the experimental data and extrapolate information, which are necessary to understand the particle-collector interaction mechanism. Also, they are useful to predict the particle behaviour in different systems and support the design of a pilot-scale experiment or real filtering system. Mathematical tools allow to estimate parameters or to estimate the distribution of particles in space and time. The software used in this study is MNMs 2018 developed by Bianco [34] member of the *Groundwater Engineering Group* of *Politecnico di Torino*.

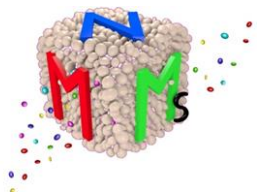

*"MNMs, which stands for Micro- and Nano-particles transport, filtration and clogging Model Suite, is a modelling tool developed in a Matlab environment for the analysis of laboratory column transport tests (1D Cartesian domains) and for the preliminary design of pilot-scale particle injections in a single well (1D radial domains)"* [34].

MNMs 2018 v. 3.017 has different available tools but only those used are described in the following list and then their equations are presented in the following chapters.

- Calculation of particle-particle and particle-collector interaction energy profiles using the

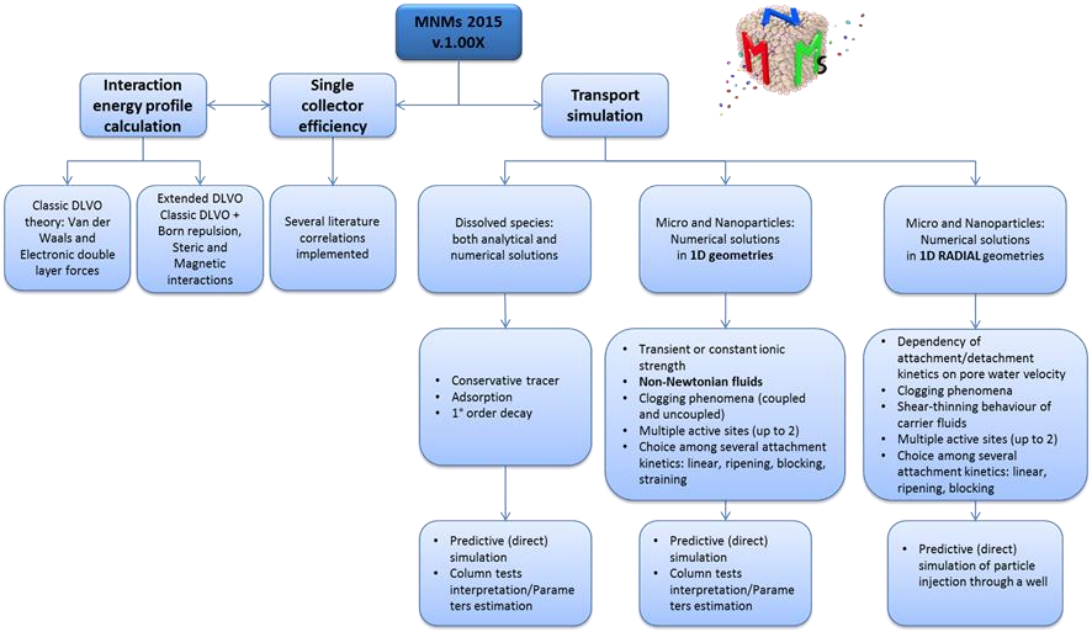


*Figure 2.4 – List of tools included in MNMS 2018. Modified from Bianco [34].*

DLVO theory. This tool is useful to foresee the particle behaviour in terms of aggregation and attachment on collector.

- Calculation of single-collector efficiency. MNMs allows to estimate the single-collector efficiency profile in function of the particle diameter using several correlations from literature. The efficiency can be estimated using the fluid shell or the collector radius.
- Simulation of the transport in 1D saturated porous media of conservative solutes. Numerical and analytical solutions are available. The analytical solution was used to estimate porosity and dispersivity form the column tracer tests.
- Simulation of the transport of colloidal particles in 1D saturated porous media. The tool allows to estimate the interaction parameters from experimental data or to simulate the behaviour of particles in a system. It is possible to simulate two concurrent interaction sites, which can be reversible or irreversible and follow linear, blocking, ripening, or straining kinetics. This tool was used to estimate interaction parameters from the particle column test ant to simulate the pilot-scale test to design the experiment.

All the tools included in MNMs 2018 are visible in the scheme of Figure 2.4.

### 2.1.4.1 Nanoparticles and porous media interaction in MNMs

In this chapter the theory of the behaviour of particles in a porous media is presented. It is mainly focused on what was used during the study of the NPs into the filters and what is implemented in MNMs.

The theory starts from the DLVO theory that explain the interaction between particles and other particle or the porous media. This section allows to understand the particle-particle or particle-collector interaction forces. The DLVO analysis is crucial to select the best interaction mechanism and model. Then, it is described the single collector contact efficiency that identifies the number of collisions between colloids and collector. The result can be added to the DLVO results to refine the model and mechanism selection. Both are crucial to better understand the behaviour of particles into a porous media. In the last section of the chapter the equations representing the particle transport in a porous media are discussed. In the first part, a general description of the equations is presented while in the second one a the description of the interaction mechanism. All the mechanisms are presented and, using

the information obtained from a DLVO analysis and single collector efficiency, it is possible to select the most appropriate to the studied problem.

#### 2.1.4.1.1 DLVO theory

The behaviour of nanoparticles into a porous media is affected directly or indirectly by the interaction forces between surfaces [35]. The main forces acting are the result of several contributions, mainly the electrostatic, Van der Waals, Born and steric forces [36]. The classical DLVO theory (*Derjaguin-Landau-Verwey-Overbeek*) describes the interaction potential between two charged surfaces. It takes in account only the Van der Waals attraction and electrostatic repulsion. In this way particle-particle and particle-collector forces can be described mathematically. It is based on the superposition principle of forces [35]:

$$V_T = V_{VdW} + V_{EDL} \tag{2.1}$$

where $V$ indicates the potential energy expressed in joule. Positive potential energy profile is considered repulsive by convection while negative one is associated to attraction.

To obtain the energy profiles some assumptions are necessary. The colloids are supposed to be uniform spheres so small that porous media grains can be assumed as plates. This is necessary to estimate the particle-plate interaction. The particle-particle interaction is assumed to be half the particle-plate interaction [35].

Three different energy profiles can be analysed to explain the classic DLVO theory, one completely repulsive, Figure 2.5(a), one completely attractive, Figure 2.5(c), and one between the two extreme cases, Figure 2.5(b). In the first case the potential energy profile is mainly positive and consequently an attachment between particles and porous media is unfavourable. The same for the particle-particle interaction. The second extreme case presents a potential energy profile completely negative and consequently a favourable deposition. Summing up in the first case the electrostatic repulsion predominates over Van der Waals forces while in the second case the opposite happens. The intermediate profile can have a primary and a secondary minimum. In this case a reversible and an irreversible deposition can occur. The attachment is maybe irreversible if the particle succeeds to overcome the energy barrier and fall in the primary minimum. Instead, a reversible attachment is likely to occur when the colloid reaches the secondary minimum.

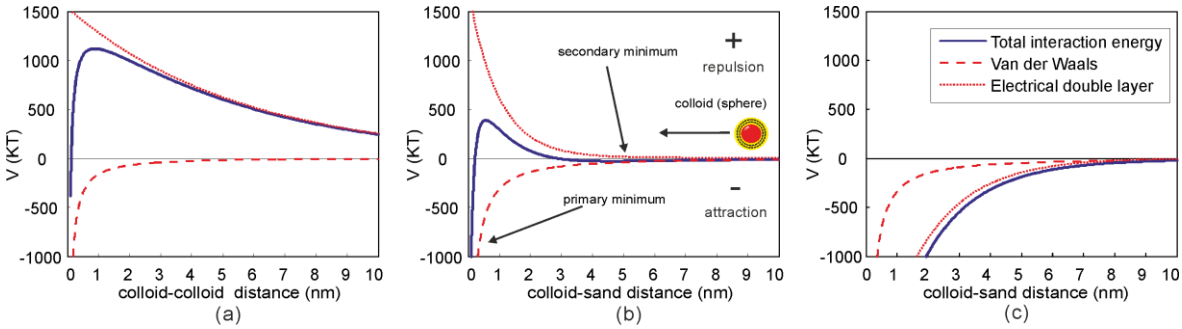


*Figure 2.5 – Interaction energy profile: a) strongly unfavourable deposition with repulsive energy profiles b) unfavourable deposition condition with a barrier to particle attachment c) favourable deposition conditions with attractive profile. Modified from Bianco [34]*

#### 2.1.4.1.1.1 Van der Waals interaction

Van der Walls potential energy profile is often calculated with the equation of Gregory [37]:

$$V_{VdW} = -\frac{H\, d_p}{6h\left(1+\frac{14h}{\lambda}\right)} \tag{2.2}$$

where $H$ is the global Hamaker constant of the system, $d_p$ is the diameter of the sphere, $h$ is the distance between the two surfaces and $\lambda$ is the characteristic wavelength of the interaction. $\lambda$ is usually assumed equal to 100 nm from the literature and also in this study it was assumed equal to this value. Gregory formulation is valid at a separation distance lower than 0.1 times the sphere diameter and for a single species of mono-valent electrolyte.

The global Hamaker constant of the system is obtained as combination of the Hamaker constants of both surfaces and the interposed medium [35, 38], Figure 2.6.

$$H \approx \left(\sqrt{H_{11}}-\sqrt{H_{33}}\right)\left(\sqrt{H_{22}}-\sqrt{H_{33}}\right) \tag{2.3}$$

#### 2.1.4.1.1.2 Electrostatic interaction

In literature different relations to estimate the electrostatic energy profile are present. Each equation is based on specific assumption and is valid a specific range of parameters. For simplicity only one equation is reported in this study.

The equation, proposed by Gregory [39], for the calculation of the electrostatic energy profile based on the linear superposition approximation is:

$$V_{EDL} = \frac{32\pi d_p \zeta}{\left(\frac{KT}{ze}\right)^2}\tanh\left(\frac{ze\phi_1}{4KT}\right)\tanh\left(\frac{ze\phi_2}{4KT}\right)\exp(-2kh) \tag{2.4}$$

where $\phi_1$ and $\phi_2$ are respectively the surface potentials of the colloid and collector, $\zeta$ is the dielectric constant of the medium, $K$ is the Boltzmann constant, $T$ is the absolute temperature, $z$ is the valence, $e$ is the electron charge, $h$ is the distance between surfaces and $k$ is the Debye-Huckel reciprocal length. The Debye-Huckel [35] is estimated as:

$$k = \sqrt{\frac{e^2 \sum_i n_{i,0} z_i^2}{\epsilon\epsilon_0 k}} \tag{2.5}$$

where $n_{i,0}$ is the bulk number concentration of ions of the i-th type and $z_i$ is the valence of the i-th ions.

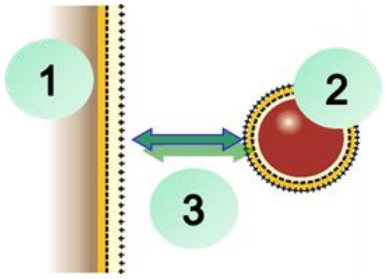


*Figure 2.6 – Conceptual model for global Hamaker constant: 1) porous media surface 2) particle surface 3) carrier fluid. Modified from Bianco [34]*

The linear superposition approximation is valid for $\phi_1 \cong \phi_2 < 60\ mV$, $k \cdot d_c > 5$ and $h \ll d_c$.

#### 2.1.4.1.2 Single collector efficiency

The deposition of particles on the porous media is made by two steps: the transport of particles from the pore fluid to the collector surface and the attachment of these particles due to the particle-collector interaction [40]. The second step is described in chapter 2.1.4.1.1, DLVO theory.

The first step is described by the single collector contact efficiency, $\eta_0$, that define the portion of particles that might touch the collector. The particles can reach the collector surface due to three mechanisms [41]: gravitational sedimentation, interception and Brownian diffusion. They are represented respectively in Figure 2.7. *Gravitational sedimentation* might happen when particles have a density higher than carrier fluid; *interception* might happen when the particle radius is higher than the distance between collector and streamline; *Brownian diffusion* is affected by temperature and particles move randomly around the streamline [34]. The single collector contact efficiency is affected by the physical and chemical characteristics of the particles (size, density, surface chemistry, temperature) and of the collector (size, porosity). The carrier fluid also affects the single collector contact efficiency with its approach velocity. In general, deposition due gravity and interception increases with increasing the size of suspended particles, while diffusion increases with the decrease of particle size [34].

The second step of deposition, called attachment, is controlled by interaction forces described by DLVO theory. The attachment efficiency, $\alpha$, describes the quantity of particles that attach on the collector with respect to the total number of collisions taking place, $\eta_0$. The product of the attachment efficiency, $\alpha$, and the single collector contact efficiency, $\eta_0$, is the single collector removal efficiency [35]:

$$\eta = \alpha \cdot \eta_0 \tag{2.6}$$

Therefore, if the interaction energy profile is completely attractive, Figure 2.5(c), the attachment efficiency, $\alpha$, can be considered equal to one and the single collector removal efficiency, $\eta$, is controlled only by the single collector contact efficiency, $\eta_0$. On the contrary, if the interaction energy profile is completely or partial repulsive, respectively Figure 2.5(a-b), the attachment efficiency must not considered equal to one. In this case the deposition might be due to the surface roughness, charge heterogeneity or retention in the secondary minimum. The attachment efficiency is therefore lower than

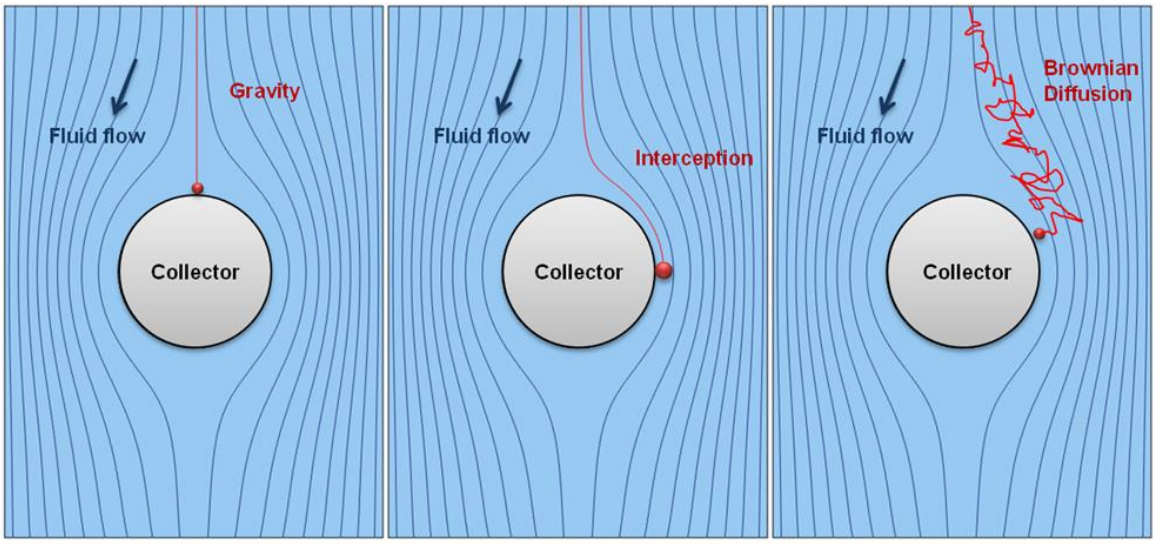


*Figure 2.7 – Particle deposition mechanisms. Modified from Messina [41].*

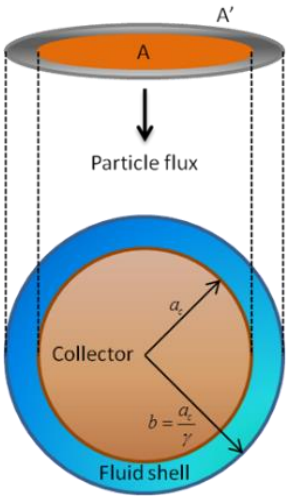


*Figure 2.8 - Schematic representation of the Happel's model. Modified from Messina [41].*

one and the single collector removal efficiency, $\eta$, is limited by the attachment efficiency, $\alpha$ [34].

While the attachment efficiency can be deduced by the interaction energy profile obtained experimentally, a lot of equation were proposed for $\eta_0$ estimation. The simplest one was formulated by Yao et al. [42] for a single sphere in an infinite fluid domain. It is defined as the ratio between the number of particles that reach the collector, $I_S$, and the number of particles entering for advection through an area equal to the projection of the collector:

$$\eta_0 = \frac{I_S}{UC_0(\pi a_c^2)} = \eta_I + \eta_D + \eta_G = \frac{3}{2}\left(\frac{a_p}{a_c}\right)^2 + 4.04\left(\frac{2a_cU}{D}\right)^{-\frac{2}{3}} + \frac{V_s}{U} \tag{2.7}$$

where $U$ is the approach velocity, $C_0$ is the influent particle concentration, $a_c$ and $a_p$ are respectively the collector and particle radius, $D$ is the diffusion coefficient, and $V_S$ is Stokes particle settling velocity. The single collector removal efficiency is composed of three terms, respectively the efficiency due to interception, $\eta_I$, diffusion, $\eta_D$,and gravity, $\eta_G$. However, for very small or very big particle size and very low fluid velocity, Yao's approach fails. In such extreme conditions, it predicts efficiency values larger than one, lacking of any physical meaning [34]. More single collector contact efficiency equations exist that are been developed in time that are going to be used in this study. For simplicity, their equations are not reported.

To take in account the presence of multiple collectors or the porosity a different model is used. The Happel's model. It takes into account not only the particles coming from the collector projection but from the fluid shell projection [41]. A schematic representation is visible in Figure 2.8 and the single collector contact efficiency equations commonly used is:

$$\eta_{0,\gamma} = \frac{I_S}{UC_0(\pi b^2)} = \gamma^2 \frac{I_S}{UC_0(\pi a_c^2)} = \gamma^2 \eta_0 \tag{2.8}$$

where $b$ is the fluid shell radius and $\gamma$ is a porosity dependent parameter defined as $\gamma = (1-\epsilon)^{\frac{1}{3}}$.

#### 2.1.4.1.3 Nanoparticles transport in porous media

The behaviour of micro- and nanoparticles in a saturated porous media is described by a modified advection-dispersion equation. It describes the dual-phase, non-equilibrium interaction between liquid and solid phase due to the physical and physic-chemical interactions [43, 44]. The solid matrix can be heterogenous regarding the affinity with particles of the carrier fluid. More than one interaction site must be considered in this case and a number of equations, equal to the number of interaction sites, is necessary. The particle concentration, $S$, deposited on the porous media is equal to the sum of the i-th concentration, $S_i$, deposited in each site. Advection-dispersion equation in a 1D isotropic system can be written as:

$$\begin{cases} \frac{\partial}{\partial t}(\epsilon C) + \sum_i (\rho_b S_i) + \frac{\partial}{\partial x}(v_x C) - \frac{\partial^2}{\partial x^2}(\epsilon D C) - v_s C_s = 0 \\ \frac{\partial}{\partial t}(\rho_b S_i) = \epsilon k_{a,i} f_{att,i} C - \epsilon k_{d,i} f_{det,i} S_i \end{cases} \quad (2.9)$$

where $\epsilon$ is the porosity, $v_x$ is the Darcyan flow velocity along the $x$ direction, $C$ is the colloid concentration in the carrier fluid, $S$ is the colloid concentration in the solid phase, $D$ is the dispersion coefficient, $\rho_b$ is the bulk density of the porous media, $v_s$ is the volumetric flow rate per unit of aquifer representing sources, and $C_s$ is the concentration of the source.

In the second equation $k_{a,i}$ and $k_{d,i}$ are respectively the attachment and detachment rate coefficient, $f_{att,i}$ and $f_{det,i}$ are generic function modelled in function of the problem. The $i$ identifies the i-th retention mechanism and interaction site. A more detailed explanation of the interaction mechanisms and correlated functions is necessary, and it is done in the following chapters.

### a. Mechanical filtration

When particles are larger than or about as large as the smallest pores, the physical mechanism of mechanical filtration takes place [35]. It is typical of micro-size particle or colloidal aggregation. The filtration is typically irreversible and modelled by a linear irreversible attachment kinetic [34]. A schematic representation is visible in Figure 2.9(a) with the values of the two functions, $f_{att}$ and $f_{det}$.

### b. Straining

It is defined as “the trapping of colloid particles in the downgradient pore throats that are too small to allow particle passage” [45]. Straining maybe happens when the ratio between particle dimension and soil gran size, $d_{50}$, is greater than 0.002 [46]. Because it can be a reversible mechanism, the detachment function is equal to one. When straining is the interaction mechanism, particles flow in the larger pores because in the smallest ones they tend to aggregate and to be entrapped. The number of dead-end pores decrease with the increasing of the distance gram the injection point. Increasing distance, particles tend to maintain a streamline passing into larger pores [34]. The attachment function used to model straining is [46]:

$$f_{att} = \left[\frac{d_{50} + x}{d_{50}}\right]^{-\beta_{str}} \quad (2.10)$$

A schematic representation is visible in Figure 2.9(b) with the values of the two functions, $f_{att}$ and $f_{det}$ and parameters explanation. The fitting parameters is $\beta_{str}$ and it determines the particle spatial

distribution.

### c. Clean bed filtration

The clean bed filtration interaction mechanism is often used to describe the initial stage of deposition because the particle-collector interaction energy is not modified by the presence of other deposited ones [47]. It can be described with an attachment function, $f_{att}$, equal to one and a detachment function equal to zero, $f_{det}$, as visible in Figure 2.9(c). Blocking and ripening are supposed to be negligible, that is the clean bed assumption [35]. The attachment coefficient, $k_a$, was formulated as function of the single collector efficiency and the attachment efficiency [48]:

$$k_a = \frac{3(1-\epsilon)}{2d_{50}} \alpha v_e \eta_0 \tag{2.11}$$

where $v_e$ is the effective velocity obtained from the ration between Darcy velocity and porosity. When the collector has a concentration of attached particles able to affect the particle-collector interaction with the particle-particle interaction, a linear reversible attachment and blocking or ripening model can be used [34].

### d. Blocking

Blocking occurs when the repulsive interaction energy between particles is greater than the attraction energy with the collector [49, 50]. The visual representation is visible in Figure 2.9(d). A Langmuirian function is often used to model blocking [51]:

$$f_{att} = 1 - \frac{S}{S_{max}} \tag{2.12}$$

where $S_{max}$ is the maximum particles concentration in the solid phase fixed the chemical parameters.

### e. Ripening

When the attraction between particles is greater than the attraction with the collector, the attached

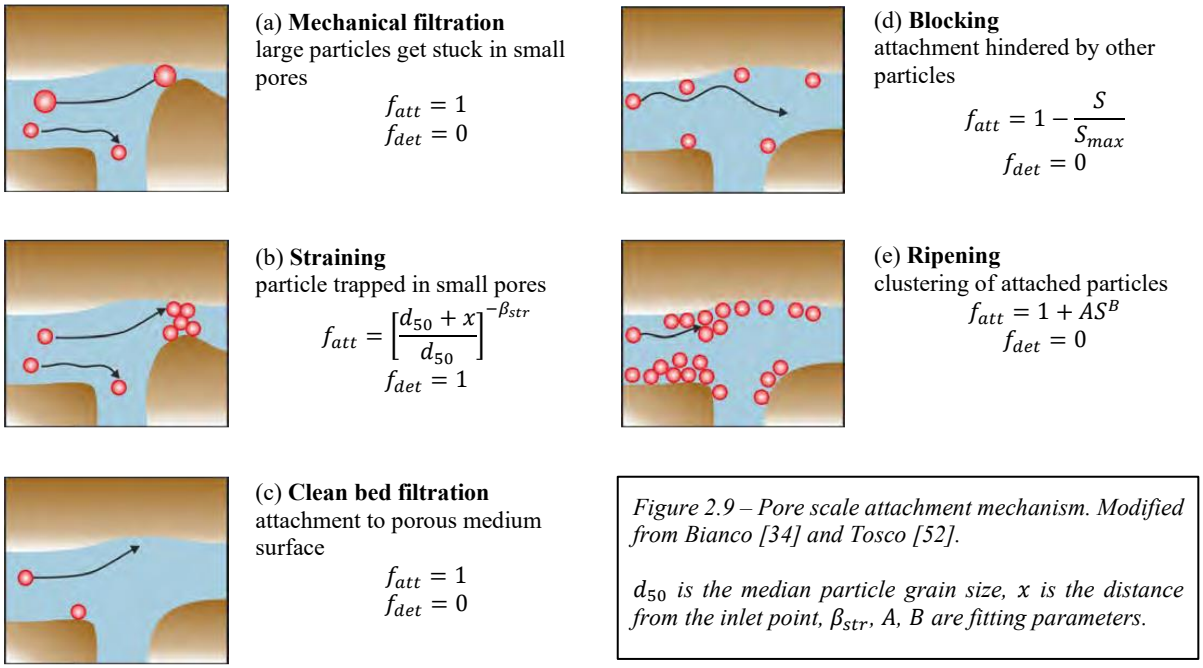


*Figure 2.9 – Pore scale attachment mechanism. Modified from Bianco [34] and Tosco [52].*

*$d_{50}$ is the median particle grain size, $x$ is the distance from the inlet point, $\beta_{str}$, $A$, $B$ are fitting parameters.*

particles attract the particles in the bulk solution. The consequence is an increase in the attachment rate, till clogging of the porous media [34]. The visual scheme is visible in Figure 2.9(e). The attachment formulation was proposed by Tosco and Sethi [52]:

$$f_{att} = 1 + AS^B \tag{2.13}$$

where $A$ and $B$ are the ripening coefficient. Both are assumed positive to increase the attachment rate increasing collector concentration $S$.

## 2.2 Methods

### 2.2.1 Physical and chemical parameters

In this chapter the description of the methods used to estimate some physical and chemical parameters is presented, which are mainly useful for the DLVO analysis. The measures are made in *Eawag* laboratory.

The first one is the Zeta Potential and it was measured by a Malvern Zetasizer. For the DLVO analysis is necessary the zeta potential of the particles and of the collector that correspond respectively to $\phi_1$ and $\phi_2$ in the equation (2.4). The nanoparticle zeta potential was measured without any pre-treatment of the sample thanks to their small size while the collector sample was treated to obtain the zeta potential value. The collector media was grinded to reduce its granulometry. This procedure allows to obtain a value of the zeta potential also for the collector because the mass of the grain not affect the potential measure. The zeta potential value is affected by the salinity of the carrier fluid. The particle and collector zeta potential was measured with two different carrier fluid: deionized water and Lake Zürich water. The zeta potential decreases generally with the increasing of the salinity of the fluid.

The second parameter that is necessary for the DLVO analysis is the ionic strength. It is equal to:

$$I = \frac{1}{2}\sum_i n_{i,0} z_i^2 \tag{2.14}$$

and it affect the Debye-Huckel reciprocal length, $k$, as visible in the equation (2.5), which in turn affect the electrostatic interaction. Because the ionic strength was not measured in the *Eawag* laboratory, it was estimated by the conductivity.

To estimate the ionic strength from conductivity some hypothesis was necessary. The first one is the assumption that the only salt present in the water is NaCl and the second one is that between the conductivity and the total dissolved solid, TDS, a linear relation is present. Based on these two hypotheses, relate the conductivity to the TDS, and estimate the concentration of NaCl in water, the estimation of ionic strength was possible. The relation between conductivity and TDS used is

$$TDS(mg/L) = 500 \cdot EC(mS/cm) \tag{2.15}$$

where $EC$ is the electrical conductivity. It comes from the *Lenntech* site. From the total dissolved solids concentration, which is the estimation of total ions in water, it is possible to estimate the concentration of NaCl using:

$$n_{NaCl}(mM) = \frac{TDS\ (mg/l)}{MW_{NaCl}\ (g/mol)} \tag{2.16}$$

where $n_{NaCl}$ is the molar concentration of the salt and $MW_{NaCl}$ is the molecular weight of NaCl equal to 58.44 mg/mol. The molar concentration of NaCl can be used in the equation (2.14) to estimate the ionic strength.

The zeta potential and conductivity measure was done for both, deionized water and Lake Zürich water but only for one filter media, sand. The particle-collector behaviour for activated carbon for both carrier fluid was supposed similar to the sand one.

### 2.2.2 Tracer tests

A tracer test is necessary to understand the hydraulic behaviour of a system. In this study many tracer tests were done both for the column and for pilot tests. They are necessary before a particle test. The tracer selected for this study is NaCl. A solution of water and salt is injected in the inlet of the porous media column and the water conductivity was measured at the end of the column using a Malvern Zetasizer with a flow cell. The shape of the tracer injection curve selected for all the tracer test of this study is a step.

When the geometry of the porous system and the flow rate are defined, it is possible to estimate the porosity and the dispersivity of the filter media. To estimate the two parameters is necessary to fit, with the method of least squares, the experimental data with an analytical solution. The experimental data were elaborated in function of the experimental setup, a different elaboration was done for the column tests and for the pilot tests. They are described respectively in the chapters 2.2.2.1 and 2.2.2.2. The analytical solution for a semi-infinite column with a 1st type, Dirichlet, inlet boundary condition without degradation is [53]:

$$\frac{C(x,t)}{C_0} = \frac{1}{2}\left\{erfc\left[\frac{x - v_e t}{2\sqrt{Dt}}\right] + \exp\left(\frac{v_e x}{D}\right) erfc\left[\frac{x + v_e t}{2\sqrt{Dt}}\right]\right\} \tag{2.17}$$

where $C$ is the solute concentration in function of time, $t$, and space, $x$, $C_0$ is the inlet solute concentration, and $D$ is dispersion coefficient computed by MNMs as $\alpha \cdot v_e$ where $\alpha$ is the dispersivity. It is obtained imposing at the partial differential equation, which describes the one-dimensional transport of a solute, the following condition [54]:

$$\begin{aligned} C(x, t = 0) &= 0 \quad for\ x \geq 0 \\ C(x = 0, t) &= C_0 \quad for\ t \geq 0 \\ C(x = \infty, t) &= 0 \quad for\ t \geq 0 \end{aligned}$$

MNMs allows to estimate porosity and dispersivity fitting the elaborated experimental date with the analytical solution using the method of least squares. The solutions provided by MNMs are obtained under the assumption of homogeneous medium and constant hydrochemical parameters.

#### 2.2.2.1 Column

The configuration of the column test, Figure 2.10, can be divided in three different parts: the injection system, the column, and the measuring system.

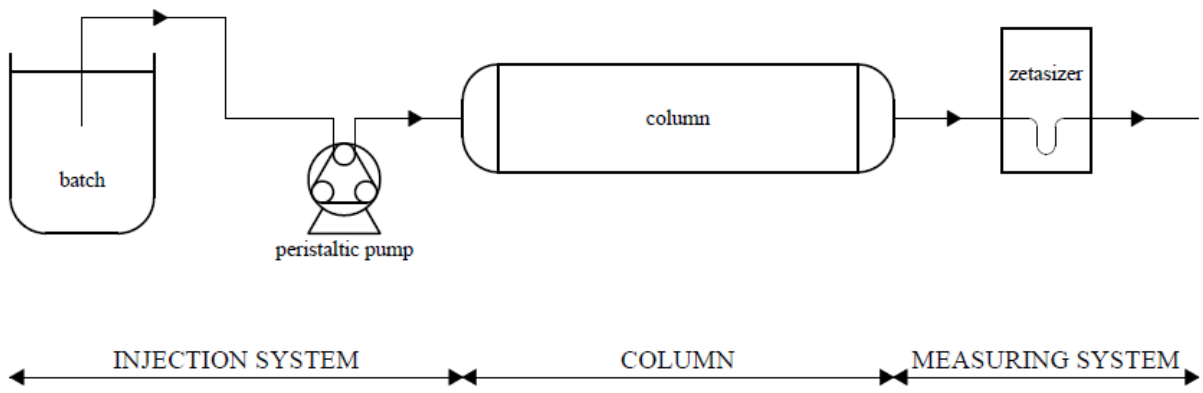


*Figure 2.10 - Column experiment scheme*

The first one is composed of a batch where is stored the solution, which has to be injected in the column, a peristaltic pump that guarantees a constant flow rate, and a tube that links the batch to the beginning of the column. In the batch a NaCl solution is used for the tracer test. Two different flow rates were used during the experiments and maintained constant by the peristaltic pump. Their values are visible in Table 2.3.

*Table 2.3 - Flow rates and porous media combinations*

| Flow rate ($m^3/s$) | Filter media |
|---|---|
| $8.33 \cdot 10^{-8}$ | Sand |
| $3.50 \cdot 10^{-7}$ | Activated carbon |

Two different flow rates were used to simulate both the conditions: a slow filtration and a rapid filtration. To reduce the number of possible combinations between flow rate and filter media, it was decided to use the lower flow rate with the sand filter, and the higher flow rate with the activated carbon filter. It is visible also in Table 2.3.

The second part of the experiment is the column. A plastic tube with a diameter of 5 cm is filled with the two different filter media: sand or activated carbon. The porous material was not been compacted in the column to simulate what happens generally in a filtering section of a water treatment plant. The filter media in a plant is not generally compacted mechanically, it is only arranged by gravity after the backwashing. The lengths of the column used during the experiments are about 11.5 cm, only one test was done with column of 5.2 cm.

The last part of the experiment is, for the tracer test, the measuring of the water conductivity. It was done with a Malvern Zetasizer using the flow cell. The instrument is connected with the end of the column by a tube.

The result of the tracer test is the breakthrough curve, which is made by the conductivity measures done by the instrument. Three data elaborations were done before using MNMs to extrapolate the hydraulic

*Figure 2.11 - Picture of a column test. Eawag*

parameter. The first one is the time correction. The solution spends time into the tubes necessary to connect the injection batch to the column and the column to the measuring instruments. This "*tubing time*" has to be subtracted to the time zero of the breakthrough curve to not overestimate the porosity of the filter media. It is function of the flow rate, but the volume is about 4 ml. Also is necessary to subtract the half of the instrumental measuring period to the time zero. The second elaboration is the subtraction of the background conductivity to the measured one. The conductivity values of the breakthrough curve are shifted of a value equal to the background value. Water has a background conductivity that is different for the deionized water and for the Lake Zürich water. The last elaboration, that is not necessary, but it allows to simplify the elaboration, is the normalization of conductivity. It is done by dividing the shifted conductivity by the maximum conductivity of the shifted breakthrough curve.

Five column tests were done combining the two porous media and the carrier fluid. Three different kind of water were used, deionized water (Dw), Lake Zürich water (LZw), and a 1:1 dilution of them. Other parameters were changed during the experimentation, like column length and injection time. In order to better represent the data, a table with the values of the main parameters in function of the porous media and the carrier fluid was done. The table is going to be proposed several times with the characteristics necessary at the consecutive interpretation and modelling.

The first passage is the estimation of the hydraulic parameters, porosity and dispersivity, from the column tracer tests. Before the estimation, a presentation of the main characteristics of the column test is necessary and the main parameters are visible in Table 2.4.

*Table 2.4 – Main column tracer test characteristics in function of filter media and carrier fluid*

| | Sand | | Activated Carbon | |
|---|---|---|---|---|
| **Dw** | Flow rate ($m^3/s$) | $8.33 \cdot 10^{-8}$ | | |
| | Column length (m) | 0.115 | | |
| | Column diameter (m) | 0.005 | | |
| | Injection time (s) | 3200 | | |
| **LZw** | Flow rate ($m^3/s$) | $8.33 \cdot 10^{-8}$ | Flow rate ($m^3/s$) | $3.50 \cdot 10^{-7}$ |
| | Column length (m) | 0.115 | Column length (m) | 0.115 |
| | Column diameter (m) | 0.005 | Column diameter (m) | 0.005 |
| | Injection time (s) | 1990 | Injection time (s) | 1270 |
| **1:1 LZw:Dw** | Flow rate ($m^3/s$) | $8.33 \cdot 10^{-8}$ | Flow rate ($m^3/s$) | $3.50 \cdot 10^{-7}$ |
| | Column length (m) | 0.052 | Column length (m) | 0.115 |
| | Column diameter (m) | 0.005 | Column diameter (m) | 0.005 |
| | Injection time (s) | 2230 | Injection time (s) | - |

The elaborated data can be used to estimate porosity and dispersivity of the filter media using MNMs as explained before in the chapter 2.2.2.

### 2.2.2.2 Pilot

The pilot plant is composed of two equal cylindrical tanks, one filled with sand and the other with activated carbon. The diameter of the tanks is 1.1 m and the depth of both the filtering zone is 1.85 m. Before the filtering zone, following the flux, a water head is present, a part of the tank with the same diameter of the filtering one but filled only with water. It allows to create a homogenous zone before the filtration. A tube collects water from the end of the filter and other one link the injection system and the

upper water head. Along the pilot some sampling points are installed. Two sampling points are present in the inlet and outlet tube, one in the upper water head, and some of them are distributed along the filtering zone. The sampling point along the filtering zone are both for water and for filtering media. The injection system is composed of a pump and a pressure valve that guarantee a constant flow rate for each tank of about 1 $m^3$/h. Upstream of the injection pump a point, where water and the necessary solution are mixed, is provided. The solution is dose by a dosing valve downstream a reservoir. A schematic representation of the pilot plant is visible in Figure 2.12.

In the case of the tracer test, salt was dissolved in the solution in the reservoir with a concentration of 70 g/L. The dosing valve guarantees a flow rate of 12 L/h of salt solution that is mixed with Lake Zürich water, which has a flow rate of 3300 L/h. The pump and the pressure valve guarantee a constant flow rate of 1 $m^3$/h for each pilot tank releasing the excess water. During the tracer test conductivity was measured in three different point, in the upper water head Figure 2.12 (a), in the middle of the filter Figure 2.12 (b) (0.85 m from the beginning of the filter), and at the end of the filter from the outlet tube Figure 2.12 (c). The outputs of the tracer test are three conductivity curves in time for each filter media.

The conductivity curve was elaborated as described in chapter 2.2.2.1 regarding the conductivity

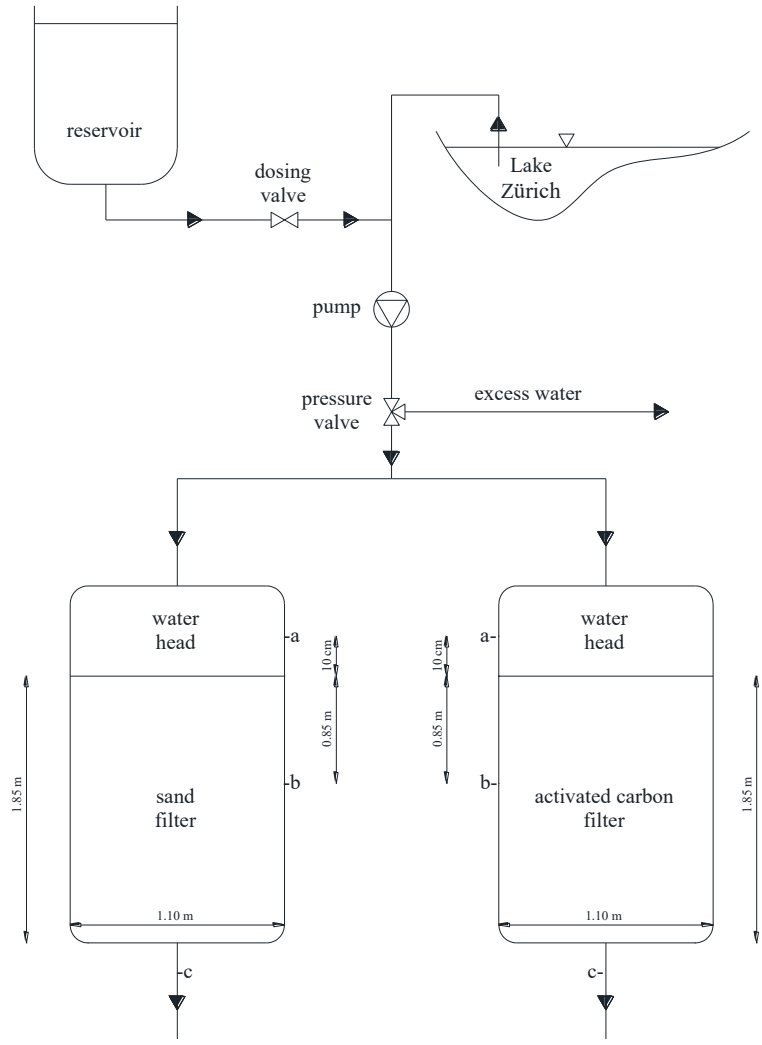


*Figure 2.12 – Pilot experiment scheme. Sampling points a) Upper water head b) Middle of the filter c) Outlet tube*

elaboration, shifting and normalization. The time correction for the pilot tracer test cannot be done as for the column tracer test because the "*tubing time*" is not known. Looking at the concentration profile at the inlet sampling point, it does not behave as an ideal PFR. If it were an ideal PFR the curve should be a perfect step like the injection one and a "*tubing time*" could was estimated. In order to make up to the lack of the "*tubing time*", the conductivity curve measured in the upper water head was used as tracer signal. The discretization of the curve was used in the boundary condition of MNMs. So, the time spent by the salt solution in the tubes is not necessary but a time correction was done because the sampling point in the upper water head is not at the beginning of the filter but 10 cm upstream. The time correction is equal to the time spent by water to do 10 cm having a flow rate of 1 $m^3/h$ in a tank with a diameter of 1.1 m, 340 s. The conductivity curve of the upper water head was used as input signal while the conductivity curve in the middle of the filter and the other one, at the end, were used to estimate porosity and dispersivity of the filter respectively at 0.85 m and 1.85 m. The results are the porosity and dispersivity in two different point of the filter for both the filter media. They are obtained creating a model on MNMs that acts as explained in chapter 2.2.2. From a 3D geometry is necessary to switch to a 1D model. The main assumption is that the concentration in the central axis is equal to the concentration of the sampling points. The schematic representation of the procedure used is visible in Figure 2.13.

### 2.2.3 Particle filtration test

The goal of the study is to understand the behaviour of plastic nanoparticles in a filter media. The tracer tests are necessary to understand the hydraulic characteristics of the porous media while the particle tests are necessary to understand the fate of NPs in a filter. All the experiment, as also explain in the chapter 2.2.2, have two step: the tracer test and the particle test. In this chapter the description of the method used to elaborate experimental data is illustrated in order to understand the particle-collector interaction parameters.

The result of the experiments for both, column and pilot, is a breakthrough curve or in the case of the pilot, several curve along the tank. The curves report the palladium concentration in function of time. As explain in the chapter 2.1.1, in order to be able to measure the concentration of nanoplastics in the

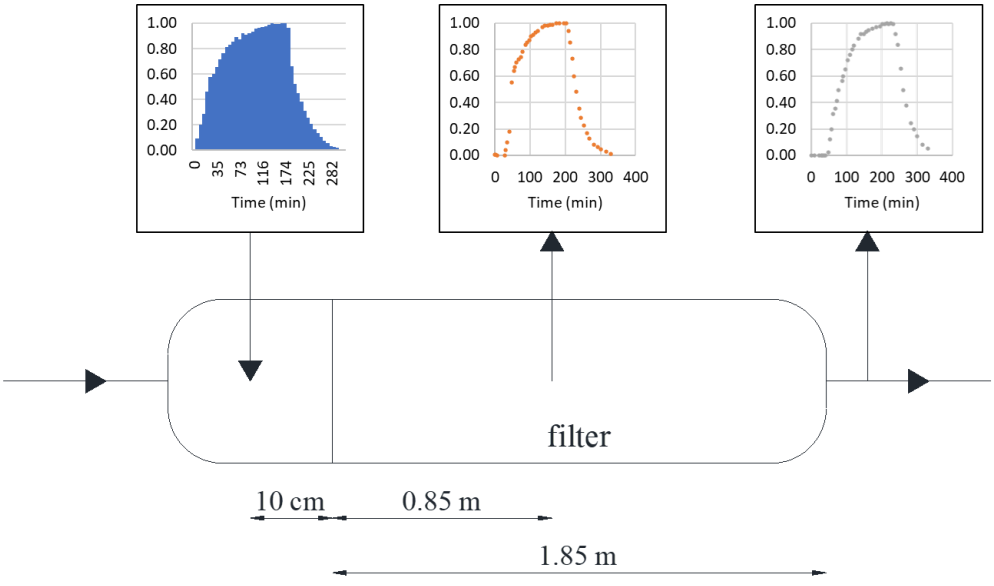


*Figure 2.13 – Schematic representation of the method used to elaborate the tracer test in MNMs*

carrier fluid, the particles are doped with palladium. To obtain the curve at the sampling points, which is at the end for the column test while along the pilot for the pilot test, an automatic sampler that collect the carrier fluid is provided. Each sample is then analysed using an ICP-MS to measure the palladium concentration. Like for the data of the tracer tests, the data elaborations of particle experiments are different for the two different scale.

After the data elaboration is possible to use the column experimental data to understand the attachment mechanism and the relative parameters. The attachment mechanisms were presented in the introduction, chapter 2.1.4.1.3. The attachment mechanism can be identified by the shape of the curve while to estimate the parameters, MNMs was used that has the tool to simulate the transport of colloidal particles in 1D saturated porous media.

When the attachment mechanism and the interaction parameters were identified from the column tests, it was possible to simulate the particle transport in the pilot plant. It is possible because the geometry of the thank, the physicochemical parameters of the materials, and the nanoparticle interaction mechanism are known. It is possible to simulate the behaviour of particles into the pilot changing the inlet particle concentration or the injection time. The goal of the simulation is to forecast the particles behaviour in the pilot plant with the two different filter media at different inlet concentration and injection time. Because some parameters, as porosity and dispersivity, are uncertain a sensitivity analysis was done. This is necessary to design the pilot-scale experiment. The inlet particle concentration and injection time must be selected in order to understand when and where the particles have to be measured and also to fall back beyond the detection limit. At the end, the experimental data coming from the pilot experiment can be compared with the results coming from the simulations.

### 2.2.3.1 Column

The experimental scheme used for the particle test is about the same of the tracer test, the visual representation is visible in Figure 2.10. Two differences can be notice: in the batch a particle solution is present and not a salt one, and the end has an automatic sampler instead of the Zetasizer. The geometries, the flow rate and the porous material are the same described in chapter 2.2.2.1.

The result of a particle column test is a breakthrough curve of palladium concentration in function of time. The first step is the data elaboration. Like for the tracer column test is necessary to shift the time of a value equal to the sum of the "*tubing time*" and the half of the average sampling period. The "*tubing time*" is equal to one of the tracer column's tests while the half of the average sampling period is different. It is equal to the half of the ratio between the volume of the samples and the flow rate of the test. Regarding to the palladium concentration it was converted to a mass concentration using the conversion factor of chapter 2.1.1, $4.0 \cdot 10^{11}$ particles/µg to transform the palladium concentration to the particle one, $1.0 \cdot 10^{-18}$ kg/particle to obtain the mass concentration. The final conversion factor, which is the product of the two different conversion factors, is $4.0 \cdot 10^{-7}$ kg/µg. It is also necessary to subtract to all the values the background concentration. This elaboration can be done with the palladium concentration or equally with the mass one.

The next step is the attachment mechanism identification. From the shape of the breakthrough curve is possible to identify the possible attachment mechanism. It is preferable to extrapolate the attachment mechanism from a longer experiment. It is also possible the define the reversibility of the mechanism looking at the tail of the curve.

At the end, because the geometry of the system, boundary and initial conditions Table 2.5, the

physicochemical parameters of particles and filter media and the attachment mechanism were defined, it is possible to use MNMs to estimate the attachment parameters fitting the experimental breakthrough curve with the least squares method.

*Table 2.5 – Inlet concentration and injection time for the particle column tests*

| | Sand | | Activated Carbon | |
|---|---|---|---|---|
| **Dw** | $C_{IN}$ (kg/m$^3$) | 0.0021 | | |
| | Injected PV (-) | 1.4 | | |
| **LZw** | $C_{IN}$ (kg/m$^3$) | 0.0012 | $C_{IN}$ (kg/m$^3$) | 0.0028 |
| | Injected PV (-) | 1.3 | Injected PV (-) | 1.6 |
| **LZw: Dw** | $C_{IN}$ (kg/m$^3$) | 0.0025 | $C_{IN}$ (kg/m$^3$) | 0.0024 |
| | Injected PV (-) | 16.5 | Injected PV (-) | 14.5 |

### 2.2.3.2 Pilot simulation

The pilot test is necessary to understand the particle behaviour in a system with a higher scale than a column, but it is necessary to design it, creating a model and simulating different situations. The geometry of the pilot is known, it has a diameter of 1.10 m and a filter depth of 1.85 m, it is visible in Figure 2.12. Two different filter are tested, one with sand and the other with activated carbon. The characteristics of the filter media are in chapter 2.1.2. The flow rate is the same for the two filters, equal to 1 m$^3$/h. These properties are also visible in Table 2.6.

*Table 2.6 - Pilots properties*

| Diameter m | Length m | Flow rate m$^3$/s | Filter media - | Filter density kg/m$^3$ | Grains diameter µm |
|---|---|---|---|---|---|
| 1.10 | 1.85 | $2.8 \cdot 10^{-4}$ | Sand | 2650 | 450 |
| 1.10 | 1.85 | $2.8 \cdot 10^{-4}$ | Activated carbon | 448.5 | 1050 |

Porosity and dispersivity selected for the simulation were extrapolated from the result of the pilot tracer test. Because they are not certain and based on a single experiment, a sensibility analysis was done. The value used are visible in the chapter 2.3.4. The attachment mechanism and the interaction parameters come from the column tests interpretation.

Regarding to the boundary conditions, the inlet concentration and the time of injection, were decided from experimental results but also taking into account the instructions of the *Eawag*. The inlet concentration was selected similar to the inlet concentration of the column tests, 5 µg/L of palladium that corresponds to $2.0 \cdot 10^{-3}$ kg/m$^3$, using the conversion factor of $4.0 \cdot 10^{-7}$ kg/µg. The injection time was selected considering the *Eawag* disposition. The injection selected is of 6 h.

The pilot, before the beginning of the filter, is not a perfect PFR and consequently a perfect step injection signal cannot be used in the boundary conditions. It is necessary to simulate the pilot considering the hydraulic behaviour of water upper head and the inlet system. The injection signal used for the pilot has the same shape of the curve of conductivity measured during the pilot tracer test in the upper water head, Figure 2.14. It has also been necessary to extend the curve in time to reach an injection time of 6 h. In order to do so, it was necessary to extend the curve, when the maximum value was reached, of a time that lets to amount to 6 h.

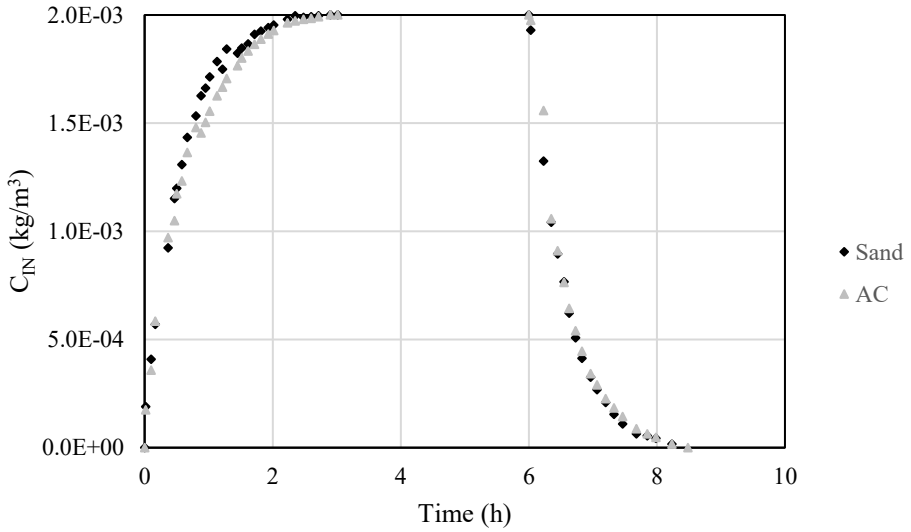


*Figure 2.14 – Sand and AC model injection steps*

Summing up two simulation was done, one for the sand and one for the activated carbon, with an injection of 6 h, shaped as the tracer curve, of particles with a concentration of $2.0 \cdot 10^{-3}$ kg/m$^3$. The flow rate and the geometry are the same for both the filter, respectively 1 m$^3$/h and a length of 1.85 m and a diameter of 1.1 m. The attachment mechanism and the interaction parameters are obtained from the column tests and are different based on the filter media. The porosity and dispersivity are obtained from the tracer test but due to their uncertain a sensitivity analysis with three different values was done. Along the pilot several sampling points are installed, visible in Figure 2.15, both for water and for the porous media.

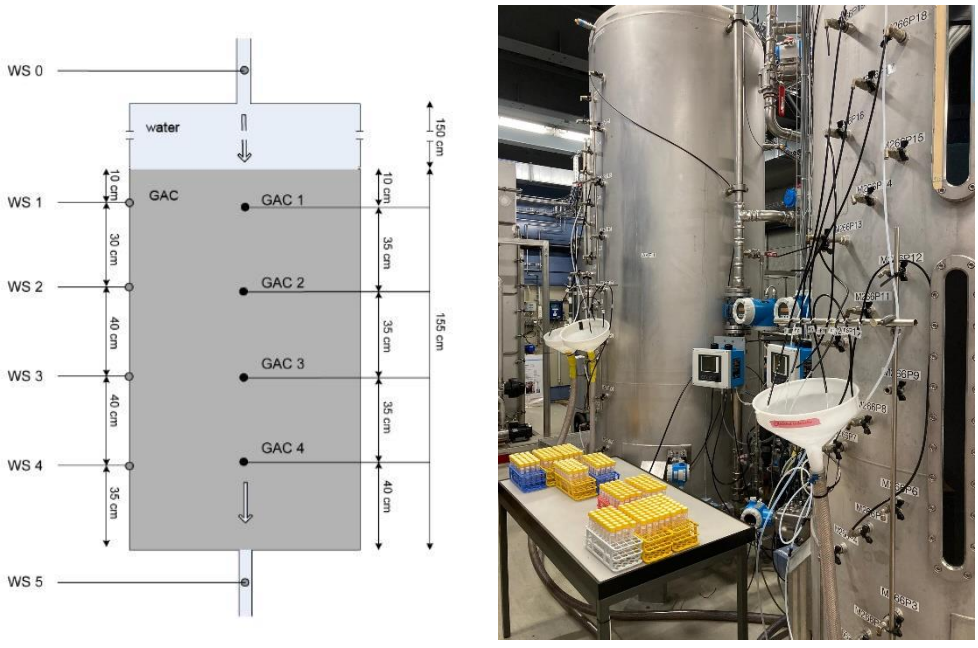


*Figure 2.15 - Water and porous media sampling point distribution, scheme and picture from Eawag*

## 2.3 Results

### 2.3.1 DLVO

The DLVO theory, used to estimate the interaction between nanoparticles and filter media, was applied only to the sand but with two different waters: deionized water and Lake Zürich water. The behaviour of particles and activated carbon is assumed to be similar to the sand one. Some parameters, necessary to create the potential energy curves, have been already showed in the previous chapters.

The experiments were conducted in a laboratory with a temperature equal to 295 K. It was assumed that the water and the laboratory temperatures are equal. Starting from particle characterization, they have a diameter equal to 190 nm (chapter 2.1.1) and, because them are covered by a layer of polystyrene, the Hamaker constant used for particles was assumed equal to $7.0 \cdot 10^{-20}$ J. The value was extrapolated from literature [55]. The particle collector potential values are visible in Table 2.7, them were measured directly in the *Eawag* laboratory. The analysis was done, as just explained, with two different kind of water. The Hamaker constant of water, hypothesized equal for the two different waters, was assumed equal to $3.7 \cdot 10^{-20}$ J. It was found in the MNMs tutorial guide. The relative dielectric constant at 295 K is equal to 78.5 for water. As explained in chapter 2.2.1, it was assumed that only NaCl is present in water, consequently the valence of dissolved ions was selected equal to 1. Also, in chapter 2.2.1, the description of the methodology used to estimate the Ionic Strength is presented for the two waters starting from the conductivity. The conductivity values measured in the laboratory are equal to 0.004 mS/cm and 0.285 mS/cm, respectively for deionized water and Lake Zürich water. The Ionic Strength estimated with the relations presented in chapter 2.2.1 is visible in Table 2.7. The last necessary parameters are the Zeta Potential of the sand in the two waters and the Hamaker constant of sand. The values of Zeta potential, coming from the experimental data of *Eawag*, are visible in Table 2.7. The Hamaker constant was found in the MNMs tutorial guide, it is equal to $6.0 \cdot 10^{-20}$ J for quartz sand.

*Table 2.7 – Experimental results of Ionic Strength and Zeta potential for the collector and the particles with deionized water and Lake Zürich one.*

| Water<br>- | Ionic Strength<br>mM | Collector zeta potential<br>mV | Particle zeta potential<br>mV |
|---|---|---|---|
| Deionized | 0.035 | -8.88±2. 19 | -37.04±2. 32 |
| Lake Zürich | 2.440 | -15.30±0. 61 | -13.10±0. 98 |

Analysing the experimental data, the particle Zeta Potential follows the theoretical trend of decreasing, in absolute value, with the increasing of the Ionic Strength. On the contrary the collector Zeta Potential does not follow the theoretical behaviour. It can be a consequence of a different grinding before the measures or an anomalous behaviour of the charge's distribution.

Using all the experimental and literature parameters and the DLVO tool of MNMs, the interaction potential curves were estimated in function of the distance. The solution used is Gregory 1975 [39], equation (2.4), which is based on the linear superposition approximation. The results are visible in Figure 2.16.

Starting with the analysis of the particle-particle interaction profiles, Figure 2.16(a), it is possible to see that in both cases, deionized and Lake Zürich waters, the profile is repulsive. Between particles a repulsion energy is present that decrease drastically with the increase of the Ionic Strength, passing from a maximum of 119.3 KT for the particles in deionized water to 8.5 KT for the Lake Zürich water. Particles in deionized water, due to the higher energy barrier, has to be more stable than in Lake Zürich

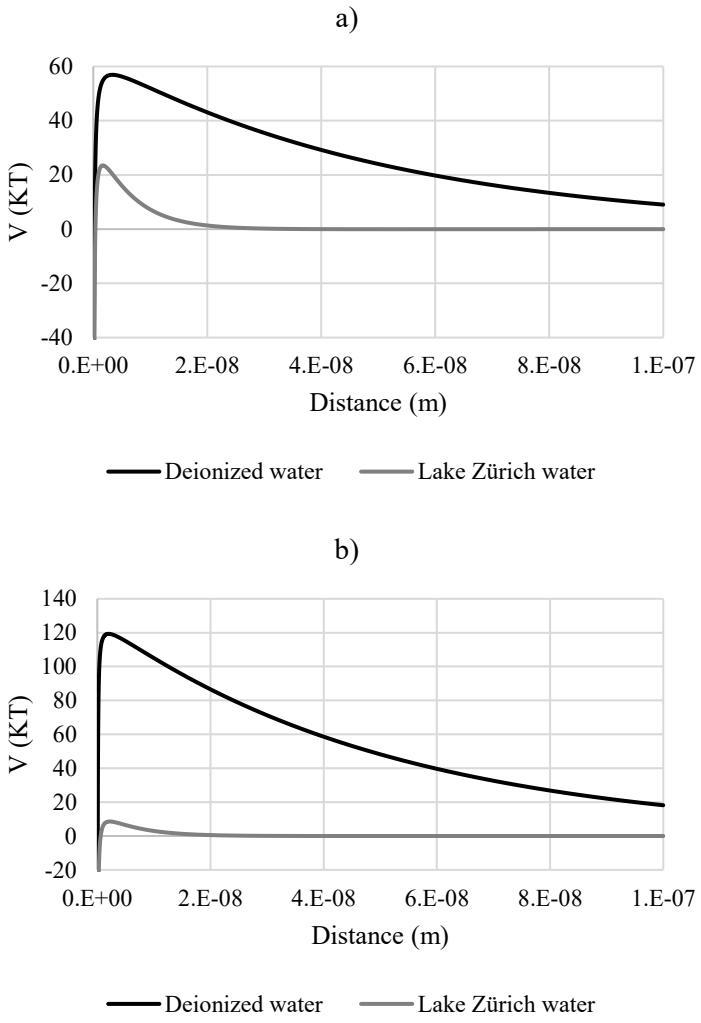


*Figure 2.16 – DLVO interaction energy profiles calculated with MNMs. a)particle-particle interaction, b) particle-collector interaction.*

water. This could confirm the impression from the *Eawag* laboratory of a more unstable suspension with the lake water.

The interaction behaviour between particles and sand has a trend equal to the particle-particle profiles. The energy barrier is higher for deionized water than for Lake Zürich water, respectively 56.9 KT and 23.5 KT. The gap between the maximum values is lower because the Zeta Potential of the collector in deionized water is, in absolute value, lower than in lake water. The attachment of particle on the filter media is easier in lake water than in deionized one.

Because the study has the goal of understanding the behaviour of NPs in the two filters during the Lake Zürich water treatment process, the grey curves are the most interesting. Both assume always positive values without considering the primary minimum. It can reflect an irreversible attachment mechanism both for particle-particle interaction and for particle-collector one. The lower energy barrier value for the particle-particle interaction can implicate an easier attachment between them than with the filter media. These considerations are useful to better understand the filtering mechanism even if it need to be supported by the other results.

### 2.3.2 Single collector efficiency

The theory of the single collector efficiency has already been explained in chapter 2.1.4.1.2. It was estimated for four different cases, two for the column tests and two for the pilot plant. Two different estimation for each scale is necessary due to the different filter media: sand and activated carbon. A summary of the four cases are visible in Table 2.8 in the *scale* and *filter media* columns. As explained in the chapters 2.2.2.1 and 2.2.2.2, the column tests was done with two different flow rate to simulate the two different filtration methods, the slow filtration in sand and the rapid filtration in activated carbon. The flow rates are 5 ml/min and 21 ml/min, respectively for the two filters. Instead, the pilot tests were done with a flow rate equal for the sand and for the activate carbon, 1 $m^3/h$ of lake water. In the Table 2.8 the results of the Darcy velocities, which is necessary to the single collector contact efficiency estimation, are visible. It was estimated as the ratio between the flow rate and the cross section.

*Table 2.8 – Single collector efficiency scheme of cases and Darcy velocity calculation*

| Scale<br>- | Filter media<br>- | Flow rate<br>$m^3/s$ | Diameter<br>m | Darcy velocity<br>m/s |
|---|---|---|---|---|
| column | sand | $8.33 \cdot 10^{-8}$ | 0.05 | $4.24 \cdot 10^{-5}$ |
| column | activated carbon | $3.50 \cdot 10^{-7}$ | 0.05 | $1.78 \cdot 10^{-4}$ |
| pilot | sand | $2.78 \cdot 10^{-4}$ | 1.10 | $2.92 \cdot 10^{-4}$ |
| pilot | activated carbon | $2.78 \cdot 10^{-4}$ | 1.10 | $2.92 \cdot 10^{-4}$ |

One other necessary parameter for the single collector contact efficiency estimation is the collector radius. They, as explain in the chapter 2.1.2, were found in literature and they are visible in Table 2.1. The sand collector was assumed equal to 450 μm while the activated carbon one was assumed equal to 1050 μm. It is also necessary the particle density that is equal to 1140 $kg/m^3$, like in chapter 2.1.1.

It is necessary to input in MNMs also some fluid characteristics: temperature, density, and dynamic viscosity. They are readable in Table 2.9

*Table 2.9 – Fluid characteristics at 295 K*

| Temperature<br>K | Density<br>$kg/m^3$ | Dynamic viscosity<br>Pa s |
|---|---|---|
| 295 | 997.8 | $9.54 \cdot 10^{-4}$ |

At the end for the single collector contact efficiency is necessary the global Hamaker constant, which was estimate with the equation (2.3). The Hamaker constants used are the same of the DLVO study. Because the DLVO analysis was done only with sand, the Hamaker constant of activated carbon has to be defined. It was assumed equal to $6.0 \cdot 10^{-20}$ J that is the same of the assumed value of quartz sand. It was found in literature [56]. In Table 2.10 a recap of Hamaker constants is visible.

The last necessary parameter to estimate the single collector efficiency, considering the fluid shell, is the porosity. It was estimated from the column particle tests and from the pilot tracer test. The motivation of the porosity selection is explained in the next chapter 2.3.3. The porosities are visible in Table 2.11. All the necessary parameters for the single collector efficiency were defined. Using MNMs the single collector efficiency in function of the particle radius was calculated for the four cases. MNMs has the possibility to estimate the single collector contact efficiency with several equations. The single collector contact efficiency in function of the particle radius for the four cases and with the several solutions, which are present in MNMs, are visible in the Appendix A. In the Appendix A the list of the solution implemented by MNMs is showed.

*Table 2.10 – Hamaker constants and Global Hamaker constant value*

| Filter | Collector Hamaker constant | Carrier fluid Hamaker constant | Particle Hamaker constant | Global Hamaker constant |
|---|---|---|---|---|
| - | J | J | J | J |
| sand | $6.00 \cdot 10^{-20}$ | $3.70 \cdot 10^{-20}$ | $7.00 \cdot 10^{-20}$ | $3.80 \cdot 10^{-21}$ |
| activated carbon | $6.00 \cdot 10^{-20}$ | $3.70 \cdot 10^{-20}$ | $7.00 \cdot 10^{-20}$ | $3.80 \cdot 10^{-21}$ |

*Table 2.11 – Porosities of the filters estimated from the column and pilot tests*

| Scale | Filter media | Porosity |
|---|---|---|
| - | - | % |
| column | sand | 45 |
| column | activated carbon | 45 |
| pilot | sand | 55 |
| pilot | activated carbon | 45 |

It is useful to compare the single collector contact efficiency. To simplify the interpretation only one solution was selected for each case, the solution that represent on average the general behaviour. The solution selected to compare the results was published by Tufenkji and Elimelech in 2004 [57]. The first comparison was done between the filter media maintaining the same scale of the problem, while the second one between the scale of the experiment but with the same collector material.

In the first comparison it is possible to notice that the single collector contact efficiency is higher for the sand than for the activated carbon. It is visible in Figure 2.17. The efficiency values for a particle radius of $1.0 \cdot 10^{-7}$ m, about the half of the particle diameter of 190 nm, are 0.30% for the activated carbon and 1.04% for the sand in the column tests. In the pilot test the efficiencies are 0.21% and 0.36%, respectively for the activated carbon and for the sand. The little difference between the single collector contact efficiencies in the pilot tests is due only to the collector radius because all the other parameters are equal. The sand has a collector radius lower than the activated carbon that increase, looking at the Yao formulation, the contact efficiency for interception and diffusion. The gap between the efficiencies in

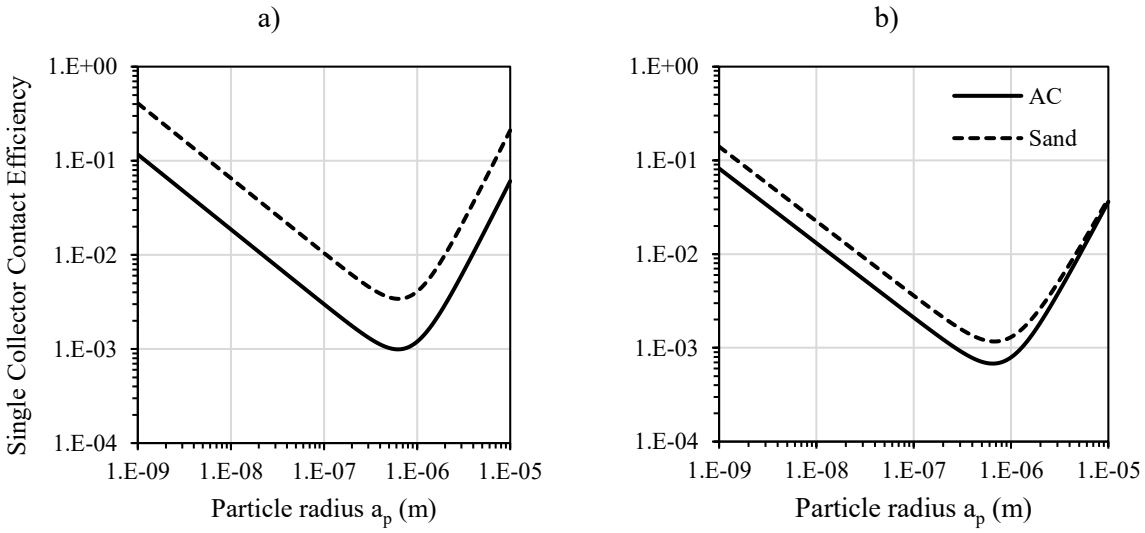


*Figure 2.17 – Single Collector Contact Efficiency comparison between sand and activated carbon maintaining the same scale problem, fluid shell model. a) columns scale, b) pilot scale.*

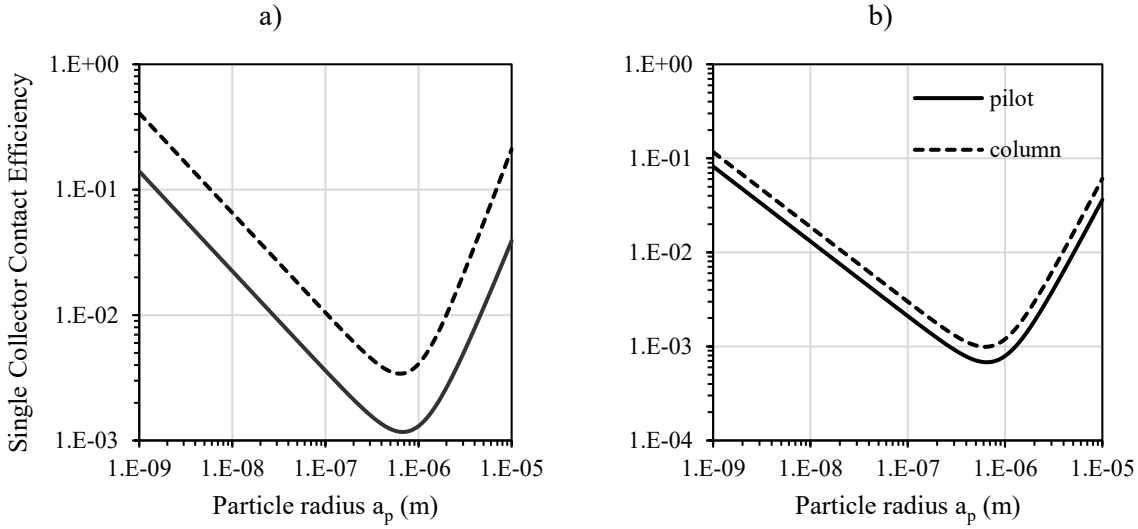


*Figure 2.18 – Single Collector Contact Efficiency comparison between scale test maintaining the same filter media, fluid shell model. a) sand, b) activated carbon.*

the column tests is greater because the Darcy velocity of the sand test is lower than the activated carbon one. The effect of the difference of the Darcy velocity is above also to the difference of porosity, which is in favour of the activated carbon. A lower porosity corresponds to a higher single collector contact efficiency because of the increase of the fluid shell. At the end, the single collector efficiency is always higher for the sand in both the scale of the experiments.

In the second comparison, Figure 2.18, the single collector efficiency is higher for the column scale test than for the pilot scale test. It is true for both the porous media used. This result can always be extrapolated from the Figure 2.17, but it is more readable. In the sand filter the single collector efficiency, for a particle radius of $1.0 \cdot 10^{-7}$ m, is 1.04% for the column test and 0.36% for the pilot test. Instead, in the activated carbon filter, the efficiency is 0.30% for the column scale and 0.21% for the pilot one. The difference for the activated carbon is very small because, without counting the collector radius that is the same, the porosity assumed is equal and the velocity is very similar Table 2.8. on the contrary, the difference for the sand is significant. It is made by the difference of the Darcy velocity, lower for the column test Table 2.8, even if it is attenuated by the lower porosity of the pilot plant.

*Table 2.12 - Single Collector Contact Efficiency values for a particle radius of $1.0 \cdot 10^{-7}$ m, without fluid shell model*

| | | **Scale of the test** | |
|---|---|---|---|
| | | **Column** | **Pilot** |
| **Filter** | **Activated Carbon** | 0.15% | 0.10% |
| | **Sand** | 0.70% | 0.18% |

The single collector contact effciency was estimated also without the fluid shell. It does not take into account the porosity. The effect is a general reduction of the efficiency. The four graphs are visble in Figure 2.19. The single collector contact efficiencies, for a particle radius of $1.0 \cdot 10^{-7}$ m, are consultable in Table 2.12.

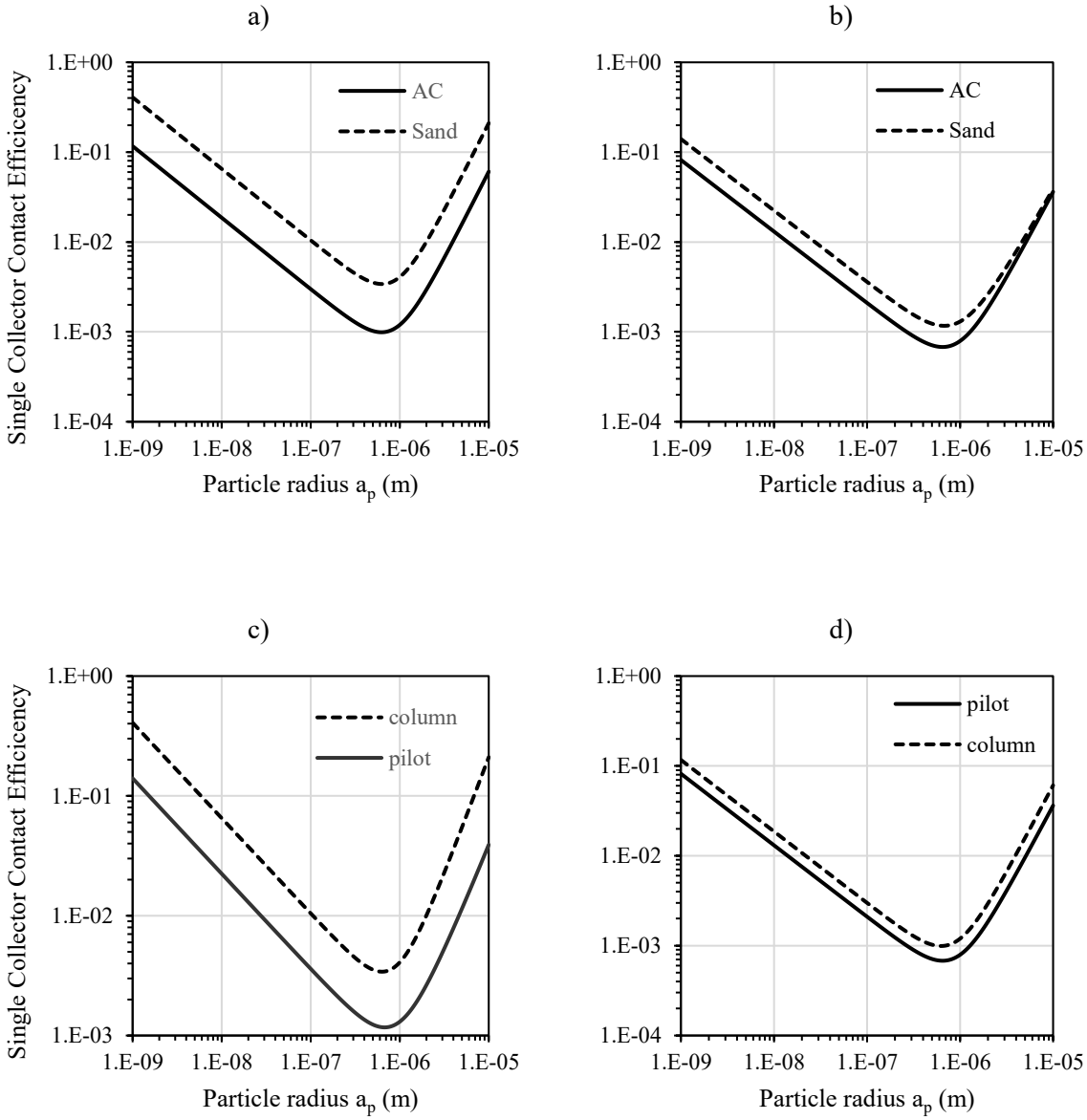


*Figure 2.19 - Single Collector Contact Efficiency comparison without fluid shell model. a) column scale – filter media comparison, b) pilot scale – filter media comparison, c) sand – experiment scale comparison, d) activated carbon – experiment scale comparison.*

### 2.3.3 Column test interpretation

#### 2.3.3.1 Tracer tests

After the elaboration of the experimental breakthrough curve, like explain in chapter 2.2.2.1, using MNMs is possible to estimate porosity and dispersivity fitting experimental data and equation (2.17) with the least squares method. The fitting results are visible in Appendix B while the porosity and dispersivity are visible in Table 2.13.

*Table 2.13 - Porosity and dispersivity estimated by the tracer column tests*

| | Sand | | Activated Carbon | |
|---|---|---|---|---|
| **Dw** | Porosity (%) | 57.3 | | |
| | Dispersivity (m) | 0.0016 | | |
| **LZw** | Porosity (%) | 67.1 | Porosity (%) | 84.6 |
| | Dispersivity (m) | 0.0007 | Dispersivity (m) | 0.0047 |
| **LZw: Dw** | Porosity (%) | 67.6 | | |
| | Dispersivity (m) | 0.0004 | | |

Also, an experiment with activated carbon and diluted LZw was done but the tracer test had some measuring problem. The porosities estimated from the tracer test at the column scale are greater than what expected. The higher values can be a consequence of a non-perfect execution of the test together at a non-ideal tracer. Maybe a discrepancy is present between the experimental data and the elaboration or NaCl interacts with the porous media producing an increase in porosity. A better estimation can be extrapolated from the particle tests. Using the porosities of the column tracer test there was a discrepancy of time in the particle curves, the porosities were too high and consequently the fitting and experimental curves had a time discrepancy. Therefore, porosity and dispersivity were estimated also from the particle column tests, and those value are considered more correct. The value of porosity and dispersivity obtained from the particle column test are visible in Table 2.14.

*Table 2.14 - Porosity and dispersivity estimated by the particle column tests*

| | Sand | | Activated Carbon | |
|---|---|---|---|---|
| **Dw** | Porosity (%) | 50.0 | | |
| | Dispersivity (m) | 0.0020 | | |
| **LZw** | Porosity (%) | 55.0 | Porosity (%) | 47.0 |
| | Dispersivity (m) | 0.0007 | Dispersivity (m) | 0.0025 |
| **LZw: Dw** | Porosity (%) | 55.0 | Porosity (%) | 43.0 |
| | Dispersivity (m) | 0.0010 | Dispersivity (m) | 0.0030 |

### 2.3.3.2 Particle test

In all the column, after the tracer test, a particle test was done. Adding at the experimental parameters and geometries used for the column tracer test, the porosity and the dispersivity defined in Table 2.14, the density and the diameter of the porous media defined in Table 2.1, the injection time and inlet concentration visible in Table 2.5, and the experimental data, it is possible, after having select the attachment mechanism, to estimate the interaction parameters.

The attachment mechanism definition can be done combining the result of the DLVO analysis with the breakthrough curves of particle column tests. The curves at which is better to pay attention, in order to understand the interaction mechanism, are the longer ones. The plot of them is visible in Figure 2.20, in the zoom the sand graph can be seen to better understand the shape. Looking at the breakthrough curves, it is possible to suppose that the attachment mechanism is characterized by an irreversible blocking. The DLVO analysis supports this result because of the repulsion between particle that can reduce the

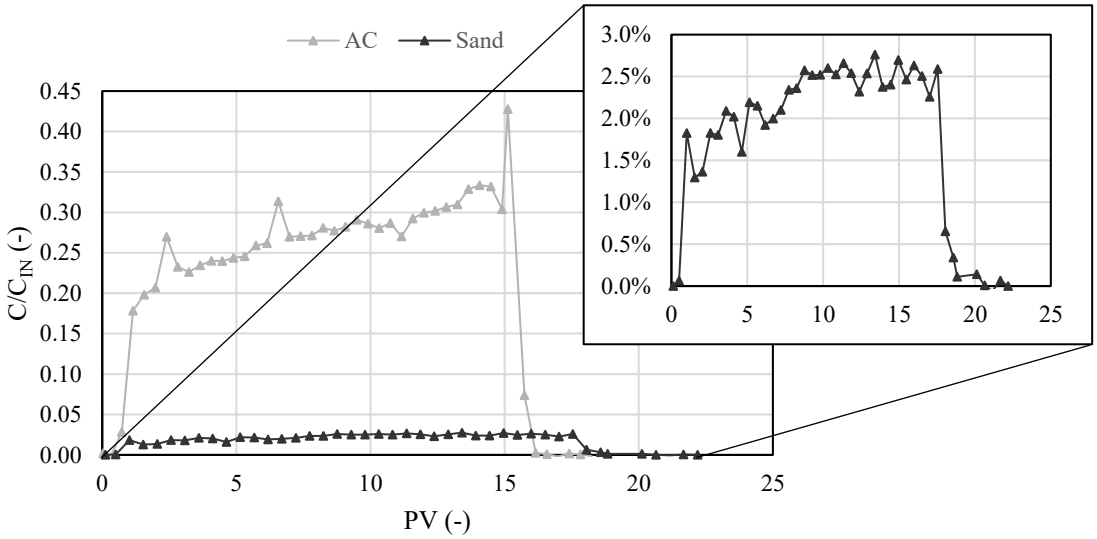


*Figure 2.20 – Long particle column test comparison*

attachment rate with the increase of the particle collector concertation. The irreversibility can be supposed due to the net decrease of particle concertation in the breakthrough tail.

After having selected the model, it is possible to estimate the interaction parameters for each column test thank to MNMs that has a tool to simulate numerically the 1D particle transport in a porous media. From the fitting of the experimental data and the model, two parameters are estimated: the attachment rate, $k_a$, equation (2.9), and the maximum blocking concentration, $S_{max}$, equation (2.12). The results are visible in Table 2.15. The experimental fitting graphs are consultable in Appendix C.

*Table 2.15 – Interaction parameters values*

| | Sand | | Activated Carbon | |
|---|---|---|---|---|
| **Dw** | Attachment rate, $k_a$ (1/s) | 0.0014 | | |
| | Maximum blocking concentration, $S_{max}$ (-) | $6.61 \cdot 10^{-6}$ | | |
| **LZw** | Attachment rate, $k_a$ (1/s) | 0.0030 | Attachment rate, $k_a$ (1/s) | 0.0022 |
| | Maximum blocking concentration, $S_{max}$ (-) | $3.94 \cdot 10^{-5}$ | Maximum blocking concentration, $S_{max}$ (-) | $3.86 \cdot 10^{-5}$ |
| **LZw: Dw** | Attachment rate, $k_a$ (1/s) | 0.0064 | Attachment rate, $k_a$ (1/s) | 0.0057 |
| | Maximum blocking concentration, $S_{max}$ (-) | $1.54 \cdot 10^{-4}$ | Maximum blocking concentration, $S_{max}$ (-) | $1.39 \cdot 10^{-4}$ |

Comparing the interaction parameters obtained for sand with deionized water and Lake Zürich water, an increase of the attachment rate and maximum blocking concentration can be notice that reflects the DLVO analysis. Increasing the salinity of water, the repulsion between particles and collector decrease and consequently an increase in both the interaction parameters. Comparing the interaction parameters obtained using the same water but with the two filters, they are comparable. The attachment rate for sand is higher than for activated carbon. It reflects the higher single collector contact efficiency of sand due to the lower Darcy velocity and the smaller grains. Comparing the experiments done with diluted Lake Zürich water, the trend between activated carbon and sand is equal, the attachment parameters are

about the same, but the attachment rate of sand is higher than AC. Comparing the parameters at different water salinity, a discrepancy between the results and the expected ones is present. They increase while ionic strength decreases. Because the pilot test was done with Zürich Lake water, the relative parameters were chosen.

### 2.3.4 1D Pilot tracer test

As explained also in 2.2.2.2 several assumptions are necessary. From a 3D geometry is necessary to switch to a 1D model. The main assumption is that the concentration in the central axis is equal to the concentration of the sampling points. Because the geometry of the pilot between the injection point and the inlet is not known, firstly it is difficult to estimate the *tubing time* and then, looking at the concentration profile at the inlet sampling point, it does not behave as an ideal PFR. If it were an ideal PFR the curve should be a perfect step like the injection one. To avoid this problem, it is possible to use the measured concentration in the inlet sampling point as injection curve in the boundary conditions of MNMs, Figure 2.13. Knowing the geometry, the flow rate, the density of the porous media, the initial and the boundary conditions, it is possible to estimate porosity and dispersivity from the experimental breakthrough.

The result of the experimental data analysis is the value of porosity and dispersivity at 1m from the top of the filter and at the end, for both the filter, Table 2.16. The curves are visible in Appendix D.

*Table 2.16 – Porosity and dispersivity, for both filters, at 1 m from the top of the filter and at the end*

| | 1 m | | End | |
|---|---|---|---|---|
| Sand | Porosity (%) | 45.5 | Porosity (%) | 51.4 |
| | Dispersivity (m) | 0.0090 | Dispersivity (m) | 0.0520 |
| Activated carbon | Porosity (%) | 58.1 | Porosity (%) | 76.6 |
| | Dispersivity (m) | 0.0493 | Dispersivity (m) | 0.0549 |

The value of porosity and dispersivity, at 1 m from the top of the filter, are more reasonable because the hydraulic behaviour of the pilot from the end of the filter to the measuring instrument is not well known. A distance of 2 m is interposed between the end of the filter and the outlet sampling point but the hydraulic behaviour is not known. The porosity was assumed for both the filter equal to 45% and, as then explained in chapter 2.3.5, due to the uncertainty a sensitive analysis was done. Dispersivity is increased of one order of magnitude in comparison to the values obtained from the column test. This is reasonable because dispersivity scales linearly with the scale of the problem. The values of dispersivity selected for the simulation are: 0.031 for the sand filter and 0.052 for the activated carbon one. Also, for the dispersivity a sensibility analysis was done.

### 2.3.5 1D Pilot simulation

The geometry, the flow rate and porous media characteristics of the two pilot-scale filters are visible in chapter 2.2.3.2, Table 2.6. In chapter 2.2.3.2 it is also explain the inlet concentration curve and the injection time, which define the initial and boundary conditions. Porosity and dispersivity were obtained from the pilot tracer test, Table 2.16 , but due to their uncertain a sensitivity analysis with three different values was done. The three porosity values simulated are 40%, 45%, 50%. Dispersivity was assumed equal to 0.006 m, 0.031 m and 0.060 m for the sand, 0.001 m, 0.052 m and 0.100 m for the activated carbon. The interaction mechanism simulated was the irreversible blocking with the interaction parameters equal to the result obtained from the column test done in the LZw, Table 2.15.

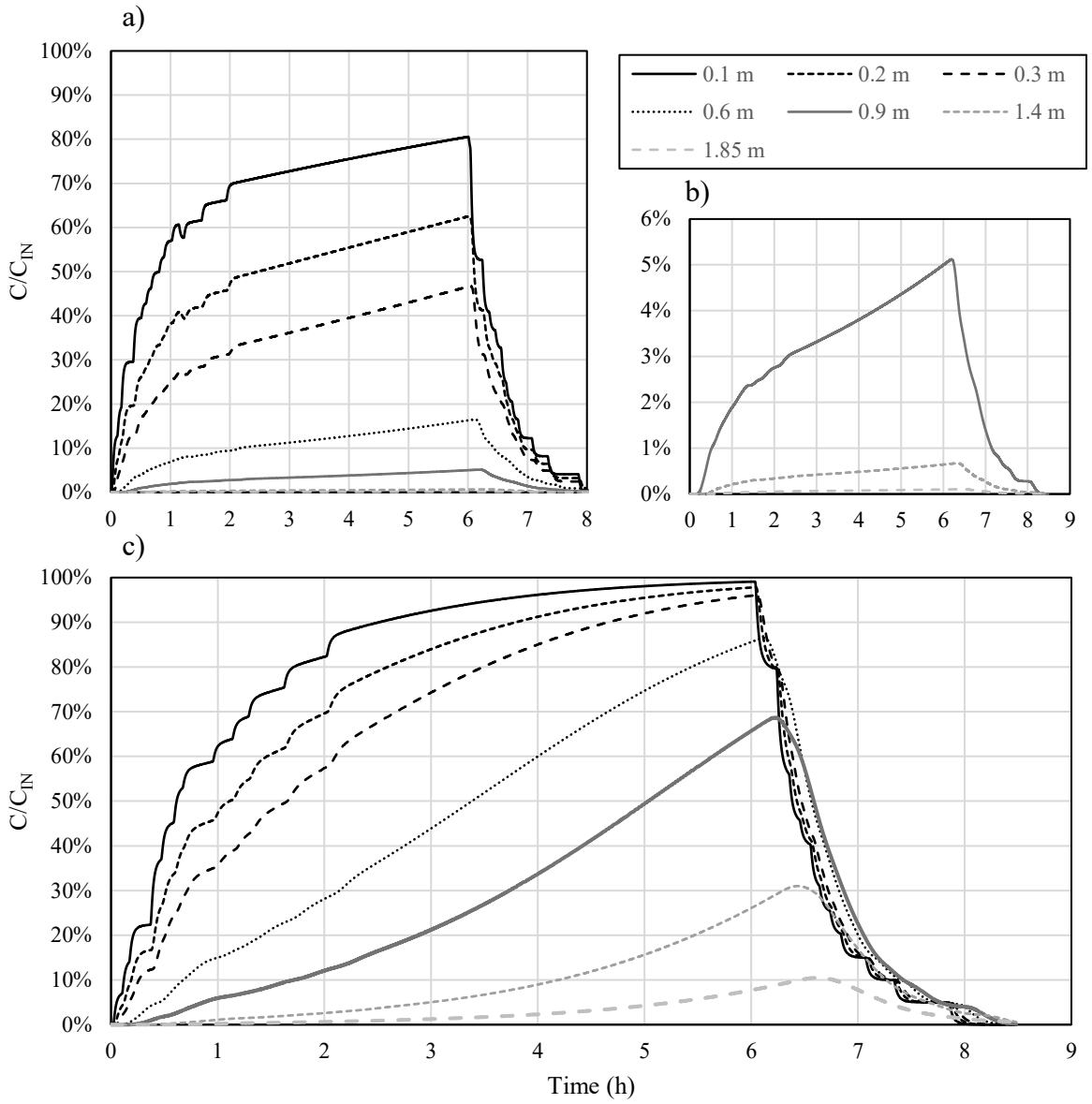


*Figure 2.21 – Particle concentrations in function of time at different distances from the top of the filter. a) sand, b) zoom of the last sand curves, c) activated carbon.*

The results are the breakthrough curves for the sand and for the activated carbon at several distances from the inlet point, the concentration distribution along the pilot in time and the effect of porosity and dispersivity on concentration at a two given points. The breakthrough curves present some steps due to the not perfect injection curve due to the necessary discretization.

The first result is the breakthrough curves of the particle concentration in time for sand and activated carbon at different distances from the top of the filter, Figure 2.21. The difference distances are the several sampling points along the pilot plant, at 10 cm, 20 cm, 30 cm, 60 cm, 90 cm, 140 cm and 185 cm.

Looking at the particle breakthrough curve in sand, Figure 2.21(a), it is possible to notice that the saturation is not reached for any distance. After 6 h of injection from the first sampling point, the particle concentration is about the 80% of the inlet one. It means that is necessary more time to saturate the first

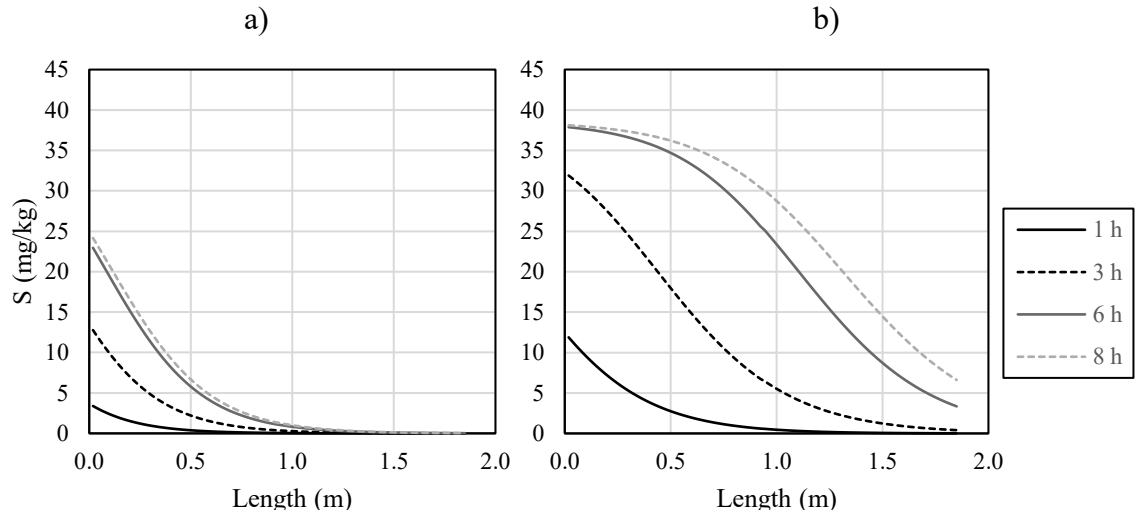


*Figure 2.22 – Porous media concentration profile at different times. a) sand, b) activated carbon.*

10 cm of the filter and consequently much more time is necessary to saturate the entire filter. From a long time analysis, 4 days are necessary to saturate it and find the inlet concertation in the last sampling point. In Figure 2.22(a) it is possible to visualize the concentration profile along the pilot filter at several times, 1 h, 3 h, 6 h and 8 h. The shape of the curves is not a saturative one and the $S_{max}$, about 39 mg/kg, had not been reached in any point of the pilot filter yet. In Figure 2.21(b) a zoom of the last three curves where it is possible to see that the breakthrough curve at 1.85 is flat. After 6 h the outlet concertation is practically null. In the activated carbon filter, Figure 2.21(c), the saturation was reached for the first sampling. In general, the particle concentrations in time are higher in the activate carbon filter.

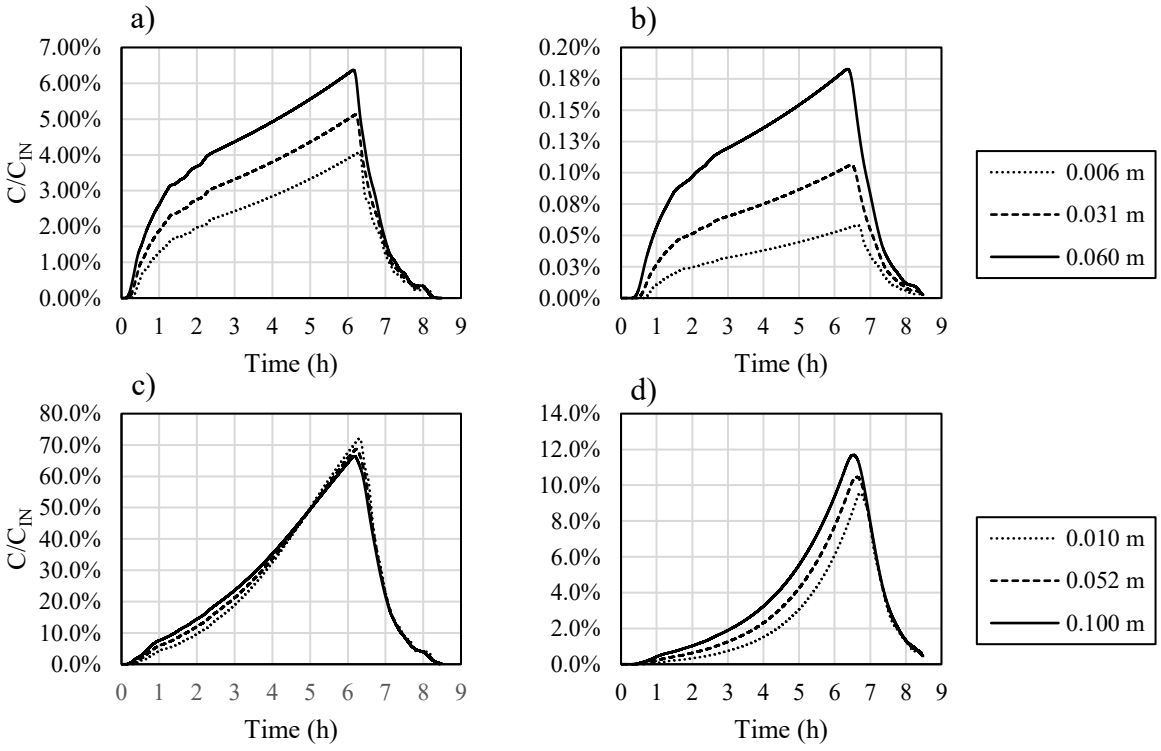


*Figure 2.23 – Sensitivity analysis on dispersivity at constant porosity, 45% for sand and 45% for activated carbon. a) Sand at 0.90 m, b) Sand at 1.85 m, c) Activated carbon at 0.90 m, d) Activated carbon at 1.85 m.*

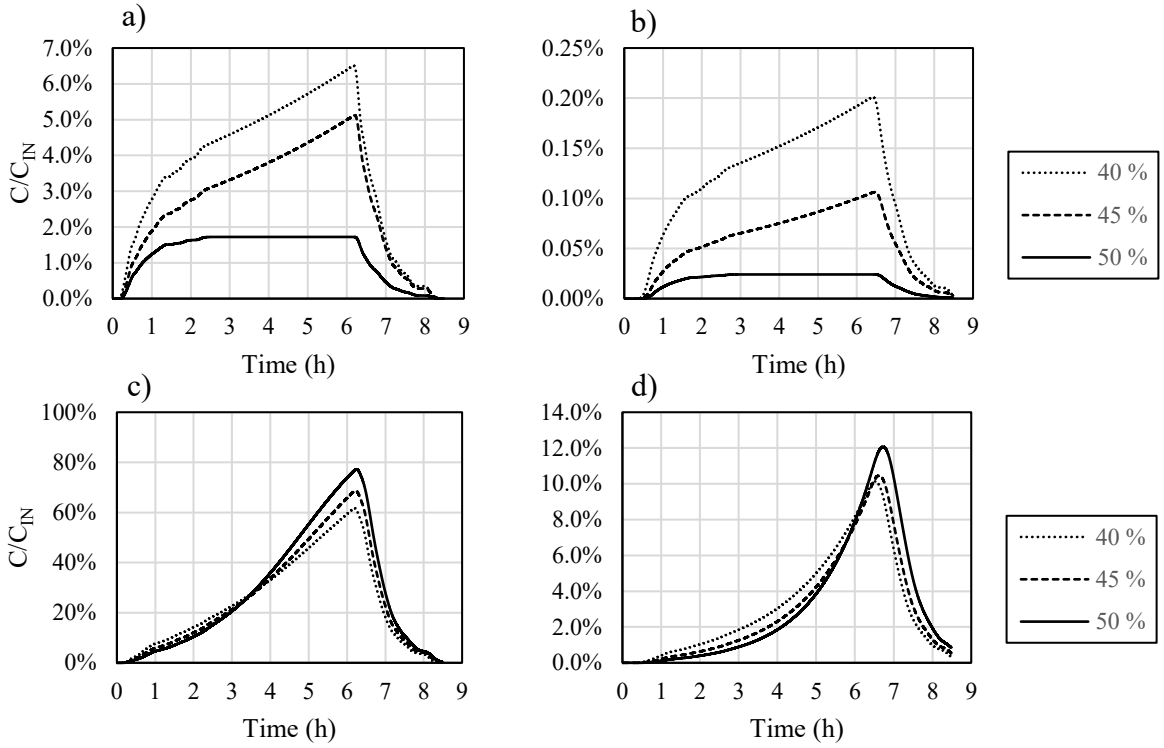


*Figure 2.24 – Sensitivity analysis on porosity at constant dispersivity, 0.031 m for the sand and 0.052 m for the activated carbon. a) Sand at 0.90 m, b) Sand at 1.85 m, c) Activated carbon at 0.90 m, d) Activated carbon at 1.85 m.*

Therefore, less time is necessary to reach the saturation of the entire pilot activated carbon filter, 18 h. After 6 h from the pilot filter it is possible to measure a particle concentration that is the 10% of the inlet one. In Figure 2.22(b) the particle concentration curves in solid phase are visible and they have a saturative shape at 6 h and 8 h.

The first important result from the simulations is that the sand filter has a higher efficiency than the activated carbon one. More time is necessary to reach the maximum saturation concentration for the entire pilot scale sand filter. After 6 h the particle concentration normalized with the inlet one is about 0% for the sand while 10% for the activated carbon. This reinforces the consideration done for the interaction energy analysis and the single collector contact efficiency.

From the sensitivity analysis done for the dispersivity at constant porosity, Figure 2.23, and for the porosity at constant dispersivity, Figure 2.24, it is possible to notice that the effects are not relevant. In the sand filter, the particle concertation would be underestimate if the dispersivity was underestimated and if the porosity was overestimated. Considering the effects at 90 cm from the top of the filter, which are more relevant, the particle concertation could range of about 2% or 4%, respectively varying dispersivity and porosity. It is also possible to see a small difference in the shape of the curves. In the activate carbon filter no effects on the shape of the curves can be seen, but the range of variation is higher. The dispersivity produces a variation of the concentration of about the 7% and the porosity of about 18%.

### 2.3.6 1D Pilot particle test and model calibration

The pilot experiment was done with conditions similar to the previous explained ones. The total injection time was of 6.3 h instead of 6 h. The simulated inlet concentration of $2.0 \cdot 10^{-3}$ kg/m$^3$ was not reached

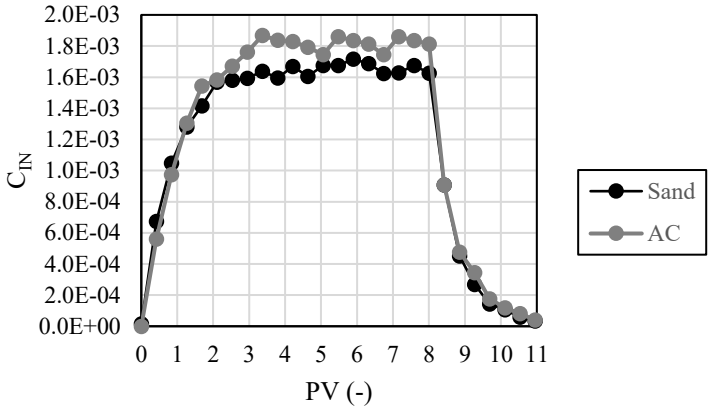


*Figure 2.25 – Pilot injection steps for sand and activated carbon*

during the pilot experimental test but respectively $1.65 \cdot 10^{-3}$ kg/m$^3$ and $1.82 \cdot 10^{-3}$ kg/m$^3$ for the sand and for the activated carbon. They are visible in Figure 2.25. Along the sand pilot test the concentration was measured at several distances from the top of the filter: 10 cm, 20 cm, 30 cm, 60 cm and 185 cm. For the activated carbon, the sampling point were also at 90 cm and 140 cm.

The sand and the activated carbon results are visible respectively in Figure 2.28 and Figure 2.28. The activated carbon curves are more regular than the sand ones, the decrease of particle concentration with the distance is gradual. The sand breakthroughs do not decrease progressively, a discrepancy between the first one and the others can be seen. After 6 h at 10 cm from the top the concentration is the 30 % of the inlet one that corresponds to a 70% of removal. Moreover, at 20 cm, at the same time, the concentration is the 5% of the inlet one. It means that a considerable removal of particles is present in the first 20 centimetres of the pilot. The reason of these phenomena can be the biological layer that is usually present on the top of the sand filters. The biological layer can reduce the space between grains increasing the retention of nanoplastics. A schematic representation is visible in Figure 2.26.

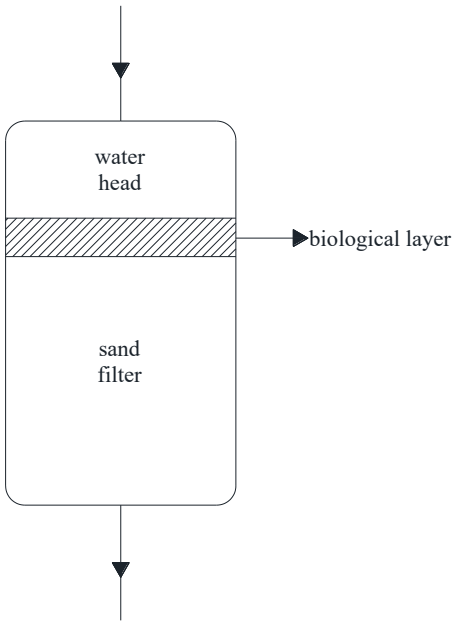


*Figure 2.26 – Scheme of the biological layer on the top of the sand filter.*

Anyway, as also underlined in the simulation paragrapher, the retention of particles is grater in the sand filter than in the activated carbon one at a same time. At long time in both filters the outlet concentration will be equal because the attachment mechanism is a "blocking", but it will be reached before in the activated carbon than in the sand. After 6 h of injection the outlet concentrations are for both about the 1.0 % of the inlet one. The difference potentially increases with longer injection times.

The last step of this study is the comparison between the pilot experimental data and the simulations. As it is reasonable, the simulation and the experimental data are different. So, the experimental data was used to consolidate and recalibrate the models. In both the cases the attachment mechanism, "blocking", which was identified from the column tests, is the same of the pilot experiments.

Starting from the sand experimental results, because of the greater attachment due to the biological layer on the top of the filter, the sand pilot model was divided in two parts. The first one represents the upper layer with the biological contribution and the second one the sand filter without the additional contribution. The scheme is visible in Figure 2.26. For the two parts different interaction parameters were estimated. The attachment rates and the maximum blocking concentrations were gotten for the first 20 cm and for the remaining 165 cm. For the top of the sand filter the values obtained are: $k_a$ equal to 0.0190 1/s and an $S_{max}$ of $1.16 \cdot 10^{-4}$. The values are greater than those calculated from the column test visible in Table 2.15. The most reasonable reason is the presence of the biological layer. Instead, the parameters of the second portion of the filter are: $k_a$ equal to 0.0030 1/s and an $S_{max}$ of $1.20 \cdot 10^{-4}$. The attachment rate is equal to the column one while the maximum saturation concentration is lower. $S_{max}$ of the column can potentially be affected by the presence of a portion of biological matter that was collected during the experimental set-up. For this reason, the value of the maximum blocking

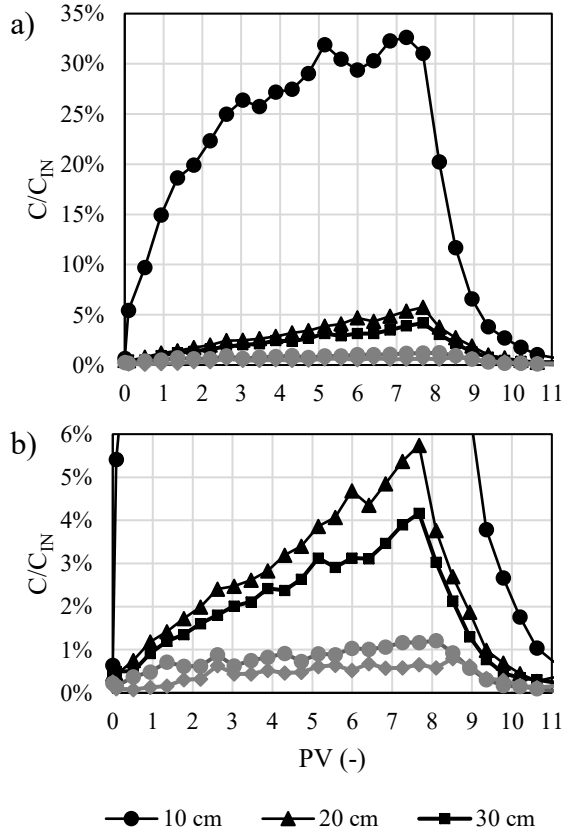


*Figure 2.28 – Sand pilot test, experimental data. a) all data, b) zoom.*

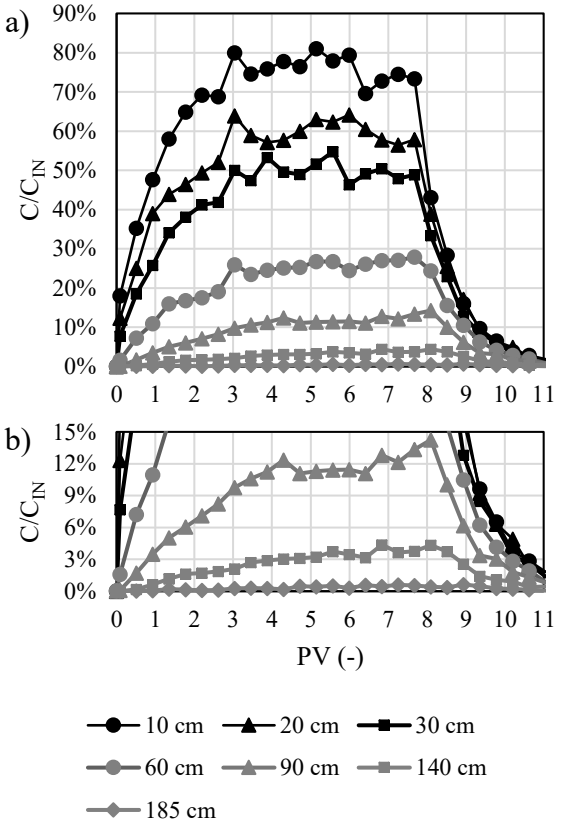


*Figure 2.28 – Activated carbon pilot test, experimental data. a) all data, b) zoom.*

concentration derived from the column test was overestimated. The result of the model recalibration is visible in Figure 2.30. The dots are the experimental data while the lines are the modeling result. The

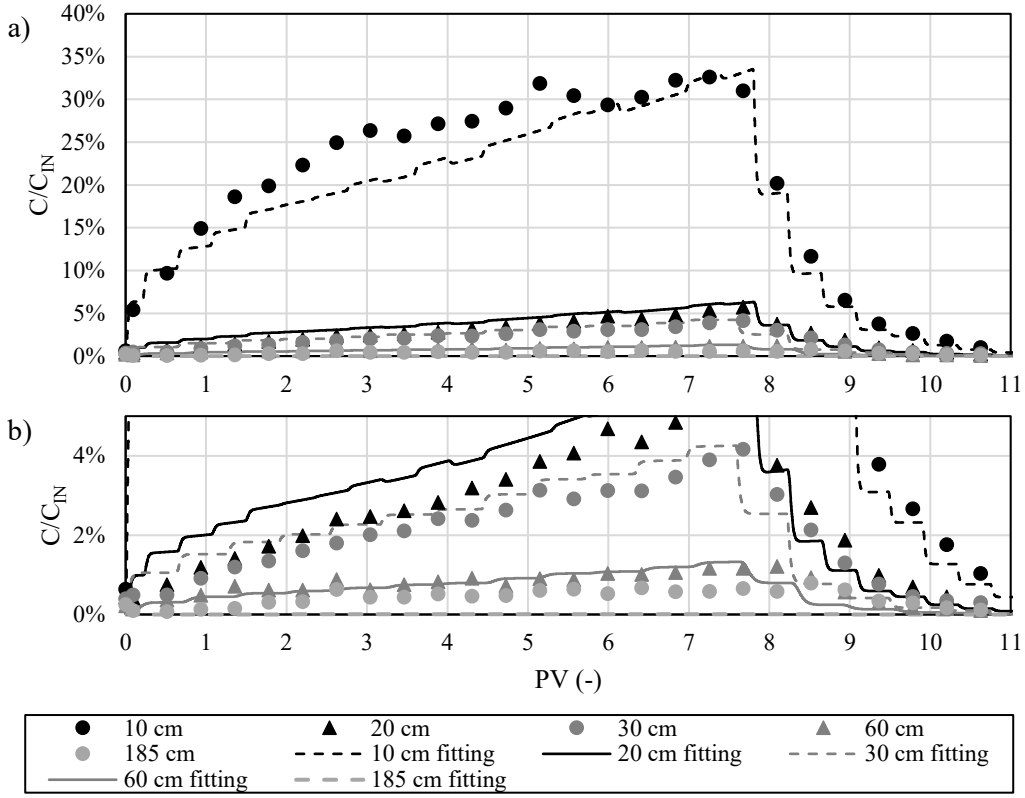


*Figure 2.30 – Sand, pilot experimental data fitting. a) all, b) zoom.*

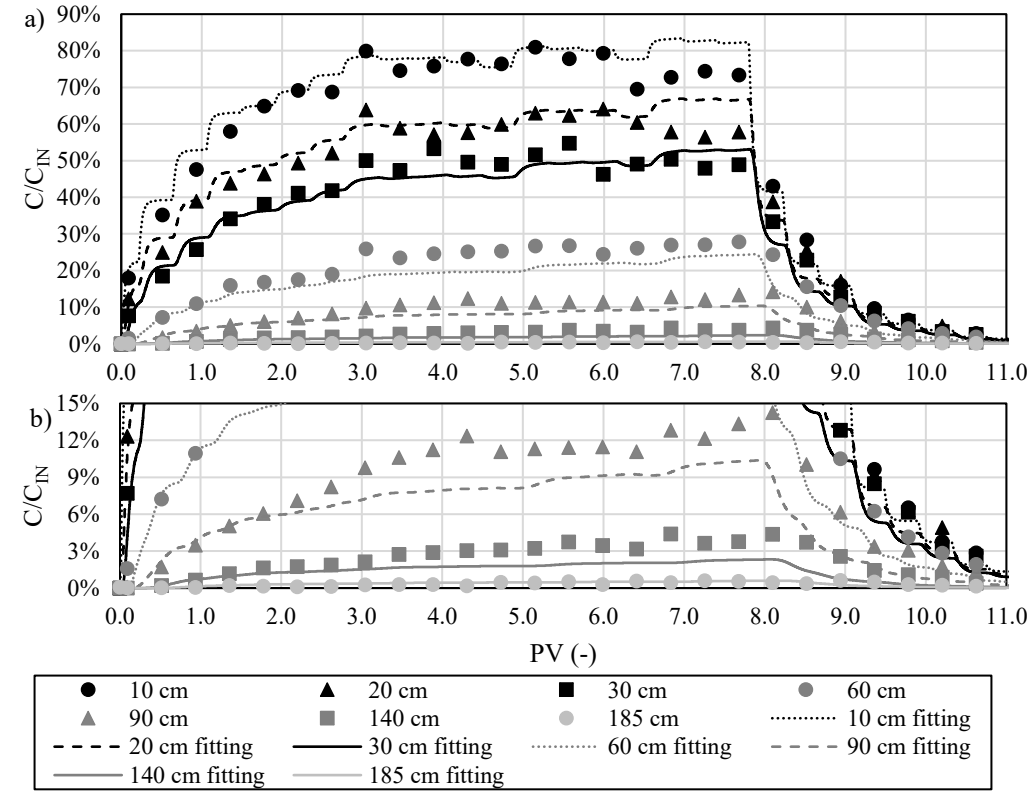


*Figure 2.30 – Activated carbon, pilot experimental data fitting. a) all, b) zoom.*

modelled breakthrough at 185 cm from the top of the filter does not fit the experimental data because of the detection limit of palladium, chapter 2.1.1.

The activated carbon filter model had only a recalibration to adjust the interaction parameters thanks to a more homogenous material along the depth. After a fitting process between the experimental data and the model the average parameters obtained are: $k_a$ equal to 0.0023 1/s and $S_{max}$ equal to $4.46 \cdot 10^{-4}$. The attachment rate is practically equal to the column one while the maximum blocking concentration is one order of magnitude bigger. The value gotten from the column tests are visible in Table 2.15. The discrepancy of the maximum blocking concentration may be due or to a scale effect or to an underestimation during the column test interpretation because of a too brief test. $S_{max}$ affects the inclination of the chart and the fitting of a brief test can generate an error in the estimation. The result of the pilot experimental fitting with the recalibrated model are visible in Figure 2.30.

### 2.3.7 Backwash time prediction

In granular media filters it is crucial to estimate the backwashing time that is the time at which the porous media needs to be cleaned with a counter-current flow. In order to estimate it, the breakthrough curves of the filter outlet at saturation was estimated by a long-time simulation. The outlet of the two filters was calculated varying the inlet concertation. The three inlet concentrations used are 0.02 kg/m$^3$, 0.002 kg/m$^3$, 0.0002 kg/m$^3$ for both sand and activated carbon. From the breakthrough curves, the removal efficiency was estimated as the complementary to one of the ratio between the concentration and the inlet one. The removal efficiency for both the filters depending on the inlet concentration can be plotted in function of time or equally PV, Figure 2.31. As it is possible to see from Figure 2.31, the removal efficiency is always higher for the sand filter than for the activated carbon one at a certain time. Indeed, it is necessary more time to decrease the removal efficiency from the 100%. For the pilot conditions, an inlet concertation of about 0.002 kg/m$^3$, 12 days are necessary to saturate the sand filter while 9 days for the activate carbon one.

As explained before the backwash is necessary to clean the grains from the NPs that are attached on the porous media in order to repristinate the removal mechanism. A removal efficiency must be identified

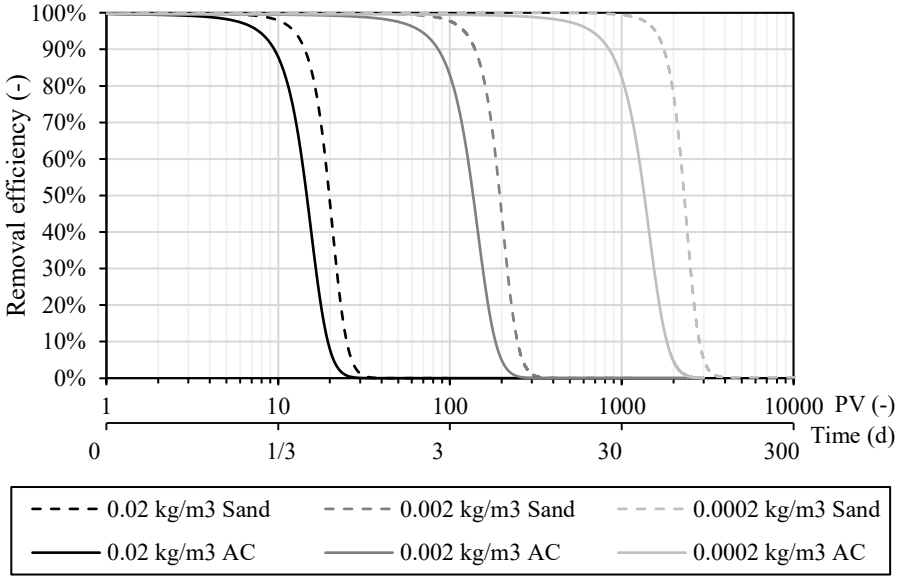


*Figure 2.31 – Removal efficiency of sand filter and activated carbon filter in function of time at three different concentration.*

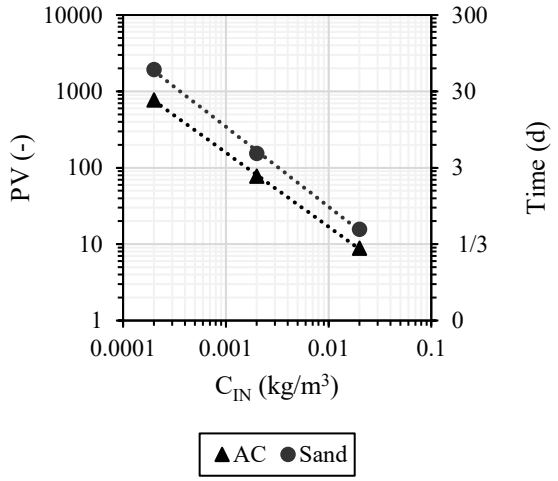


*Figure 2.32 – Backwashing time for a removal efficiency of 90% in function of the inlet concentration*

as threshold and the backwash time can be determined by the intersection of the curves with the limit. The backwash time is the period during which the filter can work guaranteeing a removal efficiency greater than the threshold fixed.

The backwashing time for a fixed removal efficiency can be plotted in function of the inlet concertation in a bi-logarithmic graph obtaining a correlation. The correlation can be useful to estimate the backwashing time for a different inlet concertation. In this case, a blocking interaction mechanism, the correlation is linear. In Figure 2.32 it is possible to see the relations for sand and activated carbon for a removal efficiency of 90%.

## 2.4 Conclusions

From this study emerged that the filtration mechanism that better describes the particle behaviour in a sand or in an activated carbon filter is “blocking”. Blocking is a saturative single-layer deposition mechanism, typical of systems where physico-chemical surface interactions are predominant. This is the case of NPs, which are characterized by a high negative surface charge. As a consequence, the filtration efficiency is expected to approach zero for both filtering materials, once all the active sites available for deposition are occupied by particles and the porous medium saturation is achieved. In support of this argumentation, a repulsive energy profile was found between the same nanoplastics and, between plastic particles and porous media. This is the result of the potential energy profile calculation using the DLVO theory, chapter 2.3.1. When nanoplastics cover the grains, reaching the maximum blocking concentration, the repulsion between particles prevent the attachment of further nanoplastics. In addition to the energy profile, the experimental breakthrough curves have a shape that is typical of a “blocking” interaction mechanism for both the scales of the experiments. The outlet concentration increases over time.

According to the model, in the long period, both filters are not able to retain nanoplastics. When the maximum blocking concentration, $S_{max}$, is reached, the outlet NP concentration is equal to the inlet one. As in all the granular media filters, a backwash is necessary to clean the grains and to allow the filters to restart. The backwashing time is one of the design parameters of a granular media filter. As explained before, in the long period the two filters have the same behaviour but a different backwashing time due to the different interaction parameters and filter media characteristics. As reported in chapter 2.3.2, the

single collector contact efficiency was found to be higher for sand than for activated carbon. Sand has a smaller grain size than the activated carbon one and the flow rate is usually lower in a sand filter than in an activated carbon filter. The result is a greater nanoplastic removal. But the results of the column tests and of the pilot test are more important than the single collector contact efficiency one, which anyway helps to characterize the NP transport. In all the experiments, the NP removal is grater for sand than for activated carbon. In the pilot experiment, the additional contribution of the organic layer significantly increases the particle retention of the sand filter.

# FINAL CONCLUSIONS

The pervasive presence of microplastics (MPs) and nanoplastics (NPs) in various environmental compartments fostered an increasing research on their possible implications on human health and environment protection. The exponential growth in the publications of documents (1439 published only in 2019), however, potentially leads to confusion. A statistical analysis of literature is therefore crucial to understand the trend of the research on MPs and NPs. The analysis presented in this thesis aimed at summarising and understanding the countries interested in the topic, the most studied environmental compartments, and the most extensive subjects. From the analysis emerged that the countries most interested in MPs and NPs are the ones that have access to seas and oceans. This is due to the fact that saltwater resulted the most studied environmental compartment. Indeed, seawater plastic pollution is one of the main environmental problem and consequently the research is growing exponentially both for marine litter and for MPs and NPs. The pollution of seas due to plastic particles is mainly caused by freshwater bodies, which transport micro- and nanoplastic from the hinterland to the shoreline. One of the main sources of MPs and NPs is the sewer of WWTPs and WTPs. Even if they contribute significantly to the water body pollution, they are not well studied yet, indeed only a small portion of documents considers the removal of micro- and nanoplastics from the treatment plants. This thesis aims at filling some gap in the knowledge by studying WWT and WWTP filters.

The most used granular media filters analysed in this study are the sand filter and the activated carbon filter. From the experimental data and from the modelling, it was found that the most appropriate interaction mechanism between NPs and the filters is “blocking”. According to the chosen mechanism, the filters are able to retain NPs because plastic particles attach on the porous media grains. However, both filters are not able to retain nanoplastics in the long period. When the maximum blocking concentration is reached, the outlet NP concentration is equal to the inlet one. To allow again the NP deposition, a backwash is necessary to clean the grains. The backwash process is always periodically done in granular media filters because their efficiency decreases in time. Some benchmarks are monitored in time during the filtration process and when one of the control thresholds is exceeded, the backwash process is run. From the backwash modelling analysis performed for the NP filtration, it results that the backwash time is grater for the sand filter than for the activated carbon one at a fixed removal efficiency for the three different modelled concentrations.

In conclusion, both the sand and the activate carbon filters are able to remove NPs from water (in this particular case the water used comes from the Lake Zürich). In reality the removal efficiency increases because in the treatment systems, the sand filter and the activated carbon one are often used in series. An experiment and a simulation of this configuration can be performed as next step of the study. Because the removal efficiency of the filters was tested mainly with a set of boundary conditions, a further step can potentially be the variation of some of them to better understand the behaviour of NPs in the two filters. One of the most interesting boundary conditions is the inlet concertation because it potentially affects the interaction mechanism and the backwashing time. The inlet concentration should be more

similar to the lake one, but the current impossibility of measuring NPs in water does not allow a correct quantification. Another important aspect that can potentially be performed is the backwashing process. The time at which the filter must be cleaned can be estimated by a simulation, but the effectiveness of the backwash has to be tested by measuring the NP concentration in the cleaning flow and in the filter media. The disposal of the backwashing solution can be a further point of interest because NPs has to be removed again from a water solution.

# Appendix A

The list of the solution used in MNMs and also visible in the following figures is:

| | Authors | Year | Symbol |
|---|---|---|---|
| [58] | Messina, Marchisio and Sethi | 2015 | η0,MMS |
| [59] | Ma et al. | 2013 | η0,MHJ |
| [60] | Nelson and Ginn | 2011 | η0,NG |
| [61] | Ma et al. | 2009 | η0,MPFJ |
| [57] | Tufenkji and Elimelech | 2004 | η0,TE |
| [62] | Rajagopalan and Tien | 1976 | η0,RT |
| [42] | Yao et al. | 1971 | η0,Y |

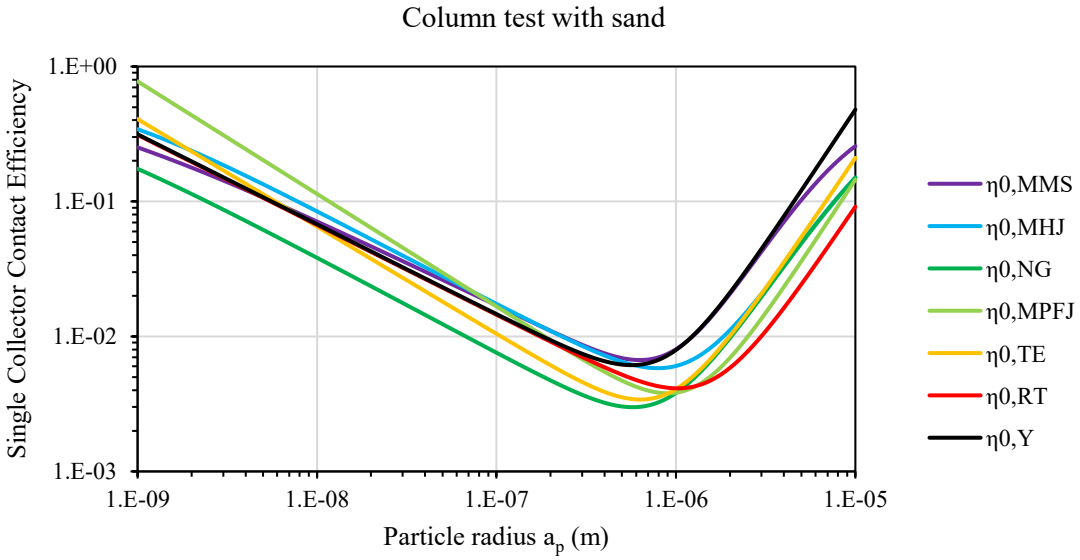


*Appendix A - Figure 1 – Single collector efficiency of column test with sand*

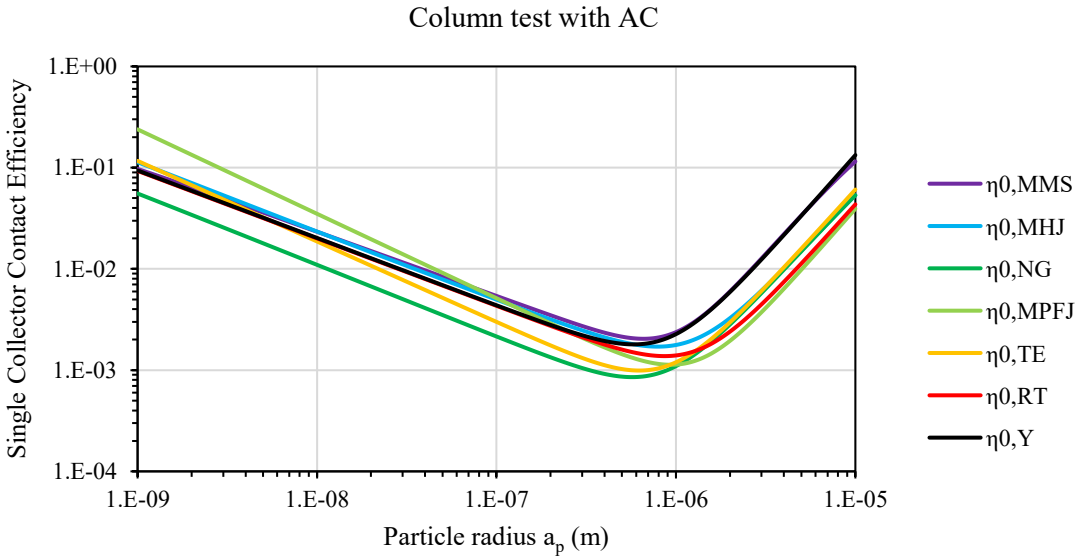


*Appendix A - Figure 2 - Single collector efficiency of column test with AC*

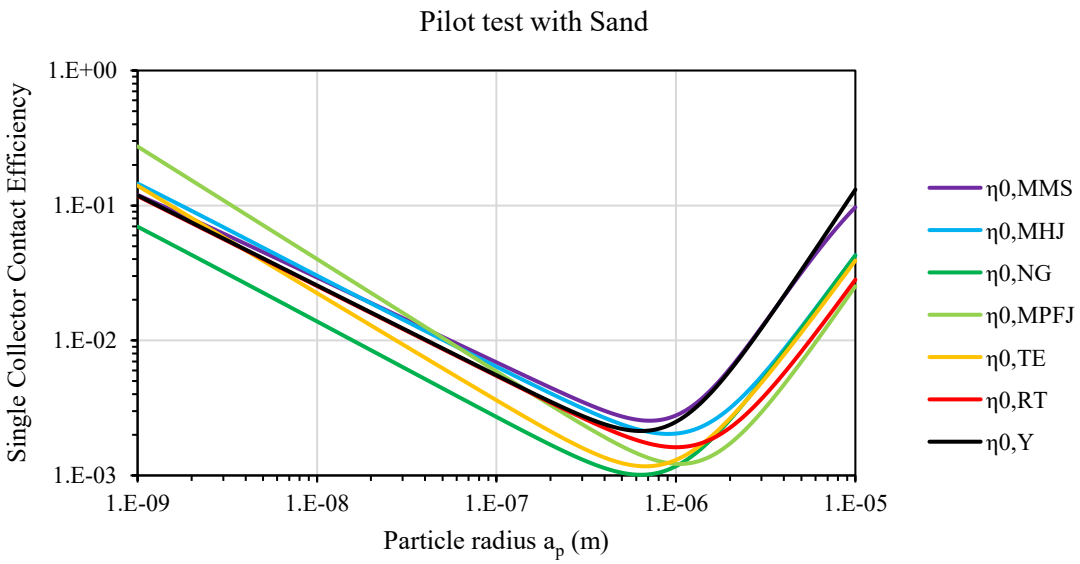


*Appendix A - Figure 3 - Single collector efficiency of pilot test with sand*

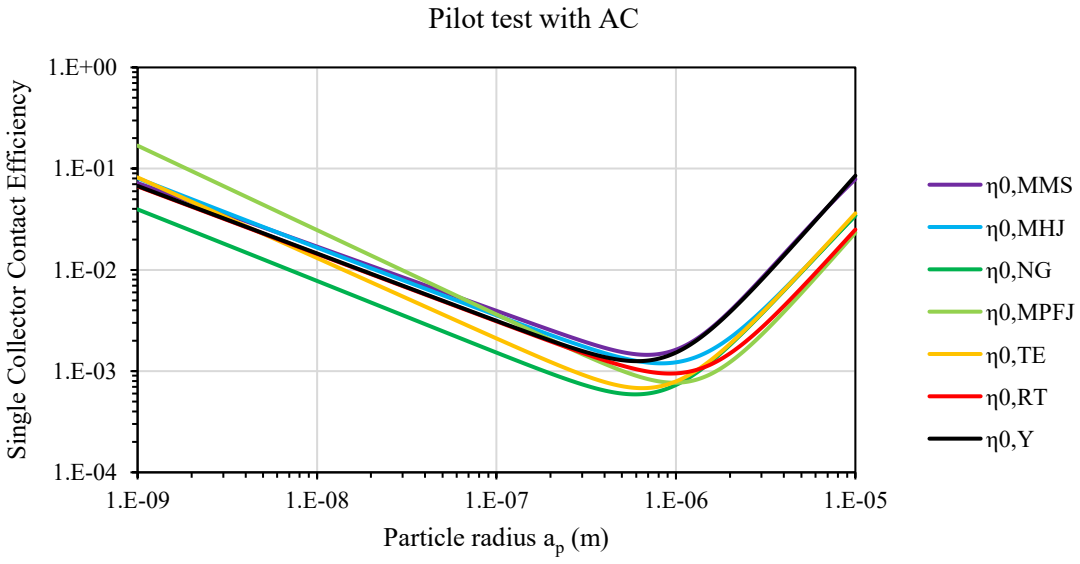


*Appendix A - Figure 4 - Single collector efficiency of pilot test with AC*

# Appendix B

In this appendix the graphs of the fitting of the column tracer test are showed.

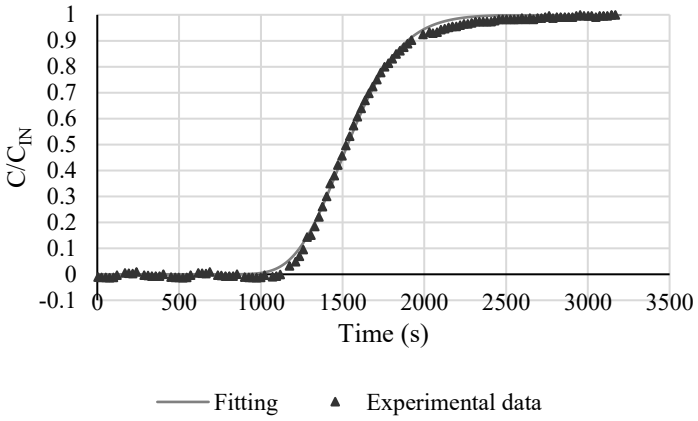


*Appendix B - Figure 1 - NaCl tracer test of Dw and Sand*

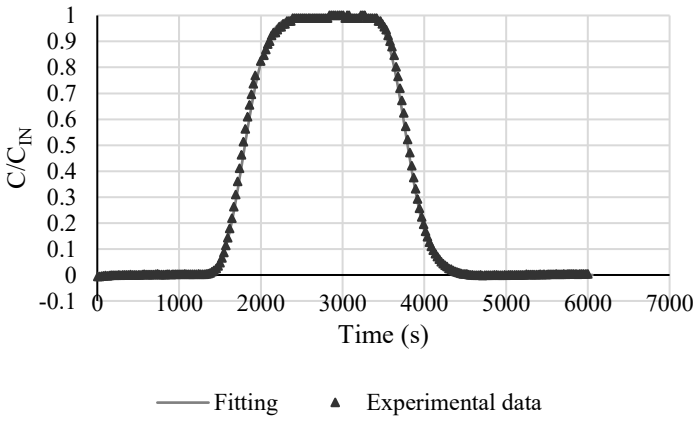


*Appendix B - Figure 2 - NaCl tracer test of LZw and Sand*

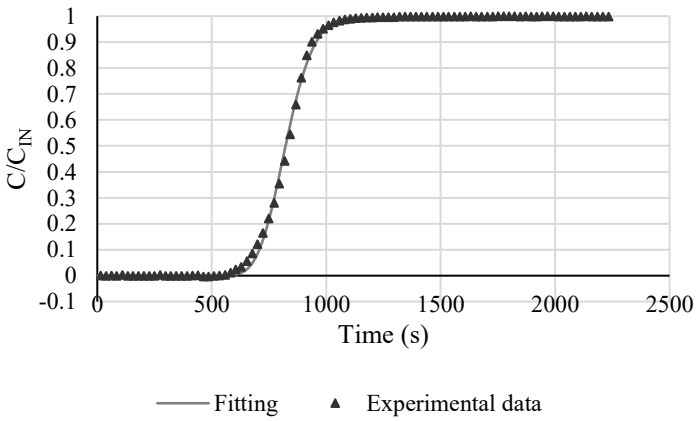


*Appendix B - Figure 3 - NaCl tracer test of 1:1 Dw:LZw and Sand*

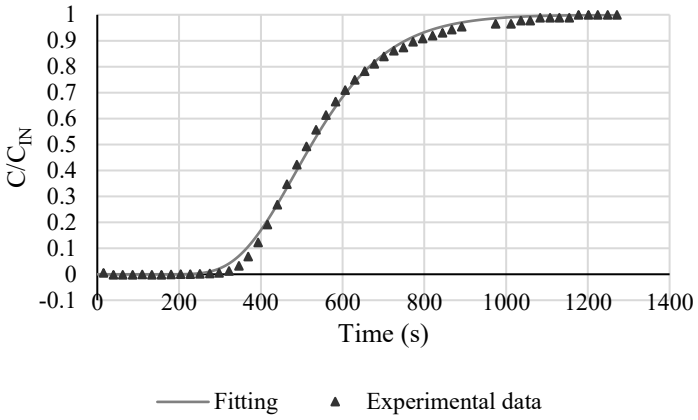


*Appendix B - Figure 4 - NaCl tracer test of LZw and Activated Carbon*

# Appendix C

In this appendix the graphs of the particle column test fitting:

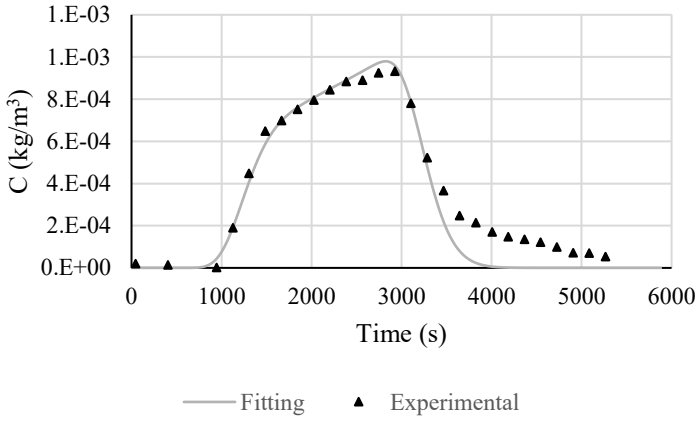


*Appendix C - Figure 1 - Sand filter with Dw*

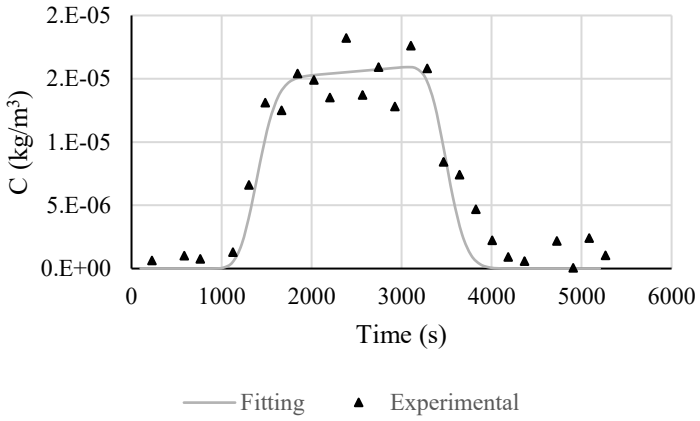


*Appendix C - Figure 2 - Sand filter with LZw*

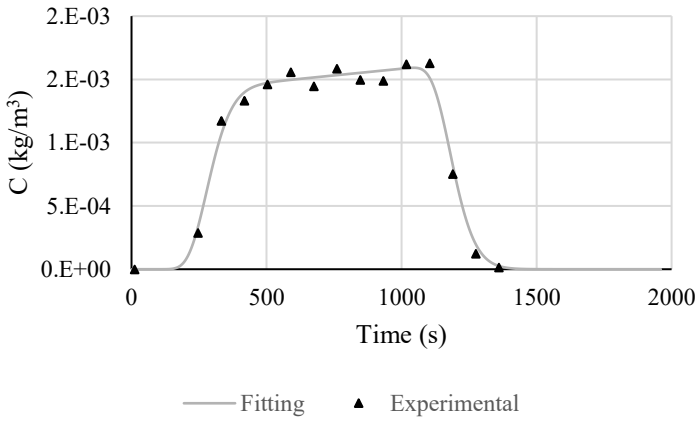


*Appendix C - Figure 3 - Activated carbon filter with LZw*

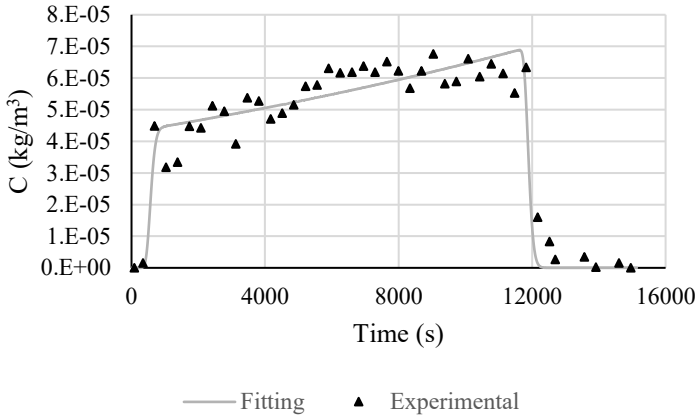


*Appendix C - Figure 4 - Sand filter with 1:1 LZw:Dw*

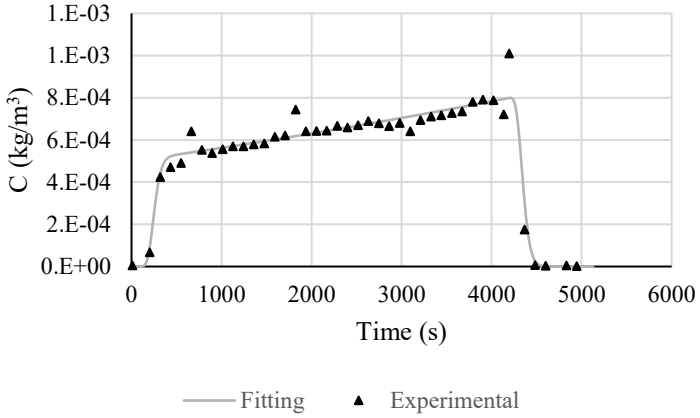


*Appendix C - Figure 5 - Activated carbon filter with 1:1 LZw:Dw*

# Appendix D

In this appendix the graphs of the pilot tracer test fitting:

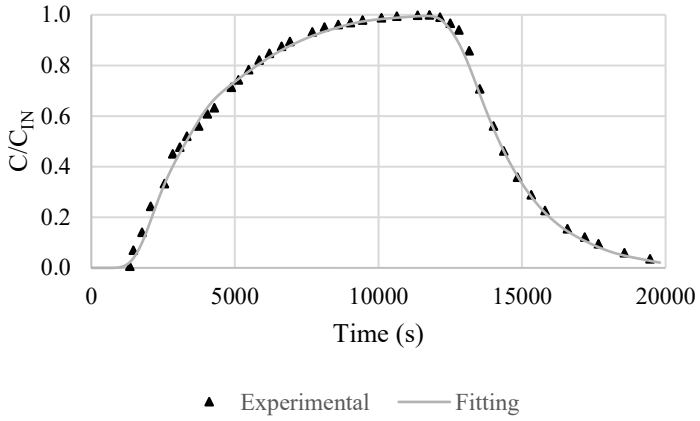


*Appendix D - Figure 1 - Sand filter, 1 m, pilot tracer test*

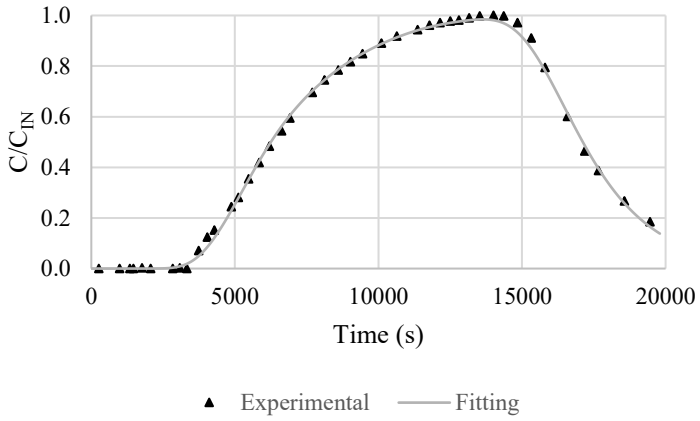


*Appendix D - Figure 2 - Sand filter, outlet, pilot tracer test*

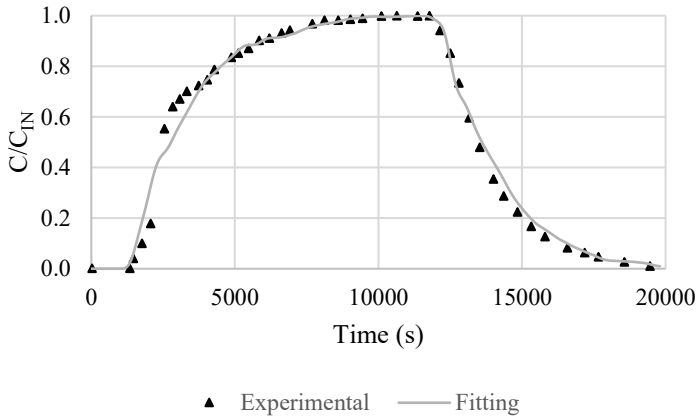


*Appendix D - Figure 3- AC filter,, 1 m, pilot tracer test*

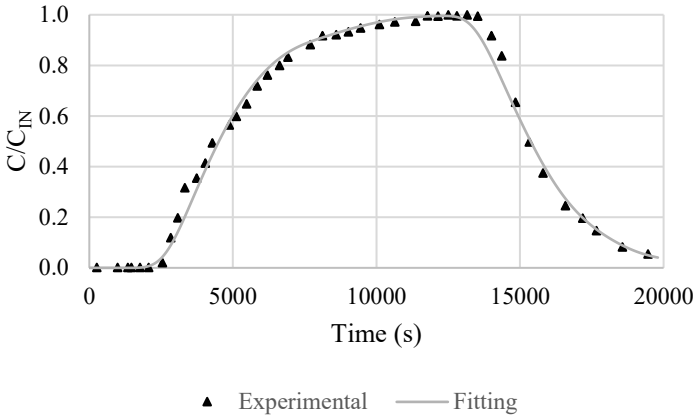


*Appendix D - Figure 4 - AC filter, outlet, pilot tracer test*

# List of figures

# List of tables

# Bibliography


1. Verschoor, A.J., *Towards a definition of microplastics : Considerations for the specification of physico-chemical properties.* Naar een definitie voor microplastics, 2015.
2. Hartmann, N.B., et al., *Are We Speaking the Same Language? Recommendations for a Definition and Categorization Framework for Plastic Debris.* Environmental Science and Technology, 2019. **53**(3): p. 1039-1047.
3. Thompson, R.C., et al., *Lost at Sea: Where Is All the Plastic?* Science, 2004. **304**(5672): p. 838.
4. Carpenter, E.J. and K.L. Smith Jr, *Plastics on the Sargasso sea surface.* Science, 1972. **175**(4027): p. 1240-1241.
5. Arthur, C., J. Baker, and H. Bamford, *Proceedings of the International Research Workshop on the Occurrence, Effects and Fate of Microplastic Marine Debris.* National Oceanic and Atmospheric Administration Technical Memorandum NOS-OR&R-30, 2009.
6. Koehler, A., et al., *SOURCES, FATE AND EFFECTS OF MICROPLASTICS IN THE MARINE ENVIRONMENT: A GLOBAL ASSESSMENT*. 2015.
7. Kershaw, P., et al., *Proceedings of the GESAMP International Workshop on assessing the risks associated with plastics and microplastics in the marine environment*. 2020.
8. Galgani, F., et al., *Guidance on Monitoring of Marine Litter in European Seas*. 2013.
9. Commision, E., *Recommendation on the definition of a nanomaterial*. 2011.
10. Katsanou, K., H.K. Karapanagioti, and I.K. Kalavrouziotis, *Plastics and microplastics in the human water cycle*, in *Microplastics in Water and Wastewater*. 2019, IWA Publishing. p. 0.
11. Da Costa, J., A. Duarte, and T. Rocha-Santos, *Microplastics – Occurrence, Fate and Behaviour in the Environment*. 2016.
12. Crawford, C.B. and B. Quinn, *Microplastic Pollutants*. 2017. 1-315.
13. Cole, M., et al., *Microplastics as contaminants in the marine environment: A review.* Marine Pollution Bulletin, 2011. **62**(12): p. 2588-2597.
14. Science Advice for Policy by European Academies, *A Scientific Perspective on Microplastics in Nature and Society*. 2019: Berlin.
15. Eriksen, M., et al., *Plastic Pollution in the World's Oceans: More than 5 Trillion Plastic Pieces Weighing over 250,000 Tons Afloat at Sea.* PLoS ONE, 2014. **9**(12).
16. Eerkes-Medrano, D., R.C. Thompson, and D.C. Aldridge, *Microplastics in freshwater systems: A review of the emerging threats, identification of knowledge gaps and prioritisation of research needs.* Water Research, 2015. **75**: p. 63-82.
17. Faure, F., et al., *Plastic pollution in Swiss surface waters: Nature and concentrations, interaction with pollutants.* Environmental Chemistry, 2015. **12**.
18. Browne, M.A., et al., *Accumulation of microplastic on shorelines woldwide: Sources and sinks.* Environmental Science and Technology, 2011. **45**(21): p. 9175-9179.
19. Mourgkogiannis, N., I.K. Kalavrouziotis, and H.K. Karapanagioti, *Questionnaire-based survey to managers of 101 wastewater treatment plants in Greece confirms their potential as plastic marine litter sources.* Marine Pollution Bulletin, 2018. **133**: p. 822-827.
20. Murphy, F., et al., *Wastewater Treatment Works (WwTW) as a Source of Microplastics in the Aquatic Environment.* Environmental Science & Technology, 2016. **50**(11): p. 5800-5808.
21. McCormick, A.R., et al., *Microplastic in surface waters of urban rivers: Concentration, sources, and associated bacterial assemblages.* Ecosphere, 2016. **7**(11).
22. Mintenig, S.M., et al., *Low numbers of microplastics detected in drinking water from ground water sources.* Science of the Total Environment, 2019. **648**: p. 631-635.
23. Carr, S.A. and J. Thompson, *Microplastics: Transport and removal at wastewater treatment plants*, in *Microplastics in Water and Wastewater*. 2019, IWA Publishing. p. 0.
24. Zhang, Y., et al., *Global trends and prospects in microplastics research: A bibliometric analysis.* Journal of Hazardous Materials, 2020. **400**: p. 123110.
25. Derraik, J.G.B., *The pollution of the marine environment by plastic debris: A review.* Marine Pollution Bulletin, 2002. **44**(9): p. 842-852.

26. Gregory, M.R., *Environmental implications of plastic debris in marine settings- entanglement, ingestion, smothering, hangers-on, hitch-hiking and alien invasions.* Philosophical Transactions of the Royal Society B: Biological Sciences, 2009. **364**(1526): p. 2013-2025.
27. Jambeck, J.R., et al., *Plastic waste inputs from land into the ocean.* Science, 2015. **347**(6223): p. 768-771.
28. Andrady, A.L., *Microplastics in the marine environment.* Marine Pollution Bulletin, 2011. **62**(8): p. 1596-1605.
29. Barnes, D.K.A., et al., *Accumulation and fragmentation of plastic debris in global environments.* Philosophical Transactions of the Royal Society B: Biological Sciences, 2009. **364**(1526): p. 1985-1998.
30. Wright, S.L., R.C. Thompson, and T.S. Galloway, *The physical impacts of microplastics on marine organisms: a review.* Environmental pollution (Barking, Essex : 1987), 2013. **178**: p. 483-492.
31. Hidalgo-Ruz, V., et al., *Microplastics in the marine environment: A review of the methods used for identification and quantification.* Environmental Science and Technology, 2012. **46**(6): p. 3060-3075.
32. Mitrano, D.M., et al., *Synthesis of metal-doped nanoplastics and their utility to investigate fate and behaviour in complex environmental systems.* Nature Nanotechnology, 2019. **14**(4): p. 362-368.
33. Benjamin, M.M. and D.F. Lawler, *Water Quality Engineering: Physical/Chemical Treatment Processes*. 2013: WILEY.
34. Bianco, C., *Modeling of the injection and long term fate of nanoparticles in groundwater systems*, R. Sethi and T. Tosco, Editors. 2017, Politecnico di Torino.
35. Elimelech, M., *Particle Deposition and Aggregation: Measurement, Modelling and Simulation*. 1998: Oxford: Elsevier Science & Technology.
36. Mark, R.W. and B. Jean-Yves, *Environmental Nanotechnology: Applications and Impacts of Nanomaterials*. 2007, New York: McGraw-Hill Education.
37. Gregory, J., *Approximate expressions for retarded van der waals interaction.* Journal of Colloid and Interface Science, 1981. **83**(1): p. 138-145.
38. Gregory, J., *The calculation of Hamaker constants.* Advances in Colloid and Interface Science, 1970. **2**(4): p. 396-417.
39. Gregory, J., *Interaction of unequal double layers at constant charge.* Journal of Colloid and Interface Science, 1975. **51**(1): p. 44-51.
40. Tien, C. and B.V. Ramarao, *Granular Filtration of Aerosols and Hydrosols*. Granular Filtration of Aerosols and Hydrosols. 2007: Elsevier Ltd.
41. Messina, F., *Pore-scale simulation of micro and nanoparticle transport in porous media*. 2015, Politecnico di Torino.
42. Yao, K.M., M.T. Habibian, and C.R. O'Melia, *Water and Waste Water Filtration: Concepts and Applications.* Environmental Science and Technology, 1971. **5**(11): p. 1105-1112.
43. Bianco, C., T. Tosco, and R. Sethi, *A 3-dimensional micro- and nanoparticle transport and filtration model (MNM3D) applied to the migration of carbon-based nanomaterials in porous media.* Journal of Contaminant Hydrology, 2016. **193**: p. 10-20.
44. Tiraferri, A., T. Tosco, and R. Sethi, *Transport and retention of microparticles in packed sand columns at low and intermediate ionic strengths: experiments and mathematical modeling.* Environmental Earth Sciences, 2011. **63**(4): p. 847-859.
45. Bradford, S.A., et al., *Physical factors affecting the transport and fate of colloids in saturated porous media.* Water Resources Research, 2002. **38**(12): p. 63-1-63-12.
46. Bradford, S.A., et al., *Modeling Colloid Attachment, Straining, and Exclusion in Saturated Porous Media.* Environmental Science & Technology, 2003. **37**(10): p. 2242-2250.
47. Logan, B.E., et al., *Clarification of Clean-Bed Filtration Models.* Journal of Environmental Engineering, 1995. **121**(12): p. 869-873.
48. Tufenkji, N. and M. Elimelech, *Deviation from the Classical Colloid Filtration Theory in the Presence of Repulsive DLVO Interactions.* Langmuir, 2004. **20**(25): p. 10818-10828.
49. Ko, C.-H., S. Bhattacharjee, and M. Elimelech, *Coupled Influence of Colloidal and*

*Hydrodynamic Interactions on the RSA Dynamic Blocking Function for Particle Deposition onto Packed Spherical Collectors.* Journal of Colloid and Interface Science, 2000. **229**(2): p. 554-567.

50. Ko, C.-H. and M. Elimelech, *The "Shadow Effect" in Colloid Transport and Deposition Dynamics in Granular Porous Media: Measurements and Mechanisms.* Environmental Science & Technology, 2000. **34**(17): p. 3681-3689.
51. Tosco, T., A. Tiraferri, and R. Sethi, *Ionic Strength Dependent Transport of Microparticles in Saturated Porous Media: Modeling Mobilization and Immobilization Phenomena under Transient Chemical Conditions.* Environmental Science & Technology, 2009. **43**(12): p. 4425-4431.
52. Tosco, T. and R. Sethi, *Transport of Non-Newtonian Suspensions of Highly Concentrated Micro- And Nanoscale Iron Particles in Porous Media: A Modeling Approach.* Environmental Science & Technology, 2010. **44**(23): p. 9062-9068.
53. Ogata, A. and R.B. Banks, *A solution of the differential equation of longitudinal dispersion in porous media*, in *Professional Paper*. 1961.
54. Sethi, R. and A. Di Molfetta, *GROUNDWATER ENGINEERING - A Technical Approach to Hydrogeology, Contaminant Transport and Groundwater Remediation*. 2019: Springer.
55. Chern, C.-S., *Interfacial Phenomena.* Principles and Applications of Emulsion Polymerization, 2008: p. 23-52.
56. Peukert, W., C. Mehler, and M. Götzinger, *Application of Adsorption and Adhesion Measurements for Particle Surface Characterization.* Particle & Particle Systems Characterization - PART PART SYST CHARACT, 2001. **18**: p. 229-234.
57. Tufenkji, N. and M. Elimelech, *Correlation equation for predicting single-collector efficiency in physicochemical filtration in saturated porous media.* Environmental science & technology, 2004. **38**(2): p. 529.
58. Messina, F., D.L. Marchisio, and R. Sethi, *An extended and total flux normalized correlation equation for predicting single-collector efficiency.* Journal of colloid and interface science, 2015. **446**: p. 185-193.
59. Ma, H., M. Hradisky, and W.P. Johnson, *Extending applicability of correlation equations to predict colloidal retention in porous media at low fluid velocity.* Environmental science & technology, 2013. **47**(5): p. 2272.
60. Nelson, K.E. and T.R. Ginn, *New collector efficiency equation for colloid filtration in both natural and engineered flow conditions.* Water Resources Research, 2011. **47**(5): p. n/a-n/a.
61. Ma, H., et al., *Hemispheres-in-Cell Geometry to Predict Colloid Deposition in Porous Media.* Environmental Science & Technology, 2010. **44**(11): p. 4383-4383.
62. Rajagopalan, R. and C. Tien, *Trajectory analysis of deep-bed filtration with the sphere-in-cell porous media model.* AIChE Journal, 1976. **22**(3): p. 523-533.